Investigation of fibre optical parametric amplifiers in telecommunications.

Jamshidi Far, Mehdi

Investigation of Fibre Optical Parametric Amplifiers in Telecommunications

Mehdi Jamshidi Far, BSc, MSc

A thesis submitted to Swansea University in the fulfilment of the requirements for the degree of

Doctor of Philosophy

School of Engineering

September 2010

ProQuest LLC.
789 East Eisenhower Parkway
P.O. Box 1346
Ann Arbor, MI 48106 – 1346

To my mother
for her never-ending love and sacrifices…

Abstract

Fibre optical parametric amplifiers have been attracting much attention since their first demonstrations. They are capable of providing a high amount of gain over large bandwidth ranges. Since what we call a fibre optical parametric amplifier is technically a combination of one or two pumps and a suitable highly-nonlinear fibre, their evolution is closely dependent on the improvements in the highly-nonlinear fibre technology and on that of the pumps.

Recently, the advent of silica-based highly-nonlinear fibres with proper dispersion characteristics and the availability of high-power erbium-doped fibre amplifiers capable of delivering several Watts of continuous-wave power have led to great improvements in achieving better performances with fibre optical parametric amplifiers. The fibre length required is reduced and fibre optical parametric amplifiers can be operated in the continuous-wave regime, which is necessary for being useful in telecommunications.

This work is a report of an investigation of different aspects of fibre optical parametric amplifiers. After reviewing the fundamentals of the operation of this kind of amplifiers, the difficulties facing them are discussed. Among these issues, the problem of nonlinear cross-talk is investigated in more details. I experimentally proved that by reducing fibre length, it is possible to keep the crosstalk in a tolerable range. The amplification of 26 communication channels modulated at about 40 Gb/s aggregating to the total capacity of more than 1 Tb/s, while obtaining performance results comparable to those of erbium-doped fibre amplifiers may tone down the chief criticism on the parametric amplifiers.

Two amplifiers with a record gain (60 dB for a two-pump amplifier) and a record bandwidth (270 nm in a one-pump amplifier) were demonstrated and it has been shown that there might be possibilities for improving the adverse effect of the Raman gain on the flatness of the gain spectra of the parametric amplifiers at the expense of losing some gain.

A sample of a newly-developed bismuth-oxide highly-nonlinear fibre is used to construct a novel scheme for wavelength demultiplexing, and the possibility of simultaneous time- and wavelength demultiplexing is discussed.

Declaration

This work has not been previously accepted in substance for any degree and is not being concurrently being submitted in candidature for any degree.

Signed.....(Mehdi Jamshidi Far)

Date...31 Jan 2011.....

Statement 1

This thesis is the result of my own investigations, except where otherwise stated. Where correction services have been used, the extent and the nature of the correction is clearly marked in a footnote(s).

Other sources are acknowledged by footnotes giving explicit references. A bibliography is appended.

Signed.....(Mehdi Jamshidi Far)

Date....31 Jan 2011.....

Statement 2

I hereby give consent for my thesis to be available for photocopying and for inter-library loan, and for the title and the summary to be made available to outside organisations.

Signed.....(Mehdi Jamshidi Far)

Date...31 Jan 2011.....

Contents

Acknowledgements

I would like to express my endless gratitude to my supervisor Professor Michel. E. Marhic from whom I have learnt a lot and to whom I am indebted to the extent certainly far beyond the words. He is the epitome of 'stability' to me. I have never found a shred of impatience in him. Neither have I witnessed any trace of anger in his attitude. He has inarguably never been in the state of rush. Through him I have had the touch of gaining profound respect free from spitefulness. The very word of 'respect' does get its real value in my terminology as an entrant inseparable from his name. I have constantly been trying my utmost to show it in any conversation we had and in every single email I sent. How much I missed to benefit from his knowledge and character is and will undoubtedly be my sole regret when thinking about my PhD.

I also wish to thank Professor Periklis Petropoulos and Professor Nick Doran for acting as the external and the internal examiners in the examination board of my thesis.

The financial support from EPSRC is gratefully acknowledged.

I wish to extend my thankfulness to my lifelong friends Shahab, Hossein, Saeed, Amir(s) and all others in Swansea and around the world for having been such a huge support in hard times and for sharing memorable moments.

I am lost for words to offer my sincerest thanks to my best ever friend Dr. Armand Vedadi. Armand! To put it in a nutshell, thank you for all those incessant helps and encouragements. Thanks for all the lessons you taught me. I will never forget how eagerly you showed me how to put two pieces of fibre in the splicer and press the 'fuse button' as the first lesson in Lab work, and then how proudly you said: "Yes, this is splicing."

My sincerest thanks go to my brothers and sisters for taking so much care of their youngest brother all the time. I specially thank my sister, Sima, for taking care of my education from the time I was a schoolboy right through to my PhD.

I thank Tarla for entering my life right on time and for bringing love into it. She coloured my life in the period of writing-up when it had become so black-and-white. Her kind help in preparing and arrangement of the References is greatly appreciated.

I thank and commend my late father for the sacrifice he made throughout his life.

No body has been and will ever be able to thank his/her mother adequately. Words prove to be too inefficient and too far from complete to appreciate mothers for their uniqueness. I wrote 17 sentences, none seemed perfect enough so I chose not to say anything. I know that she knows what I wish to say.

List of tables

List of illustrations

Abbreviations

ASE	Amplified spontaneous emission
AWG	Arrayed waveguide grating
BER	Bit-error rate
BERT	Bit-error rate tester
Bi2O3	Bismuth oxide
Bi-HNLF	Bismuth-oxide highly nonlinear fibre
BPF	Band-pass filter
DPSK	Differential phase shift keyed
DSF	Dispersion-shifted fibre
DWDM	Dense wavelength-division multiplexing
EDFA	Erbium-doped fibre amplifier
FOPA	Fibre optical parametric amplifier
FWM	Four-wave mixing
GeO_2	Germania
GVD	Group velocity dispersion
HF	Holey fibres
HNLF	Highly-nonlinear fibre
IM	Intensity modulation
IR	Infra-red
MI	Modulation-instability
MOF	Microstructured optical fibres
NLO	Nonlinear optics
NLSE	Nonlinear Schrodinger equation

OEO	Optical-electrical-optical
OPA	Optical parametric amplifier
OSA	Optical spectrum analyzer
OSNR	Optical signal to noise ratio
PBS	Polarisation beam splitter
PDL	Polarisation-dependent loss
PM	Phase modulator
PMD	Polarisation-mode dispersion
PRBS	Pseudo-random bit sequence
PSG	Phase-sensitive gain
PSP	Principal states of polarisation
RA	Raman amplifier
RIN	Relative intensity noise
RZ	Return-to-zero
SBS	Stimulated Brillouin scattering
SFG	Sum-frequency generation
SMF	Single-mode fibre
SOA	Semiconductor optical amplifier
SOP	State of polarisation
SPM	Self-phase modulation
SRS	Stimulated Raman scattering
SSFM	Split-step Fourier method
THG	Third-harmonic generation
TL	Tunable laser
WDM	Wavelength-division multiplexing
XGM	Cross-gain modulation
XPM	Cross-phase modulation

ZDW	Zero-dispersion wavelength

Introduction

The invention of lasers is considered to be one of the greatest invention of the 20th century. Lasers, which were named 'the solution looking for problems' were soon used for a countless number of applications, and there is a little doubt that their use for communication was the most influential application of them that changed the world and societies. However, this was not until the invention of optical fibres, the right medium for lasers to propagate and convey information. Optical fibres provide a genuinely enormous amount of capacity for data transmission. Their capacity was exploited by wavelength-division multiplexing (WDM) systems in which a large number of laser lights neighbouring at a close distance to each other are accommodated in the fibre each transmitting a large amount of data.

Any communication channel, in addition to other impairments, exhibits some loss and optical fibres are no exception. Their loss, which was originally about 1000 dB/km, was soon reduced to very low values of the order 0.2 dB/km, and it was the actual beginning of practical optical communications. Nonetheless, this amount of loss itself is very limiting as it will attenuate the signal by 20 dB after 100 km of transmission. Then the signal needs to be regenerated if it is to propagate further. Traditionally regeneration was performed by optical-electrical-optical (OEO) converters; that is at every 100 km the optical signal was converted to electrical domain and back to optical domain with proper power to continue its way. The complexity of OEO regenerators, their limited speed and high cost was the motivation for the development of optical amplifiers capable of compensating the fibre loss directly in the optical domain.

To this end, several possibilities were investigated and various kinds of amplifiers each exploiting different amplification mechanism were developed. These include erbium-doped fibre amplifiers (EDFAs), Raman amplifiers (RA), semiconductor optical amplifiers (SOA) and fibre optical parametric amplifiers (FOPA).

Fibre optical parametric amplifiers, which are the subject of this dissertation, have been attracting a lot of attention since their first demonstrations in 1980s. They are capable of providing high amount of gain over large wavelength range, and in that sense fulfil the basic expectations from an amplifier. However, owing to the absolute superiority of their competitors, namely EDFAs, they have not been constructed and used commercially so far. EDFAs are quite easy and inexpensive to build, and their gain is not polarisation dependent. In addition, 32 nm of gain bandwidth of EDFAs has been well enough to meet the demand of the market.

What is called a fibre optical parametric amplifier technically consists of one or two intense optical waves, which are named pump(s) and a fibre with suitable dispersive properties. The pump(s) transfer their energy to the signals while propagating along the fibre and amplify the signals. The energy transfer is through a nonlinear process known as four-wave mixing (FWM). The efficiency of the amplification mechanism depends on the extent to which the nonlinear effects are enhanced inside the amplifier fibre. Therefore, special kinds of fibres have been designed with intentionally enhanced nonlinearity. They are called highly-nonlinear fibres (HNLFs) in general. The other requirement of an OPA, namely the pump, is normally obtained from a laser light which has been amplified by another amplifier. EDFAs are normally used for this purpose.

The evolution of OPAs is then closely dependent on the availability of suitable HNLFs and high-power EDFAs to provide the pump for the OPA. Recently, with the advent of successful technologies for the production of HNLFs and at the same time the availability of very high-power EDFAs, OPAs have enjoyed great improvements. In addition, although the acceptability of OPAs has been affected by the success of EDFAs in the past two decades of the evolution of the optical communications, by the alarming rate of the growth in demand for larger capacities and data rates their use is conjectured to be reconsidered in telecommunication industry.

The main features of OPAs that make them potentially attractive for a variety of applications are as follows.

Increasing gain bandwidth with increased pump power

The gain bandwidth of OPAs can be extended by increasing the pump power. This provides a means to achieve very wide bandwidth of several hundreds of nanometres. The bandwidth of EDFAs and RAs are fundamentally limited to tens of nanometres.

Arbitrary centre wavelength

While this feature also exists in RAs, the centre wavelength of the gain bandwidth of EDFAs is fixed. The centre wavelength of OPAs can be chosen almost arbitrarily provided the right pump and fibre are available. This can be very important especially for those applications for which suitable amplifiers are missing. Recently, the IR communication is finding desirability and OPAs can be a candidate for such systems.

Large gain

It is relatively easy to obtain very large gain values in OPAs. Since the parametric gain is only available in one direction the possibility of unwanted oscillations is minimised in OPAs. Such back-reflections define a maximum value of about 60 dB of gain for EDFAs, while continuous-wave and pulsed gains of 70 dB have been reported in OPAs. Such high gains are useful in free-space optical communication.

Wavelength conversion

In OPAs another wave, which is called the idler, is generated at a new wavelength concurrently with the amplification of the original signal. The idler inherits all the properties of the signal and is virtually an exact copy of it. Thus OPAs can be used as wavelength convertors, which is a very desirable functionality in optical networks.

Spectral inversion

In fibre OPAs, the idler spectrum is symmetric to the signal spectrum with respect to the centre frequency. This property is called spectral inversion and can be useful in mitigating some detrimental effects such as dispersion.

Instantaneous response

Since the amplification mechanism in OPAs is based in the third-order nonlinear response of the glass, which is very quick, the response of OPAs is also agile, and for most of the applications can be assumed instantaneous. This enables the fibre OPAs to perform some signal processing tasks at very high speeds.

Low noise figure

While OPAs can exhibit noise figures comparable to that of EDFAs, in the phase-sensitive operation their noise figure is reducible to below 3 dB.

Unidirectional gain and spontaneous emission

Vacuum fluctuations can be amplified in any optical amplifier and thus give rise to amplified spontaneous emission (ASE). Due the fact that the parametric gain is only available in the direction of the pump the ASE of fibre OPAs would only be propagating in one direction (the direction of the pump). Moreover, as the parametric gain is polarisation-dependent the ASE will be naturally polarised. Thus, OPAs can be efficient sources of ASE, which is useful in some applications such as biomedical photonics and sensing.

Despite the desirable features mentioned above briefly, OPAs do not tick all the boxes. In fact, there are a few issues that raise questions on the usefulness of OPAs. Therefore, these problems are required to be fixed completely before OPAs can attain popularity and find their way to commercial production. This thesis is a report on an investigation of a number of different aspects of OPAs. The outline of this dissertation is as follows.

In Chapter **1**, the very basic principles of nonlinear optics and specifically nonlinearities in optical fibres together with different nonlinear effects that appear inside optical fibres are reviewed. Specifically, the FWM process as the underlying process of the OPAs operation is described and basic equations describing the amplification mechanism of OPAs is reviewed.

In Chapter **2**, I have discussed some of the chief problems of OPAs and have tried to highlight the description of the problem and review the recent advances.

In Chapter **3**, I have discussed the gain and bandwidth-related issues of OPAs with emphasis on one-pump arrangement. We have presented the results of the operation of two OPAs with a record gain and a record bandwidth.

In Chapter **4**, I have discussed in details the problem of nonlinear crosstalk in OPAs as one of the most important issues facing OPAs. I have presented the results of two of my experiments showing promising performance of OPAs with regard to the crosstalk problem.

In Chapter **5**, I have briefly reviewed the recent advances in the highly nonlinear fibre technology. I investigated a sample of a non-silica HNLF based on bismuth-oxide for OPA work. Although they were found not perfectly appropriate for OPAs at present, we exploit a novel wavelength-division demultiplexing method using such fibres.

Chapter 1. Nonlinear effects in optical fibres

Any actual physical phenomenon of any discipline of science can be fundamentally regarded as the reaction of a system to an input, providing a response (output). The presence of some sort of nonlinearity in the response of any real system is a very well-established concept. Hence, absolutely linear systems can only exist in idealised mathematical models but nowhere in reality, and optics is not an exception. When light penetrates into a medium there is some nonlinear response. Nonlinearities in optics and more specifically in optical communications are sources of some difficulties, however, like many other phenomena in physics they can be investigated for beneficial aspects as well. The whole subject of this thesis is fibre OPAs, which are based on such optical nonlinearities. In this chapter, we review the origin of nonlinear optical processes and focus on the physical fundamentals that OPAs are based on.

1.1. Nonlinear optics

The advent of laser light in 1960 distinctly separated the realm of optics into two eras with a great contrast. This happened because the brightness of the light that a researcher could have in his laboratory increased by a factor of 10^{12}. Before such a tremendous improvement, the well-known perfectly linear Maxwell's equations could handle almost everything concerning light. Classically light was considered to be an electro-magnetic wave. Such waves could be superposed and propagate, but could not interact to transfer energy, and their frequencies remained the same before and after propagation. After lasers came into reality, everything needed to be revised drastically as they were strong enough to force matter to respond in a nonlinear manner. Although scientists were familiar with some nonlinear interactions for some time, the strong stimulation to open a new area of research dedicated to nonlinear optical processes came only after the lasers were born.

Nonlinear optics (NLO) originates from the fact that the response of materials to the presence of electric fields is nonlinear, which leads to a vast range of interesting physical phenomena such as sum-frequency generation (SFG), third-harmonic generation (THG), four-wave mixing and so on. The main manifestation of all these nonlinear processes is that waves interact with each other (and possibly with matter) and possibly generate waves at new frequencies.

In general, there are two different aspects to be considered when studying NLO: one is to determine the response of the matter to the applied electrical field, which indeed is the matter of modelling and quantifying the response; the other one is to investigate the effect of this response on the electro-magnetic wave itself when propagating in matter [**1**].

The response of matter to an applied electrical field, as far as the electric dipole approximation holds, can be studied by the polarisation density vector $\vec{P}$, which appears in Maxwell's equations. Nonlinearities are included in the response by introducing nonlinear terms via nonlinear higher-order susceptibilities. If we express $\vec{P}$ as the sum of linear and nonlinear parts as:

$$\vec{P}(\boldsymbol{r},t) = \vec{P}_L(\boldsymbol{r},t) + \vec{P}_{NL}(\boldsymbol{r},t) \tag{1.1}$$

then each part can be written as [**2**]:

$$\vec{P}_L(\boldsymbol{r},t) = \varepsilon_0 \int_{-\infty}^{t} \chi^{(1)}(t-\tau).\vec{E}(\boldsymbol{r},\tau)d\tau \tag{1.2}$$

$$\begin{aligned}\vec{P}_{NL}(\boldsymbol{r},t) = \varepsilon_0 \int_{-\infty}^{t} dt_1 \int_{-\infty}^{t} dt_2 \times \chi^{(2)}(t-t_1,t-t_2):\vec{E}(\boldsymbol{r},t_1)\vec{E}(\boldsymbol{r},t_2) + \\ \varepsilon_0 \int_{-\infty}^{t} dt_1 \int_{-\infty}^{t} dt_2 \int_{-\infty}^{t} dt_3 \times \chi^{(3)}(t-t_1,t-t_2,t-t_3) \vdots \\ \vec{E}(\boldsymbol{r},t_1)\vec{E}(\boldsymbol{r},t_2)\vec{E}(\boldsymbol{r},t_3) + \cdots\end{aligned} \tag{1.3}$$

$\chi^{(i)}$is the i^{th} order susceptibility, and in general, it is a tensor of order i+1. The symbols $\vec{E}$ and $\vec{P}$ represent the electric field and the polarisation density vector. In the time domain, the nonlinear response can be viewed as an extension of the convolution theory

of linear systems. In the frequency domain, nonlinear susceptibilities can be written in terms of the frequencies of the interacting waves and those of the resulting waves. For instance, the third-order susceptibility responsible for THG is written as $\tilde{\chi}^{(3)}(\omega_4;\ \omega_1, \omega_1, \omega_1)$ where $\omega_4 = \omega_1 + \omega_1 + \omega_1$.

Although Eqs. (**1.2**) and (**1.3**) is in tensor form in general, a simplified view is obtained by assuming the electrical field to be polarised along one direction and by neglecting time delays in the response. Equation (**1.1**) is then reduced to the scalar form of:

$$P = \varepsilon_0 \chi^{(1)} E + \varepsilon_0 \chi^{(2)} EE + \varepsilon_0 \chi^{(3)} EEE + \cdots \qquad 1.4$$

The origin of the generation of new frequencies can be readily understood from this equation. Due to the nonlinear response of dielectric dipoles to the presence of an intense electric field, which is called the pump in the literature, dielectric dipoles start radiating not only at the pump frequencies but also at some newly generated frequencies i.e. P contains newly generated frequencies in addition to those of the pump (E). This is due to the higher powers of E appearing in the equation. The radiation at these new frequencies acts as new sources in the wave equation derived from Maxwell's equations:

$$\nabla \times \nabla \times \vec{E} = -\frac{1}{c^2}\frac{\partial^2 \vec{E}}{\partial t^2} - \mu_0 \frac{\partial^2 \vec{P}}{\partial t^2}. \qquad 1.5$$

If certain conditions are met, the new waves can propagate and grow.

The nonlinear optical processes are divided into two main categories based on whether the matter contributes in energy transfer to and from the waves or just mediates the energy transfer among them. In the former case, the phenomenon is called an active process. Inelastic process is another term used for this type of interaction where the medium is actively involved in energy transfer by the means of optical phonons (Raman scattering) or acoustic phonons (Brillouin scattering). In the passive case, the process is called elastic process in which the medium is not involved directly in the interaction.

1.2. Nonlinearity in optical fibres

As mentioned in the previous section, the response of a medium to the presence of high-intensity light becomes nonlinear and optical fibres are no exception. In the field of optical communication, thorough investigation of nonlinearities and their adverse and constructive effects has been the topic of an enormous amount of research activities. In the context of signal transmission and WDM systems, the immediate detrimental impact of nonlinearities is the cross-talk generated between the channels, while soliton communication are a good example of the useful aspects of nonlinearity.

In optical fibres, which are made of glass, the second-order susceptibility, $\chi^{(2)}$, is not present and thus the lowest-order nonlinear susceptibility is the third-order $\chi^{(3)}$. It is due to the amorphous (non-crystalline) molecular arrangement of silica (SiO_2). Indeed, the second-order susceptibility and in general even-order susceptibilities vanish for mediums with inversion symmetry such as silica. Tensor calculation also yields that out of 81 elements of $\chi^{(3)}$ only 21 are nonzero, and among them three elements are independent. Normally, the three independent elements are assumed to be $\chi^{(3)}_{xxxx}$, $\chi^{(3)}_{yyyy}$ and $\chi^{(3)}_{zzzz}$ [**1**], [**2**].

The nonlinear phenomena in optical fibres originating from the third-order susceptibility fall into two main classes with regard to what we mentioned in the preceding section. One type, which is purely electronic in origin and falls in the category of passive or elastic optical processes, is due to the fact that the refractive index of the material is modified slightly by applying an electric field. In other words, refractive index is dependent on the intensity of the electric field in the fibre. In the literature, this phenomenon is known as the optical Kerr effect and in its simplest form can be stated by introducing the nonlinear refractive-index coefficient, n_2, as [**3**]:

$$n = n_0 + n_2|E|^2 \qquad 1.6$$

where n_0 is the weak-field refractive index and $|E|^2$ is the intensity.

The nonlinear refractive index n_2, is an intrinsic property of any material and is related to the third-order susceptibility as:

$$n_2 = \frac{3}{8n_0} Re\left(\chi^{(3)}_{xxxx}\right) \quad 1.7$$

As mentioned above, the optical Kerr effect is of electronic origin; indeed it is due to the nonlinear response of bound electrons of molecules. Since electrons are very light, they can move very quickly in response to an applied electrical field. As a result, their response is very fast and assumed to be almost instantaneous. Hence, time delays in their response can be neglected and the susceptibility can be written as:

$$\chi^3(t,t,t) = \chi^3\delta(t)\delta(t)\delta(t) \quad 1.8$$

In the frequency domain, this statement would mean that we assume $\tilde{\chi}^3$ to be independent of frequency.

The dependence of the refractive index on the applied electric field (optical Kerr effect) means that the refractive index seen by a propagating wave can be modified by another wave or even by itself. The latter case leads to a nonlinear effect, which is known as self-phase modulation (SPM); that is, the phase of the wave is altered by an amount that is proportional to the intensity of the field. In the former case, the phase of a wave is modified by another wave through an effect called cross-phase modulation (XPM).

One other important process in which three (or four) waves are involved is known as four-wave mixing. In FWM three waves at frequencies $\omega_1, \omega_2, \omega_3$ mix together to generate another wave at the frequency $\omega_4 = \pm\omega_1 \pm \omega_2 \pm \omega_3$. FWM is the underlying process of OPAs, different aspects of which are the subjects of this report.

In order for strong nonlinear interaction to take place in a fibre, the extent to which the fibre exhibits nonlinearity is of a great importance. Since working with susceptibilities is often complicated, for the majority of design and/or research purposes in optical fibres, it is more convenient to work with another quantity called the fibre nonlinearity coefficient γ. It is a measure of the extent of nonlinearity in the fibre and is defined as

$$\gamma(\omega) = \frac{n_2(\omega)\omega}{cA_{\text{eff}}}. \quad 1.9$$

The parameter A_{eff} in the above expression is known as the effective mode area of the fundamental fibre mode and is defined as

$$A_{\text{eff}} = \frac{\left(\iint_{-\infty}^{\infty} |F(x,y)|^2 dxdy\right)^2}{\iint_{-\infty}^{\infty} |F(x,y)|^4 dxdy} \qquad 1.10$$

As it is seen from Eq. (**1.9**), γ in general is frequency dependent, and it can depend on spatial coordinates as well. However, for most of the time a single value reported at the zero-dispersion wavelength (ZDW) of a fibre is sufficient. It is seen from the definition of γ that it is related to the intrinsic nonlinearity of the material of a fibre through n_2. It is also dependent on the effective area of the fibre A_{eff}, which is not unexpected as the smaller the effective area is the tighter the light is confined, which in turn implies increased irradiance. Hence, in order to increase the value of γ, one should find materials with high n_2 for the fibre core and/or design waveguides with reduced A_{eff}. We will present some ideas in Chapter **5**, which have been developed to address this issue.

The nonlinearity coefficient γ incorporates the effect of nonlinearity into the wave propagation equation, which in the linear case includes only the effects of the fibre attenuation and the chromatic dispersion. The combined effect of these three factors is beautifully reflected in the modified nonlinear Schrodinger equation (NLSE), which is written as:

$$\frac{\partial A}{\partial z} + \beta^{(1)}\frac{\partial A}{\partial t} + i\beta^{(2)}\frac{\partial^2 A}{\partial t^2} + \frac{\alpha}{2}A = i\gamma|A|^2 A \qquad 1.11$$

This equation describes the evolution of the slowly-varying complex amplitude of the propagating wave, $A(z,t)$, as the main quantity of interest. $\beta^{(1)} = {v_g}^{-1} = d\beta/d\omega$ relates to the group velocity and $\beta^{(2)} = d^2\beta/d\omega^2$ is the group velocity dispersion (GVD) parameter. The fibre attenuation is accounted for by α.

In addition to the nonlinear processes, which were named in the preceding, there are two other phenomena, which originate from the third-order susceptibility, namely stimulated Raman scattering (SRS) and stimulated Brillouin scattering (SBS). In contrast to the Kerr effect, these phenomena have molecular causes. They are inelastic interactions and

the matter is involved directly in the energy exchange. In the following, each of these processes is described in brief.

1.3. Elastic nonlinear processes

1.3.1. Self-phase modulation

The dependence of the refractive index on the intensity of an applied electric field manifests itself by introducing a phase shift to the field. This phenomenon, which is called self-phase modulation, was first observed in optical fibres as early as 1974 [**4**] and has been studied extensively since then [**4**]-[**6**]. The main features of SPM can be examined by analysing the NLS equation in the absence of dispersion. In the limit when GVD is assumed zero the NLSE of Eq. (**1.11**) can be written as

$$\frac{\partial A}{\partial z} + \frac{\alpha}{2}A = i\gamma|A|^2A \qquad 1.12$$

It is useful to define the normalised amplitude $U(z,t)$ such that $A(z,t) = \sqrt{P_0}\exp\left(\frac{-\alpha}{2}z\right)U(z,t)$, where P_0 is the initial optical power of the field [**2**]. We can then rewrite Eq. (**1.12**) in terms of $U(z,t)$:

$$\frac{\partial U}{\partial z} = i\frac{e^{-\alpha z}}{L_{NL}}|U|^2U \qquad 1.13$$

where L_{NL} is defined as $(\gamma P_0)^{-1}$, and it is called the nonlinear length. Using $U = |U|\exp(i\varphi_{NL})$ in Eq. (**1.13**) we obtain

$$\frac{\partial|U|}{\partial z} + i\frac{\partial\varphi_{NL}}{\partial z}|U| = i\frac{e^{-\alpha z}}{L_{NL}}|U|^3 \qquad 1.14$$

Equating the real and imaginary parts of Eq. (**1.14**) leads to

$$\frac{\partial|U|}{\partial z} = 0 \qquad 1.15$$

$$\frac{\partial \varphi_{NL}}{\partial z} = \frac{e^{-\alpha z}}{L_{NL}} |U|^2 \tag{1.16}$$

It is seen from Eq. (**1.15**) that the temporal intensity of the optical field does not change with distance i.e. $|U(z,t)| = |U(0,t)|$. The nonlinear phase shift introduced at the distance $z = L$ is obtained from Eq. (**1.16**) as

$$\int_0^L \partial \varphi_{NL}(z,t) = \int_0^L \frac{e^{-\alpha z}}{L_{NL}} |U(z,t)|^2 \, \partial z \tag{1.17}$$

Since $|U(z,t)| = |U(0,t)|$, $\varphi_{NL}(L)$ is found to be:

$$\varphi_{NL}(L) = \frac{L_{\text{eff}}}{L_{NL}} |U(0,t)|^2 \tag{1.18}$$

The quantity L_{eff} that appears in many instances in nonlinear optics accounts for the fact that the decrease in the intensity of the field due to attenuation weakens the effect of nonlinearity. This means that the effective length of nonlinear interactions is less than the fibre length due to loss. For a fibre length L, the effective length is defined as

$$L_{\text{eff}} = \frac{[1 - \exp(-\alpha L)]}{\alpha} \tag{1.19}$$

The reason for naming this process as self-phase modulation is clear from Eq. (**1.18**); propagating along the fibre, the optical field acquires a phase shift that is proportional to its intensity and related to the distance. The maximum phase shift is obtained when the intensity is maximum i.e. $|U(z,t)|^2 = 1$ and it is

$$\varphi_{\text{max}} = \frac{L_{\text{eff}}}{L_{NL}} = \gamma P_0 L_{\text{eff}} \tag{1.20}$$

If we consider optical pulses, the time dependence of the phase shift leads to spectral changes. Temporally varying phase implies that the instantaneous optical frequency deviates across the pulse from its central value. The deviation $\delta\omega$ is given by [**2**]:

$$\delta\omega = -\frac{\partial \varphi_{NL}}{\partial t} = -\frac{L_{\text{eff}}}{L_{NL}}\frac{\partial}{\partial t}|U(0,t)|^2 \qquad 1.21$$

The time dependence of the instantaneous optical frequency of the field indicated by Eq. (**1.21**) is referred to as frequency chirping [**2**]. It is seen that the deviation of the optical frequency depends on the shape of the pulse. Consequently, the effect of SPM on the spectrum of the pulse depends on its shape and initial chirp. Figure **1.1.** shows the variation of (a) the nonlinear phase shift and (b) the induced frequency chirp across the pulse at $L_{\text{eff}} = L_{\text{NL}}$ for a Gaussian pulse and a super-Gaussian pulse with the temporal profile defined as [**2**]

$$U(0,t) = \exp\left[-\frac{1+iC}{2}\left(\frac{t}{T_0}\right)^{2m}\right] \qquad 1.22$$

where T_0 is the pulse width and $m = 1$ for Gaussian pulses and $m > 1$ for super-Gaussian pulses. The quantity C is called the chirp-factor and determines the initial chirp.

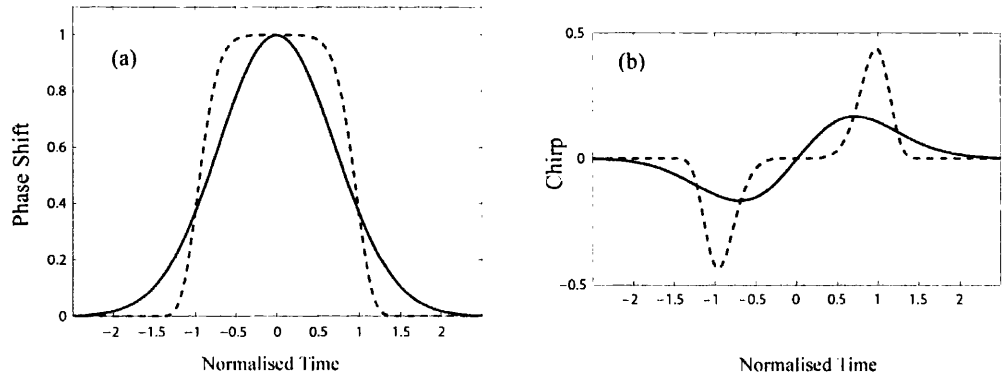

Figure 1.1. Nonlinear phase shift (a) and SPM-induced chirp (b) at $L_{\text{eff}} = L_{\text{NL}}$; solid curve (Gaussian pulse) and dashed curve (super-Gaussian pulse $m = 3$). The pulses are initially unchirped.

In Figure **1.2.**, the evolution of pulse spectra over a length of $10L_{\text{NL}}$ is depicted for a Gaussian and a super-Gaussian pulse. Both pulses are initially unchirped. It is seen that both spectra experience a broadening, which is always the case when the optical pulse in unchirped. For super-Gaussian pulse the amount of broadening is much less and the

energy is concentrated mainly near the central frequency. This can be understood by considering that the SPM-induced chirp for this pulse occurs at the rising and falling edges of the pulse and the central region of the pulse does not experience considerable chirp. As a result most of energy is carried over the flat region of the pulse, which is associated with lower frequencies.

For a Gaussian pulse, the spectral broadening is substantial as there is a continuous chirping across almost the whole length of the pulse. If the duration of the pulses is reduced to extremely small values of the order 1 ps, the initially broad spectra can be further broadened over very wide spectral region especially when SPM is accompanied by other nonlinear processes such as four-wave mixing; a phenomenon known as supercontinuum generation.

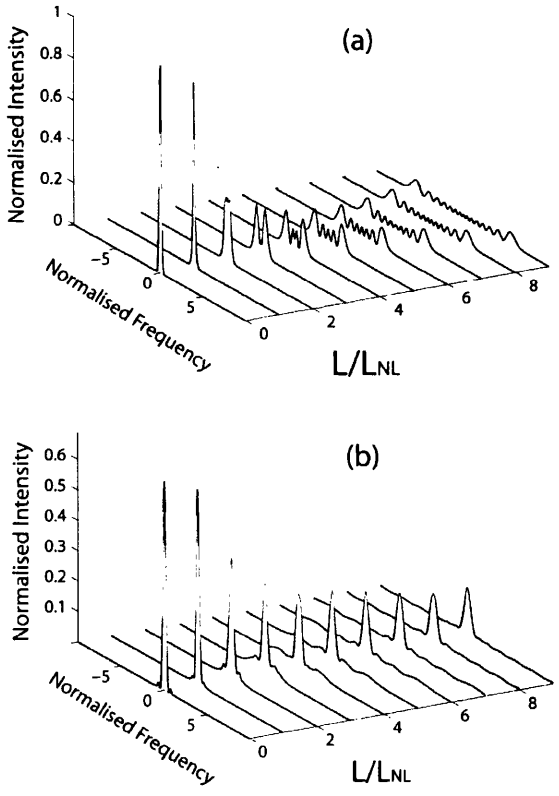

Figure 1.2. Evolution of the spectrum of a Gaussian (a) and a super-Gaussian (m=3) (b) pulse over the length 0 to $10L_{NL}$.

As mentioned earlier, the effect of SPM depends on the initial chirping that the pulse may have in addition to the shape of the pulse [**6**]. Figure **1.3.** shows the evolution of a Gaussian pulse, which is (a) positively and (b) negatively chirped. In the case of negative chirp, it is seen that at $L=5L_{NL}$, the spectrum of the pulse is compressed rather than broadening. It is due to the fact that the SPM-induced chirp cancels the initial chirping for that length. Again after that length, the spectrum is broadened.

A noteworthy point in fibre optical amplifiers such as OPAs is that the pulse experiences a gain in the amplifier. This in turn means that the fibre loss is replaced by the gain of the amplifier, which implies that the effective length will be more than the actual fibre length. Hence, the effects of SPM can be more pronounced. Moreover, in most OPAs the fibre used is highly-nonlinear with γ values about 20 $W^{-1}km^{-1}$. Therefore L_{NL} is reduced.

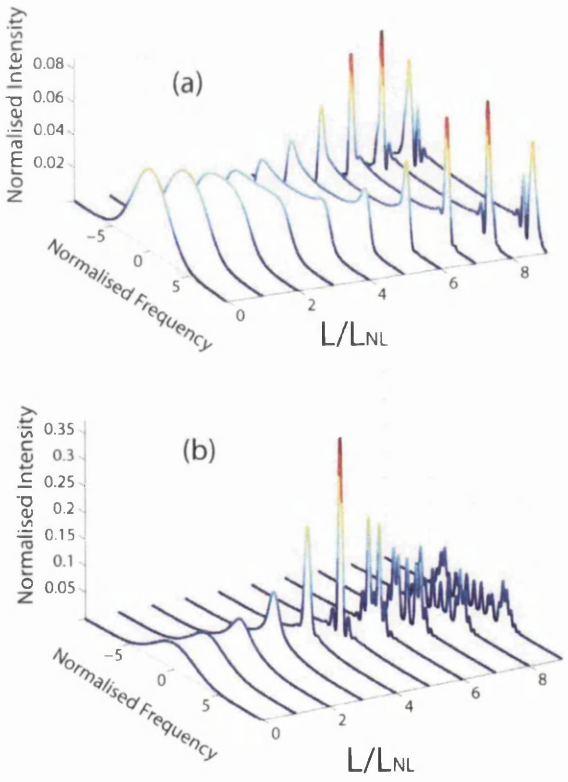

Figure 1.3. Evolution of the spectrum of (a) positively and (b) negatively chirped Gaussian pulse over the length 0 to $10L_{NL}$. The chirp-factor is 10 for both cases.

1.3.2. Cross-phase modulation

An intense electric field modulates the refractive index not only for itself but also for all other waves co-propagating with it. Hence, a mutual interaction is produced for two optical waves either at different frequencies or even at the same frequencies but with different polarisation states. This phenomenon is called cross-phase modulation. Cross-phase modulation is always accompanied by SPM. The effects of XPM are similar to SPM in the sense that the optical waves acquire a phase-shift proportional to the intensities of other waves [7]. Considering two waves at frequencies ω_1 and ω_2, the XPM between them can be analysed by writing the total electric field as

$$\vec{E} = \frac{1}{2}\hat{x}[E_1 \exp(-i\omega_1 t) + E_2 \exp(-i\omega_2 t)] + c.c. \quad 1.23$$

Here we consider two collinearly polarised waves. Assuming CW operation the complex amplitudes E_j can be written as

$$E_j = F(x,y)A_j(z)\exp(i\beta_j z) \quad 1.24$$

where $F(x,y)$ is the transverse distribution of the waves, which we have assumed to be the same for the two fields. Substituting Eqs. (**1.23**) and (**1.24**) in NLSE, one obtains two coupled equations for the evolution of the amplitudes of the fields as

$$\frac{\partial A_1}{\partial z} = i\gamma(|A_1|^2 + 2|A_2|^2)A_1 \quad 1.25$$

$$\frac{\partial A_2}{\partial z} = i\gamma(|A_2|^2 + 2|A_1|^2)A_2 \quad 1.26$$

We have assumed that the nonlinear coefficient γ is identical for the two fields. From Eqs. (**1.25**) and (**1.26**) it is seen that each optical field acquires a phase shift proportional to the intensity of its own and to that of the other wave. Moreover, for identical intensities the effect of XPM is twice stronger than that of SPM.

If we consider two optical pulses instead of two CW waves, XPM would lead to similar effects as SPM in changing the temporal shape and spectrum of the pulses. Moreover, since the mutual effect of the waves is not symmetric the changes in shape and spectrum of the pulses will be asymmetric.

1.3.3. Four-wave mixing

Among the nonlinear processes that take place in optical fibres, FWM is a prolific one in terms of the number of different techniques, applications and devices proposed and implemented based on it [**7**]-[**12**]. FWM is the underlying process of parametric gain, which is the gain process used in OPAs. This section briefly reviews the origin of parametric gain.

In FWM, as the name implies, four different waves at frequencies ω_i (i=1–4) are coupled via the third-order nonlinearity $\chi^{(3)}$. The processes such as FWM in which several waves interact and the medium is passively mediating the interaction are known as parametric processes as well [**2**].

Quite a large number of interactions can take place by injecting four waves into an optical fibre. From a microscopic point of view, these interactions can be seen as radiations by electric dipoles at new frequencies. However, these radiations do not lead to noticeable macroscopic outcome unless certain conditions are met. Indeed, the radiations must be at right frequencies in order to be constructive and build up to propagating waves with a net power. This can be seen by considering the nonlinear terms of the polarisation density vector $\vec{P}$ when injecting four waves at different frequencies. If, for simplicity, we assume all four waves to be linearly polarised in one direction, the total electric field can be written as:

$$\vec{E} = \frac{1}{2}\hat{e}\sum_{i=1}^{4} E_i e^{j(\omega_i t - \beta_i z)} + c.c. \qquad 1.27$$

Considering the nonlinear part of dielectric polarisation originating from $\chi^{(3)}$ and using Eq. (**1.3**), it can be written as:

$$\vec{P}_{NL} = \frac{1}{2}\hat{e}\sum_{i=1}^{4} P_i e^{j(\omega_i t - \beta_i z)} + c.c. \qquad 1.28$$

Expanding each component of $\vec{P}_{NL}$, we find that it consists of a large number of terms involving the products of three electric fields. For instance, P_4 can be expressed as [**2**]

$$P_4 = {}^{3\varepsilon_0}/_4 \chi^{(3)}_{xxxx}[|E_4|^2E_4 + 2(|E_1|^2 + |E_2|^2 + |E_3|^2)E_4 + 2E_1E_2E_3\exp(j\theta_1) + 2E_1E_2E_3{}^*\exp(j\theta_2) + \cdots] \qquad 1.29$$

where θ_1 and θ_2 are defined as

$$\theta_1 = (\beta_1 + \beta_2 + \beta_3 - \beta_4)z - (\omega_1 + \omega_2 + \omega_3 - \omega_4)t,$$

$$\theta_2 = (\beta_1 + \beta_2 - \beta_3 - \beta_4)z - (\omega_1 + \omega_2 - \omega_3 - \omega_4)t.$$

Each term in the expansion of P_4 is responsible for a certain phenomenon. For example, the first four terms describe the SPM and XPM effects and the remaining terms result from the frequency mixing of all four waves. The effectiveness of such interactions depends on the phase mismatch between E_4 and the associated term, which is governed by θ_1, θ_2 or a similar quantity. In fact, significant interaction occurs if the phase mismatch vanishes.

The four-wave mixing process, which is responsible for optical amplification in OPAs, is the interaction between one or two intense waves (pumps) and a weak wave (signal), which is the wave to be amplified. Based on whether we use one or two pumps the resulting OPA is called one-pump or two-pump OPA. In fact, a one-pump OPA can be considered as a two-pump OPA in which the spacing between the two pumps is zero. Therefore, in order not to lose generality, we describe a two-pump OPA here.

Injecting two pumps at frequencies ω_1 and ω_2 together with the signal at the frequency ω_3, another wave is generated at frequency $\omega_4 = \omega_1 + \omega_2 - \omega_3$ in the process. This new wave is called the idler. The generation of an idler is one of the features of OPAs we will describe in more details later on in this section. It is seen that the idler is generated

automatically at such a frequency that leads to the time-varying part of the phase mismatch to be zero.

The coupling among the four interacting waves in an OPA yields four coupled equations describing the evolution of their amplitudes. Different authors with different notations and definitions for variables have derived these equations. Here we use the notation used in [**3**] to write the equations as:

$$\frac{dA_l}{dz} = i\gamma\left[|A_l|^2 A_l + 2\sum_{j\neq l=1}^{4}|A_j|^2 A_l + 2A_m A_n A_k{}^* e^{i\varepsilon\Delta\beta z}\right], \qquad l = 1-4 \tag{1.30}$$

Here $\Delta\beta = \beta_1 + \beta_2 - \beta_3 - \beta_4$ and the integers k, l, m, n and ε are such that:

for $l = 1$ or 2, $\varepsilon = 1$ and $k = 3-l$, $m = 3$, $n = 4$;

for $l = 3$ or 4, $\varepsilon = -1$ and $k = 7-l$, $m = 1$, $n = 2$.

In the right hand side of the Eq. (**1.30**) again the effects of SPM, XPM and FWM are clearly distinguishable.

The origin of parametric gain can be realized in the solution of the OPA equations mentioned above. In conventional OPAs, the pump(s) are much stronger than the signal, and thus their amplitude can be assumed unchanged along the fibre. This regime is known as no pump depletion and greatly simplifies the solution. Moreover, the effect of FWM on the pump(s) can also be neglected so that pump(s) are modified only because of SPM and XPM. Considering these simplifications, the pump equation can be written as:

$$\frac{dA_k}{dz} = i\gamma(P_k + 2P_l)A_k = ip_k A_k \qquad k = 1,2, \quad l = 3-k, \tag{1.31}$$

where $p_k = \gamma(P_k + 2P_l)$. $P_i = |A_i|^2$ is the optical power.

The solution of Eq. (**1.31**) can be readily written as:

$$A_k(z) = A_k(0)e^{ip_k z}, \qquad k = 1,2. \tag{1.32}$$

It is clearly seen from Eq. (**1.32**) that the effect of SPM and XPM express as a phase-shift in the pump waves.

For signal and idler, the SPM and the XPM between the signal and the idler can be neglected. We can readily validate neglecting those terms by considering their small magnitude in comparison with other terms. The signal and idler equations then take the form:

$$\frac{dA_k}{dz} = i\gamma(2P_1 + 2P_2)A_k + 2i\gamma A_1 A_2 A_l{}^* e^{-i\Delta\beta z} \tag{1.33}$$

$$= 2i\gamma(P_1 + P_2)A_k + ir_k A_l{}^* e^{i(p_1+p_2-\Delta\beta)z} = ip_k A_k + ir_k e^{iq_k z} A_l{}^*$$

where

$$p_k = 2\gamma(P_1 + P_2) = 2\gamma P_0, \qquad q_k = p_1 + p_2 - \Delta\beta,$$

$$r_k = 2\gamma A_1(0)A_2(0), \qquad k = 3,4, \qquad l = 7 - k.$$

As seen from the Eq. (**1.33**), r_k is the quantity governing the magnitude of the FWM coupling coefficient among the four waves. Since $r_3 = r_4$, we simply denote both by r.

It can be shown (Ref [**3**]) that by defining $\kappa = p_3 + p_4 - p_1 - p_2 + \Delta\beta$ and making the change of variable

$$C_k = A_k \exp\left[i\left(\frac{\kappa}{2} - p_k\right)z\right], \qquad k = 3,4, \tag{1.34}$$

an equation can be obtained for C_k as:

$$\frac{d^2C_k}{dz^2} - g^2 C_k = 0, \qquad k = 3,4, \tag{1.35}$$

where g is the parametric gain coefficient and is given by

$$g^2 = r^2 - \left(\frac{\kappa}{2}\right)^2. \tag{1.36}$$

The quantity κ can be interpreted as the total propagation constant or wavevector mismatch. Writing $\kappa = \Delta\beta + \Delta\beta_{NL}$ and introducing $\Delta\beta_{NL} = p_3 + p_4 - p_1 - p_2 = \gamma P_0$, we can arrive at an important interpretation, which describes the philosophy of OPAs: a nonlinearity-induced phase mismatch, $\Delta\beta_{NL} = \gamma P_0$, counterbalances the phase mismatch term of dispersion so that the waves interact efficiently. Hence, the larger $\Delta\beta_{NL}$ is, which can be obtained by increasing either γ or P_0, the wider the bandwidth over which the phase mismatch can be counterbalanced. This implies larger gain bandwidth, and it is a unique feature of OPAs that bandwidth can be increased by increasing the pump power.

The solution of Eq. (**1.35**) gives the output fields as linear combinations of e^{gz} and e^{-gz}. Making use of the initial conditions, we find that

$$C_k(z) = A_k(0)\cosh(gz) + \frac{i}{g}\left[\frac{\kappa}{2}A_k(0) + rA_l^*(0)\right]\sinh(gz), \tag{1.37}$$

$$k = 3,4, \quad l = 7 - k.$$

In the above equation it is seen that $C_3(z)$ and subsequently $A_3(z)$ depend on the initial amplitude and phase of the idler. This introduces another very attractive property of OPAs, which is the possibility of phase-sensitive amplification.

In conventional OPAs, there is no idler at the input i.e. $A_4(0) = 0$. For this case the signal-to-idler power conversion efficiency can be defined and calculated as:

$$G_i(z) = \left|\frac{A_4(z)}{A_3^*(0)}\right|^2 = \left|\frac{r}{g}\sinh(gz)\right|^2 \tag{1.38}$$

The signal power gain can be expressed as

$$G_s(z) = G_i(z) + 1. \qquad 1.39$$

The introduced OPA equations have also been solved for different cases including the effect of fibre attenuation, pump depletion, Raman gain and any other effects, which OPAs are subject to.

The parametric amplification process in OPAs can also be interpreted from a quantum mechanical point of view as well, which leads to interesting results. The energy transfer process can be viewed as annihilation of photons of pumps in pairs and creation of photons at signal and idler frequencies. The relation between the frequencies $\omega_1 + \omega_2 = \omega_3 + \omega_4$ assures energy conservation. In addition, the wavevector matching guarantees the (approximate) conservation of momentum. Figure 1.4. depicts the concept.

The annihilation of one photon from each pump (two photons from the single pump in the one-pump case) and creation of photons at signal and idler must happen simultaneously. This means that signal and idler are exact copies of each other down to the quantum level. Even the temporal distributions of the photons are the same. From a communication standpoint, the idler inherits the modulation format and other properties of the signal. This can be used in designing optical networks where it is frequently needed that we route one channel at a new wavelength.

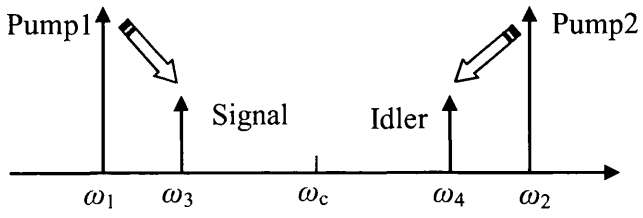

Figure 1.4. Frequency assignment for a two-pump OPA. Two photons from the pumps are annihilated and two photons are created simultaneously at signal and idler frequency.

1.4. Inelastic nonlinear process

1.4.1. Stimulated Raman scattering

First observed by C.V. Raman in 1928, the Raman process is a nonlinear process in which an optical wave at frequency ω_p transfers part of its energy to another wave at a lower energy ω_s [**13**]. The former wave is named pump as a convention in nonlinear optical processes and the latter is called the Stokes wave. From a quantum mechanical point of view, the process can be seen as the scattering of a photon of energy $\hbar\omega_p$ by a molecule to another photon of energy $\hbar\omega_s$, where $\hbar\omega_s < \hbar\omega_p$. The remainder of the energy is absorbed by the molecule to vibrate. Such molecular vibrations in the wave-particle duality are quantized to particles known as optical phonons, which are described by their energy and momentum. The reverse interaction is also possible in which a photon absorbs the energy of a phonon to make a transition to a higher-energy photon. However, this process is not efficient as it is much improbable for a photon to find a phonon of the right energy and momentum. As long as the quantum mechanical description is considered, it is worth noting that for amorphous structures such as silica, the possible vibration states expand over a wide range [**14**], which means that the scattering is possible over a very broad (40 THz) continuum [**15**]. The efficiency of the Raman process is strongly frequency-dependent. The Raman-gain coefficient $g_R(\Omega)$, where $\Omega = \omega_p - \omega_s$ represents the frequency detuning between the pump and the Stokes wave, is the most important quantity describing the Raman process and its frequency dependence [**2**]. It has been measured for fused silica for the two cases of parallel and orthogonal pump and Stokes wave (Figure **1.5.**). The spectrum is normalised such that $g_R(\Omega) \approx 1\times10^{-13}$ at a pump wavelength $\lambda_p = 1$ μm. It is seen that the gain coefficient almost vanishes for the orthogonal case. For the parallel case, there is a broad peak at around 13.2 THz and another peak at around 15.4 THz. The concentration of the gain is around 13.2 THz [**2**], [**16**]-[**17**]. From the quantum mechanical description, it can also be concluded that in contrast to parametric gain, the Raman gain can be provided to a backward propagating Stokes wave as well.

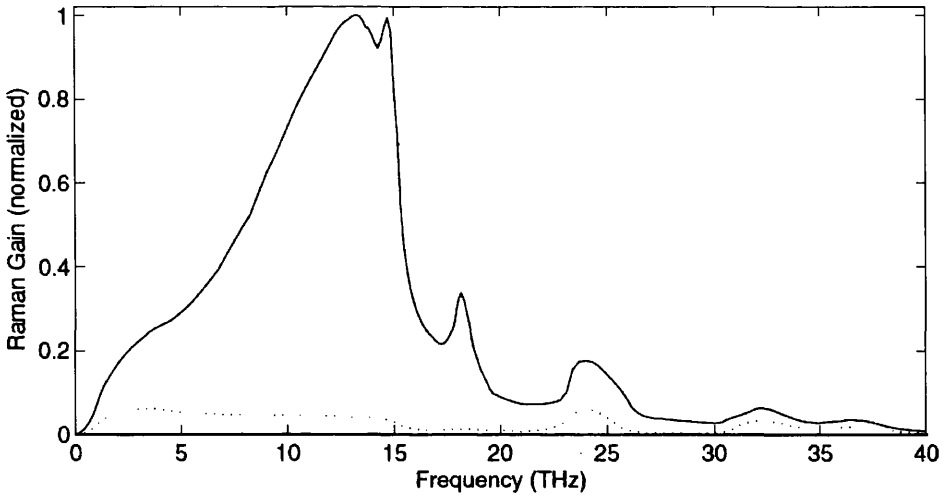

Figure 1.5. Normalised Raman gain for fused silica and parallel (solid) and orthogonal (dashed) pump-signal SOPs (After Ref [2]).

The energy transfer from a pump to a Stokes wave through the Raman process implies the possibility of optical amplification. Indeed, if an intense pump is injected into a fibre together with a weak probe, the probe can be amplified provided that it falls within the gain spectrum of the Raman process. The efficiency of the energy transfer depends on the power of the pump wave. Moreover, if the pump power is large the probe is amplified exponentially. This can be seen by considering a simplified case of propagation of a CW pump with intensity I_p along with a weak probe of intensity I_s. Such a situation then can be described by two coupled equations [**18**]:

$$\frac{dI_s}{dz} = g_R I_p I_s - \alpha I_s, \tag{1.40}$$

$$\frac{dI_p}{dz} = -\frac{\omega_p}{\omega_s} g_R I_p I_s - \alpha I_p \tag{1.41}$$

where α accounts for the fibre attenuation and is assumed to be frequency independent. It can be verified that in the absence of fibre losses,

$$\frac{d}{dz}\left(\frac{I_s}{\omega_s} + \frac{I_p}{\omega_p}\right) = 0 \tag{1.42}$$

This states that the total number of photons in the Raman process remains unchanged; that is, similar to FWM, the annihilation of the pump photons and creation of the Stokes photons occurs concurrently.

The above-mentioned coupled equations can be readily solved if we assume that the pump is not depleted; that is the pump wave is much stronger than the Stokes wave. Then the pump is only affected by the fibre attenuation and its evolution can be written as:

$$I_p = I_0 \exp(-\alpha z) \tag{1.43}$$

where I_0 is the initial pump intensity.

Substituting Eq. (**1.43**) in Eq. (**1.40**) and solving that equation yields the Stokes wave evolution as:

$$I_s(L) = I_s(0) \exp(g_R I_0 L_{\text{eff}} - \alpha L) \tag{1.44}$$

where L is the fibre length.

The above calculations show how a probe launched with an intense pump can be amplified through the Raman process. Since the signal in the absence of the pump is $I_s(L) = I_s(0) \exp(-\alpha L)$, the gain is defined as $G = \exp(g_R P_0 L_{\text{eff}}/A_{\text{eff}})$ [**2**]. In fact, such a mechanism has been used to construct optical amplifiers, which are known as Raman amplifiers [**19**]-[**21**]. They offer quite interesting features such as a broad amplification bandwidth and arbitrary centre wavelength for amplification. However, the amplification requires the availability of a pump at a proper frequency which is about 13.2 THz away from the signal to be amplified. Another feature is the possibility of distributed amplification; that is the transmission fibre itself can be used for amplification.

1.4.1.1. Coupled Amplitude Equations

The simplified formulation described in the preceding is not sufficient for describing the evolution of the pump and the Stokes fields since the effects of the pump depletion, SPM, XPM and GVD are ignored. A unified description thus is often necessary to incorporate these effects all together. We did not mention the effect of FWM since it is

often assumed to be inefficient for most of the cases of interest for the Raman process. However, such a description will be introduced in Chapter **2** in order to describe the mutual interaction between parametric and Raman gain. In order to do so, we need to review the full description of the Raman process first. To this end, we will closely follow the formulation of [**2**], however, we will deviate from that approach in favour of preparing the ground for the discussion of Chapter **2**. Specifically, we will assume CW operation and hence leave out the time-dependence of the amplitudes.

In order to include the Raman effect in the nonlinear wave propagation equation, the first step is to separate the third-order susceptibility into two parts. This can be done by revising Eq (**1.8**) to [**22**]

$$\chi^{(3)}(t,t,t) = \chi^{(3)}R(t)\delta(t)\delta(t) \tag{1.45}$$

where $R(t)$ is the nonlinear response function normalised such that $\int_{-\infty}^{+\infty} R(t)dt = 1$. The nonlinear response function should include both the electronic and nuclear contributions as

$$R(t) = (1-f)\delta(t) + fh_R(t) \tag{1.46}$$

The first term on the right-hand side of the above equation accounts for the electronic part, which is assumed to be instantaneous for the reason discussed in section**1.2**. The function $h_R(t)$ is the Raman response function whose duration is of the order 0.1 ps. The quantity f is the relative strength of molecular contribution and it is found to be 0.18 for typical silica-based fibres [**22**], [**23**].

With these assumptions the NLSE, after some algebra, can be rewritten as

$$\frac{\partial A}{\partial z} + \beta^{(1)}\frac{\partial A}{\partial t} + \frac{i\beta^{(2)}}{2}\frac{\partial^2 A}{\partial t^2} + \frac{\alpha}{2}A \tag{1.47}$$

$$= i\gamma A(z,t)\int_0^{\infty} R(t')|A(z,t-t')|^2 dt'$$

Assuming the pump and the Stokes waves to be aligned to the x-axis the electrical field can be written as

$$E(r,t) = \frac{1}{2}\hat{x}\{A_p \exp\left[i(\beta_p z - \omega_p t)\right] + A_s \exp\left[i(\beta_s z - \omega_s t)\right] + c.c. \quad 1.48$$

where A_p and A_s are the complex amplitudes of the pump and the Stokes field, respectively. β_i and ω_i for $i = p$ or s are the propagation constant and the angular frequency of the pump and the Stokes wave. Substituting Eq. (**1.48**) into Eq. (**1.47**) and assuming CW operation and neglecting the fibre attenuation, one can obtain two coupled equations describing the evolution of the complex amplitudes as:

$$\frac{\partial A_p}{\partial z} = i\gamma(1-f)\left(|A_p|^2 + 2|A_s|^2\right)A_p + D_p(z,t) \quad 1.49$$

$$\frac{\partial A_s}{\partial z} = i\gamma(1-f)\left(|A_s|^2 + 2|A_p|^2\right)A_s + D_s(z,t) \quad 1.50$$

In the above equations, the Raman contributions D_p and D_s have the form

$$D_j(z,t) = i\gamma f A_j \int_{-\infty}^{t} h_R(t-t')\left[|A_j(z,t')|^2 + |A_k(z,t')|^2\right]dt'$$

$$+\gamma f A_k \times \int_{-\infty}^{t} h_R(t-t')A_j(z,t')\,A_k^*(z,t')\exp[\pm i\Omega(t-t')]dt' \quad 1.51$$

where $j,k = p$ or s and $j \neq k$, $\Omega = \omega_p - \omega_s$ is the Stokes shift.

With regard to the CW assumption, the integral in Eq. (**1.51**) can be performed analytically to give a simple form as

$$D_j(z,t) = i\gamma f\left[\left(|A_j|^2 + |A_k|^2\right)A_j + \tilde{h}_R(\pm\Omega)|A_k|^2 A_j\right] \quad 1.52$$

where $\tilde{h}_R(\Omega)$ is the Fourier transform of the $h_R(t)$ and the negative sign corresponds to $j = s$. The real and imaginary parts of $\tilde{h}_R(\Omega)$ have been measured for orthogonal and parallel polarised pump and Stokes waves as shown in Figure **1.6.** It is important to note that the imaginary part of $\tilde{h}_R(\Omega)$ is related to the Raman gain. In fact, with regard to the above equations, the Raman-gain coefficient can be described as $g_R = 2\gamma f \mathrm{Im}[\tilde{h}_R(\Omega)]$.The real part of $\tilde{h}_R(\Omega)$ leads to Raman-induced index changes. We will

see in section **2.1** that because of the Raman contribution to the index changes, it can affect drastically the phase-matching conditions in an OPA, and thus modify its gain spectra.

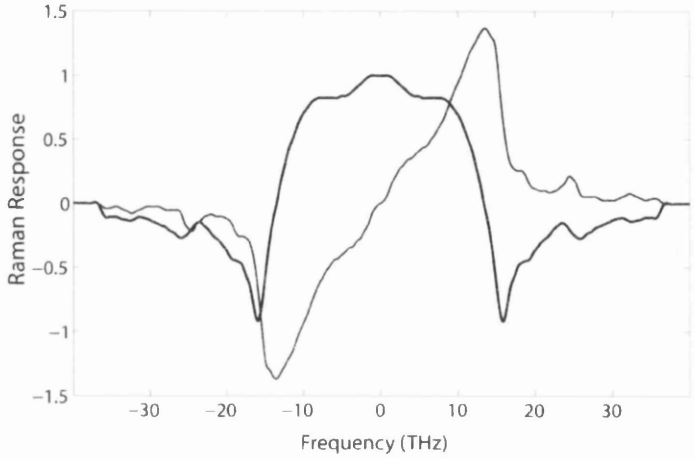

Figure 1.6. Real (thick) and imaginary (thin) parts of the Raman response for parallel pump-signal SOPs. (Courtesy of A. Vedadi.)

The Raman-gain coefficient and response curves both show a radical decrease for the case when the pump and the Stokes wave are orthogonally polarised. In fact, the Raman process is polarisation-dependent and a full vector description is necessary to analyse the situation in which the pump and the Stokes wave are not linearly co-polarised. In such an analysis the Raman nonlinear response function itself is divided into two parts including an isotropic and an anisotropic part of the nuclear response with a relative strength i.e. $h_R = f_a h_a + f_b h_b$. We skip such a description and only point out the fact that the Raman gain almost vanishes for orthogonal states of polarisations (SOPs).

1.4.2. Stimulated Brillouin scattering

Similar to SRS, stimulated Brillouin scattering is a nonlinear process in which a pump is scattered into another wave downshifted by the Brillouin shift $\Omega_B = \omega_p - \omega_s$. When an optical wave is injected into a fibre, the thermally excited acoustic waves scatter the wave into a backward-propagating wave by Bragg diffraction [**2**]. The incident and the reflected waves form an interference pattern, which reinforces the acoustic wave and leads to the simultaneous growth of both the acoustic wave and the reflected wave until a steady-state is reached [**3**]. Figure 1.7. shows schematically the interaction. The acoustic wave, which modulates the refractive index of the medium, can be seen as a Bragg grating moving at the acoustic velocity v_A. The scattered light is then

downshifted in frequency because of the Doppler shift [**2**]. The Brillouin downshift then becomes a function of the acoustic velocity and can be written as

$$\nu_B = \Omega_B/2\pi = 2n_p v_A/\lambda_p \qquad 1.53$$

The quantity v_A is very dependent on the material forming the core and the cladding of the fibre, and hence, the Brillouin shift is much dependent on the physical properties of the material as well. For example, for silica fibres, it is around 11 GHz at λ_p = 1550 nm while it is about 9.18 GHz for bismuth-oxide based fibres (Figure **1.8**). The measurement of the Brillouin shift for a bismuth-oxide fibre is performed by me using the heterodyne technique. The explanation of the experiment is presented at the end of this section.

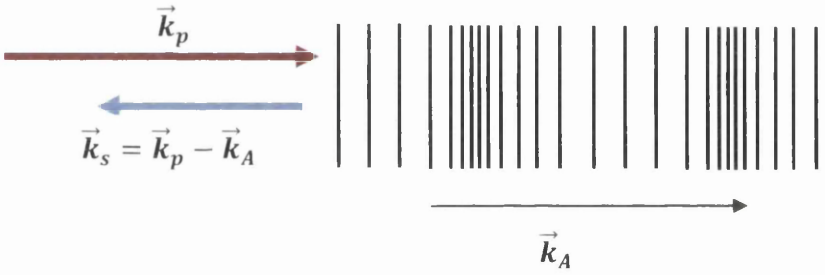

Figure 1.7. Schematic description of Brillouin interaction; the acoustic wave propagates at velocity v_A.

The Brillouin gain spectrum is very narrow compared with the gain spectrum of SRS. Its width is related to the acoustic phonon lifetime and is of the order of 20 MHz (FWHM) with a Lorentzian shape about the peak value. However, the gain coefficient of SBS is much larger than that of Raman process. Theoretical considerations show that the peak gain coefficient is almost independent of the pump wavelength and is about 3 to 5×10^{-11} m/W, which is almost three orders of magnitude larger than the peak Raman-gain coefficient [**2**].

The growth of the Stokes wave in a CW or quasi-CW pumping regime is governed by a set of two equations as:

$$\frac{dI_p}{dz} = -g_B I_s I_p - \alpha I_p \qquad 1.54$$

$$-\frac{dI_s}{dz} = g_B I_s I_p - \alpha I_s \qquad 1.55$$

where I_p and I_s are the intensities of the pump and the Stokes wave, respectively, and α accounts for the fibre attenuation. The negative sign on the left handside of Eq. (**1.55**) indicates the backward propagation of the Stokes wave.

Using these equations, a critical power is defined as the pump power for which the reflected optical power equals the transmitted optical power that emerges from the other end of the fibre [**18**]. It is found to be

$$\frac{g_B(\Omega_B)P_{cr}L_{eff}}{A_{eff}} \approx 21 \qquad 1.56$$

It is seen that P_{cr} depends on the length of the fibre. As g_B is large for SBS, the threshold is reached for small values of pump power and prevents injecting strong pumps into the fibre.

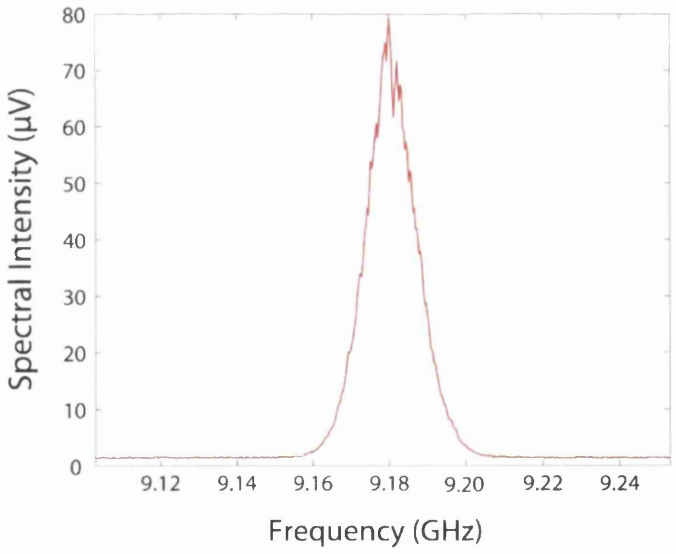

Figure 1.8. Brillouin gain spectra as a function of frequency detuning for bismuth-oxide highly nonlinear fibre (Bi-HNLF). (see Chapter **5**).

1.4.2.1. Measurement of the Brillouin gain spectrum for bismuth-oxide highly nonlinear fibre

The experimental setup shown in Figure 1.9 was used to measure the Brillouin gain spectrum of the Fig.18. The technique used in this experiment is known as heterodyne detection. The CW output of the tunable laser (TL) is divided into two branches through a 3-dB coupler. The wavelength of this laser was set to 1550 nm. One branch is amplified by an EDFA and using a circulator is coupled into the bismuth-oxide fibre. The output light is monitored on an OSA. The Brillouin back-reflected light is directed to the third arm of the circulator and is mixed with the second branch of the tunable laser by another 3-dB coupler. The output is impinged on a photo-detector (PD) and the electrical signal is analysed on as electrical spectrum analyser (ESA). Since the photo-detector responds to the intensity of the light, the electrical signal is at the frequency difference between the original light and the back-reflected light, namely the Brillouin shift.

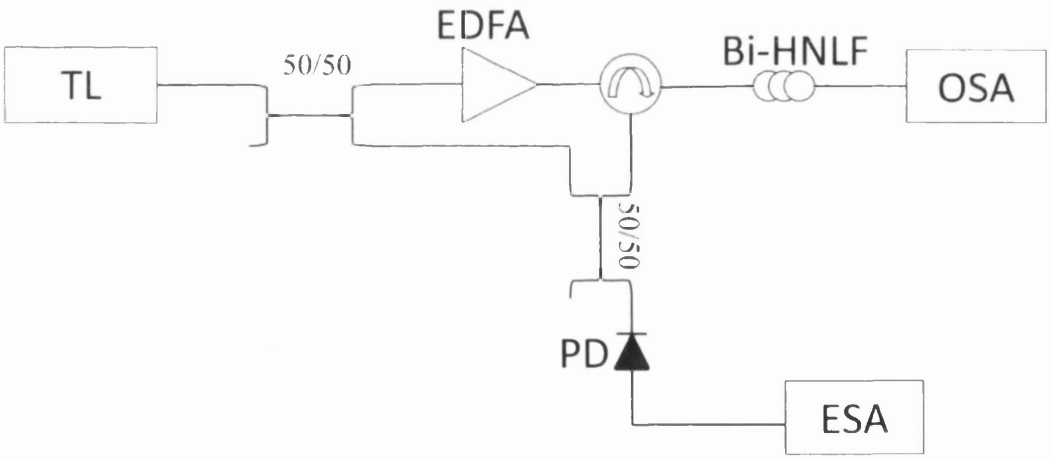

Figure 1.9. The experimental setup for the measurement of the Brillouin gain spectrum of a bismuth-oxide fibre using heterodyne-detection method. TL: tunable laser, PD: photo-detector, ESA: electrical spectrum analyser.

Summary

In this chapter, we reviewed some aspects of nonlinear optics. The existence of nonlinearity in the response of any media including glass leads to a variety of effects through which different optical waves propagating inside the medium interact with each other leading to energy exchange among them. Based on the fact that whether the

propagation medium is involved in the interaction or not the phenomenon is classified as inelastic or elastic phenomenon. SPM, XPM and FWM processes are introduced as the more important elastic processes and main aspects of them were discussed together with SRS and SBS as the important inelastic processes. FWM is the underlying process of the OPAs and thus it was discussed in a greater detail. The gain process leading to amplification in OPAs was also presented and associated equations were reviewed.

References

[1] P. G. Harper and B. S. Wherrett, *Nonlinear Optics*. United States of America: Academic press, 1977.

[2] G. P. Agrawal, *Nonlinear Fiber Optics*.4th Ed. United States of America: Academic press, 2007.

[3] M. E. Marhic, *Fiber Optical Parametric Amplifiers, Oscillators and Related Devices*. United Kingdom: Cambridge University Press, 2008.

[4] E. P. Ippen, C. V. Shank, and T. K. Gustafson, "Self-Phase Modulation of Picosecond Pulses in Optical Fibers," *Appl. Phys. Lett.*, vol. 24, pp.190-192, 1974.

[5] Y. R. Shen, and M. M. T. Loy. "Theoretical interpretation of small-scale filaments of light originating from moving focal spots," *Phys. Rev. A*, vol. 3, pp. 2099-2105, 1971.

[6] R. H. Stolen, and C. Lin, "Self-phase-modulation in silica optical fibers," *Phys. Rev. A.*, vol. 17, pp. 1448-1453, 1978.

[7] M. T. Myaing, J. Urayama, A. Braun, and T. B. Norris, "Nonlinear propagation of negatively chirped pulses: maximizing the peak intensity at the output of a fiber probe," *Opt. Express.*, vol.7, pp. 210–214, 2000.

[8] A. R. Chraplyvy, and J. Stone, "Measurement of cross-phase modulation in coherent wavelength-division multiplexing using injection lasers," *Electron. Lett.*, vol. 20, pp. 996-997, 1984.

[9] S. Coen, M. Haelterman, P. Emplit, L. Delage, L. Simohamed, and F. Reynaud, "Experimental investigation of the dynamics of a stabilized nonlinear fiber ring resonator," *J. Opt. Soc. Am. B.*, vol. 15, pp. 2283-2293, 1998.

[10] D. K. Serkland, and P. Kumar, "Tunable fiber-optic parametric oscillator," *Opt. Lett.*, vol. 24, pp. 92–94, 1999.

[11] E. Ciaramella, and S. Trillo, "All-optical signal reshaping via four-wave mixing in optical fibers," *IEEE Photon. Technol. Lett.*, vol. 12, pp. 849–851, 2000.

[12] R. Slavık, F. Parmigiani, J. Kakande, C. Lundstrom, M. Sjodin, P. A. Andrekson, R. Weerasuriya, S. Sygletos, A. D. Ellis, L. Gruner-Nielsen, D. Jakobsen, S. Herstrom, R. Phelan, J. O'Gorman, A. Bogris, D. Syvridis, S. Dasgupta1, P. Petropoulos, and D. J. Richardson, "All-optical phase and amplitude regenerator for next-generation telecommunications systems," *Nature Photonics,* vol. 4, pp. 690-695, 2010.

[13] C. V. Raman, "A new radiation," *Indian J. Phys.*, vol. *2*, pp. 387-398, 1928.

[14] Y. R. Shen, "Nonlinear optical susceptibilities," in *The Principles of Nonlinear Optics* ,4th Ed. New York: Wiley, 1984, pp.13-41.

[15] R. H. Stolen, E. P. Ippen, and A. R. Tynes, "Raman oscillation in glass optical waveguide," *Appl. Phys. Lett.*, vol. 20, pp. 62–65, 1972.

[16] R. H. Stolen, "Fundamentals of Raman Amplification in Fibres," in *Raman Amplifiers for Telecommunications*, M. N. Islam, Ed. New York: Springer, 2004, 35-58.

[17] S. P. Singh, R. Gangwar, and N. Singh, "Nonlinear Scattering Effects in Optical fibres," *progress in Electromagnetics Research.*, vol. 74, pp. 379-405, 2007.

[18] R. Smith, "Optical Power Handling Capacity of Low Loss Optical Fibbers as Determined by Stimulated Raman and Brillouin Scattering," *Appl. Opt.*, vol. 11, pp. 2489-2494, 1972.

[19] L. Mollenauer, R. Stolen, and M. Islam, "Experimental demonstration of soliton propagation in long fibres: loss compensated by Raman gain," *Opt. Lett.*, vol. 10, pp. 229-231, 1985.

[20] L. F. Mollenauer, J. P. Gordon, and la. N. Islam, "Soliton propagation in long fibres with periodically compensated loss," *IEEE J. Quantum Electron.*, vol. 22, pp. 157-173, 1986.

[21] M. Nakazawa, T. Nakashima, and S. Seikai, "Raman amplification in 1.4–1.5-μm spectral region in polarization-preserving optical fibers," *J. Opt. Soc. Am. B.*, vol. 2, pp. 515-521, 1985.

[22] K. J. Blow, and D. Wood, "Theoretical description of transient stimulated Raman scattering in optical fibers," *IEEE J. Quantum Electron.*, vol. 25, pp. 2665–2673, 1989.

[23] P. V. Mamyshev and S. V. Chernikov, "Ultrashort-pulse propagation in optical fibers," *Opt. Lett.*, vol. 15, pp. 1076–1078, 1990.

[24] R. W. Boyd, *Nonlinear Optics*, 3rd Ed. United States of America: Academic Press, 2008.

Chapter 2. Problems facing OPAs

Despite many useful proposed applications for OPAs, their use as practical amplifiers in WDM systems has not been realised so far. The reason for that, in addition to the poor drive of the telecommunication industry, which is because of economic situation and the quite large amount of unused capacity of the current systems, are some structural problems. These problems can be categorised in two categories including requirements and the fundamental problems.

The requirements include a strong pump with well-defined qualities such as low noise and availability at proper wavelengths, and suitable highly nonlinear fibres to act as the amplification medium. The fibres themselves must possess suitable properties such as proper dispersive characteristics, uniform ZDW, ideally no birefringence etc.

In the not too distant future, as the demand for more capacity continues to grow, it is anticipated that the industry will urge new technologies to be developed to answer the demand and at that point OPAs might be considered as quite a mature solution. Therefore, in order to produce commercial OPAs, their problems need to be fully understood. At present these problems mainly include.

- Nonlinear FWM crosstalk
- The impact of stimulated Raman scattering
- The impact of stimulated Brillouin scattering
- Polarisation dependence of the OPA gain

Among these problems, the problem of nonlinear crosstalk is described and discussed in details together with presentation of some results in a separate chapter (see Chapter **4**). The results are promising as they show OPAs can demonstrate quite similar

performance to ubiquitous EDFAs. In this chapter we review the other three problems with improvements in addressing them.

2.1. Impact of Raman gain

As we briefly discussed in section **1.4.1**, the Raman process couples two optical waves at frequencies ω_p and ω_s if the frequency shift $\Omega = \omega_p - \omega_s$ lies in the frequency range of 0-40 THz. Its various aspects have been studied extensively in the context of Raman amplifiers and its impacts on WDM systems. Furthermore, we mentioned that the evolution of the pump and the Stokes wave can be described using a set of two coupled equations similar to those introduced in section**1.4.1.1**. The effect of FWM is usually neglected for it is not efficient in most situations concerning the Raman process. In fact, Raman amplifiers are built in such fibres that exhibit a large negative dispersion. In addition, the Raman process is most efficient for frequency excursions in the range of 13.2 THz. This translates to about 100 nm at 1550 nm. Such large frequency detunings and large dispersion make the FWM negligible.

In the context of OPAs, the gain bandwidth used to be much less than 13.2 THz on each side of the pump to run into the Raman range. However, as the gain bandwidth of OPAs extends to more than 70-80 nm, the Raman gain appears to influence the parametric process. Hence, one needs to consider the effect of Raman carefully. The situation would be more important in the case of newly introduced compound-glass highly nonlinear fibres such as bismuth-oxide highly nonlinear fibre. In such fibres, the Raman shift turns out to be much smaller than that of silica fibres. For example for Bi-HNLF it is around 25-30 nm (see Chapter **5**).

The mutual effect of the Raman and parametric gain became important in Raman amplifiers before in OPAs when it was shown that Raman gain could be suppressed to 0 or reinforced to a 3.5 times larger value if the parametric coupling is taken into account [**1**]-[**7**]. On the other side, the use of Raman gain in the so-called Raman-assisted OPAs has attracted attention [**8**]-[**10**].

In order to investigate the mutual effect of the Raman and parametric processes one needs to account for the generated idler first, which will be named the anti-Stokes wave to comply with the terminology of Raman process. By considering the anti-Stokes wave

in the equation of the electric field and substituting in the revised NLSE, a set of three coupled equations describing the three complex amplitudes can be written as [**2**]

$$\frac{1}{i\gamma}\frac{dA_a}{dz} = |A_a|^2A_a + \left(1+\tilde{R}(-2\Omega)\right)|A_s|^2A_a + \left(1+\tilde{R}(-\Omega)\right)|A_p|^2A_a + \tilde{R}(-\Omega){A_p}^2A_s^*\exp(-i\Delta\beta z) \quad 2.1$$

$$\frac{1}{i\gamma}\frac{dA_p}{dz} = |A_p|^2A_p + \left(1+\tilde{R}(-\Omega)\right)|A_s|^2A_p + \left(1+\tilde{R}(\Omega)\right)|A_a|^2A_p + \left(\tilde{R}(\Omega)+\tilde{R}(-\Omega)\right)A_aA_sA_p^*\exp(i\Delta\beta z) \quad 2.2$$

$$\frac{1}{i\gamma}\frac{dA_s}{dz} = |A_s|^2A_s + \left(1+\tilde{R}(2\Omega)\right)|A_a|^2A_s + \left(1+\tilde{R}(\Omega)\right)|A_p|^2A_s + \tilde{R}(\Omega){A_p}^2A_a^*\exp(-i\Delta\beta z) \quad 2.3$$

where $\Delta\beta = \beta(\omega_a) + \beta(\omega_s) - 2\beta(\omega_p)$ is the linear wavevector mismatch and $\tilde{R}(\Omega) = 1 - f + f\tilde{h}_R(\Omega)$ is the Fourier transform of the total nonlinear response. The phase mismatch can be written as $\Delta\beta = \beta^{(2)}\Omega^2 + \frac{\beta^{(4)}}{12}\Omega^4$ (see section **3.2.1**). In the undepleted pump assumption, Eqs. (**2.1**)-(**2.3**) yield a small-signal gain as a function of pump power, *P*, and fibre length *L* as [**11**]:

$$G = \left|\cosh(\gamma TPL) \pm \frac{i(K-\tilde{R})}{T}\sinh(\gamma TPL)\right|^2 \quad 2.4$$

where $K = -\Delta\beta/2\gamma P$ is the normalised phase mismatch and $T = \sqrt{K(2\tilde{R}-K)}$. In Eq.(**2.4**) the positive sign for the sinh term is used if the signal is injected on the anti-Stokes side. Where the gain of the amplifier is considerable ($\gamma P\mathrm{Re}[T]L \gg 1$) Eq.(**2.4**) reduces to [**12**]

$$G = \frac{1}{4}\left|1 \pm \frac{i(K-\tilde{R})}{T}\right|^2 \exp(2\gamma P\mathrm{Re}[T]L) \quad 2.5$$

This yields the combined Raman-parametric gain coefficient $g = 2\gamma P\mathrm{Re}(T)$.

Figure 2.1 shows the plot of g/g_R versus normalised phase mismatch K. It is seen that for small values of K, which means small phase mismatch ($\Delta\beta \rightarrow 0$), the combined gain drops to zero. It is referred to as parametric suppression of Raman gain as we mentioned before. Experimental verification of such effect has been reported by several authors [**2**], [**12**]. In this case the signal experiences a weak quadratic amplification.

In the case of very large phase mismatch, one can show that the gain expression in Eq. (**2.4**) reduces to that of Raman process, which is normal as in that case the parametric process is not efficient.

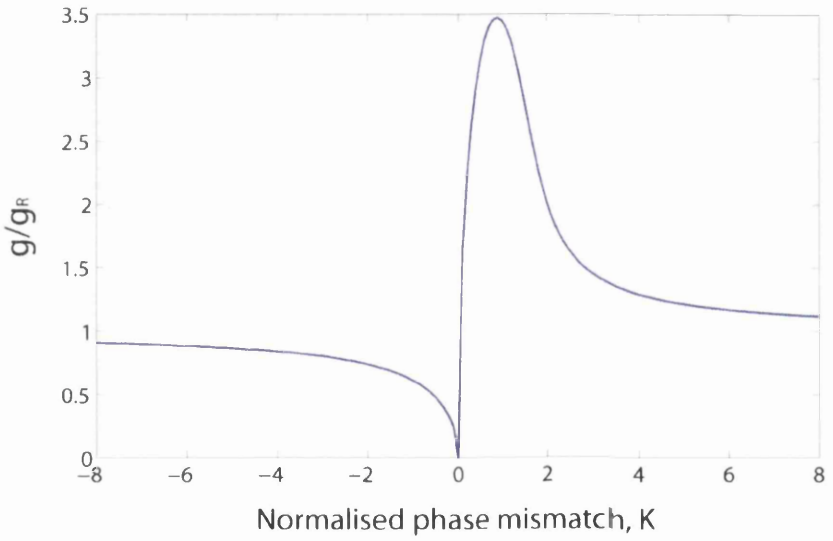

Figure 2.1. Plot of the ratio of the combined gain coefficient and the Raman gain coefficient versus the normalized phase mismatch.

One important case to be considered carefully is the phase matched case, where the nonlinear phase mismatch counterbalances the linear phase mismatch i.e. $\kappa = \Delta\beta + \Delta\beta_{NL} = 0$ (section **3.1**). This corresponds to $K = 1$ and is the case in which one expects the maximum parametric gain. In this case $T = \sqrt{2\tilde{R} - 1} \approx \tilde{R}$ and the gain expression of Eq. (**2.4**) is reduced to [**11**]

$$G = \frac{1}{4}\left|1 \pm \frac{i(1-\tilde{R})}{\tilde{R}}\right|^2 \exp(2\gamma PRe[\tilde{R}]L) \qquad 2.6$$

In this expression the exponential term depends on the real part of the nonlinear response and not on the imaginary part. The gain expression is reduced to $G = \frac{1}{4}e^{2\gamma PL}$, which is a well-known expression for maximum parametric gain in the absence of the Raman gain. In this case one would expect that the phase-matched gain would be much dependent on the real part of the Raman response $\tilde{h}_R(\Omega)$. Since $\tilde{h}_R(\Omega)$ shows a strong dip near 15.4 THz, the gain spectrum would follow such behaviour. This situation is simulated in Figure **2.2**. It is seen that for broadband OPAs, the gain spectrum has a drastic drop for 15.4 detuning, which affects the flatness of the spectrum. This has been verified experimentally in [**13**].

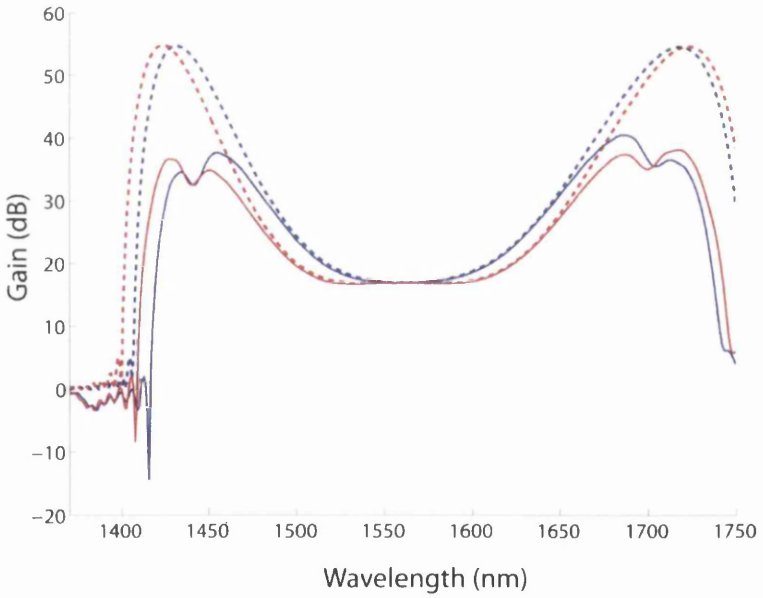

Figure 2.2. Theoretical gain spectra for pure parametric (dashed) and combined parametric-Raman gain. λ_0 = 1560 nm, γP = 3.5 km^{-1}, $\beta^{(3)}$ = 0.0516 ps^3/km, $\beta^{(4)} = -5\times10^{-4}$ ps^3/km and λ_p = 1559.5 nm (Red), λ_p = 1562 nm (Blue).

From the discussion presented so far, the implications caused by the Raman susceptibility on design of broadband OPAs are evident, and thus the effect of Raman should be accounted for carefully in the wideband OPAs. In Figure 2.3 and Figure 2.4,

the gain spectrum of two experimentally demonstrated broadband OPAs are shown for both a single-pump OPA [**14**] and a dual-pump one [**15**]. It is seen that the flatness of the gain spectra is severely affected. In an experiment (section **3.3.1.3**) we have shown such adverse impacts of the Raman process in a one-pump OPA. In the case of a two-pump OPA the situation is even more complex due to the presence of two pumps and the fact that the signal and the idler are both on the Stokes side of one pump and on the anti-Stokes side of the other pump. The phase matching condition is also more complex. Hence a numerical approach is required in order to simulate the behaviour of two-pump OPAs when the Raman gain in included.

In [**15**], it was found that small changes of 0.07 nm in the pump wavelength could greatly influence the flatness of the gain spectrum. Although an appealing gain bandwidth of about 155 nm is reached, unfortunately, the impact of the Raman gain makes it practically useless for telecommunication applications due to large fluctuations of about 15 dB.

In [**16**], we proposed that it may be possible to moderate the deteriorating effect of the Raman process by altering the state of polarisation of the signal; that is, by considering situations other than collinearly polarised pump and signal, which is the case of most practical interest. The vector analysis of mutual effect of the Raman and parametric process has received less attention due to its intricacy. In [**4**], it has been discussed for birefringent fibres and for the case of orthogonal pump and signal. The effect of polarisation-mode dispersion (PMD) is also partly investigated in [**17**]. In [**16**], we showed that by fine tuning of the pump wavelength in a range similar to that mentioned in [**15**] and by altering the polarisation states, it is possible to partially mitigate the undesirable effect of Raman. We describe the experiment in greater detail in Chapter **3**.

2.1.1. Solution of the field equations for a one-pump OPA including Raman gain and fibre loss

In the derivation of the three coupled equations introduced in this section, we did not include the effect of the fibre attenuation. It can be justified for silica-based fibres such as DSFs and HNLFs since the attenuation coefficient for them is very small and around 0.5 dB/km and 1 dB/km, respectively.

However, for novel holey fibres (HFs) and fibres composed of compound-glass such as the one we mentioned, Bi-HNLF, in addition to small Raman shift, the fibre attenuation

coefficient is very large. For Bi-HNLF, for example, it is around 2000 dB/km. This invalidates the assumption of negligible loss. On the other hand, deriving closed-form solutions for the field equations is often very helpful, specifically for simulation purposes. In the following, we present such a closed-form solution, with a trivial change in the notations, for the case of a one-pump OPA including the Raman effect and the

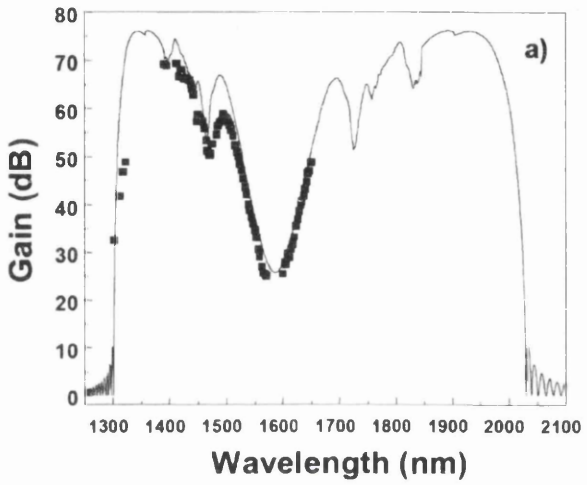

Figure 2.3. Gain spectrum of a one-pump OPA with 730 nm bandwidth and 80 W pulsed peak-power. (After Ref [14]).

fibre attenuation together.

Similar to section **1.4.1** we characterised the stimulated Raman scattering by the third-

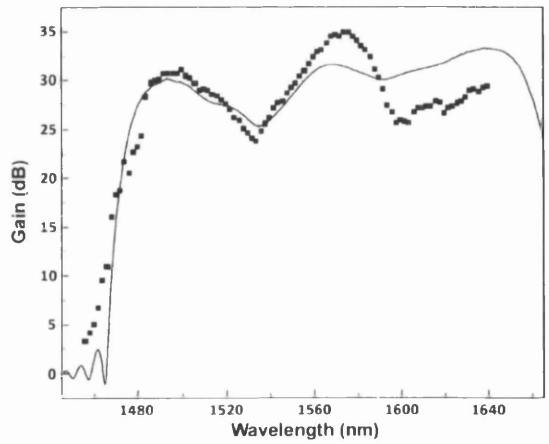

Figure 2.4. Gain spectrum of a CW two-pump OPA with 155 nm bandwidth. (After Ref [15]).

order susceptibility$\chi_R^{(3)}(\Omega) = f\chi^{(3)}\tilde{h}_R(\Omega)$, where $\Omega = \omega_3 - \omega_1$and $\omega_1$and $\omega_3$are the pump and signal frequencies, respectively. We designate the part of nonlinearity that is purely electronic in origin by $\chi_e^{(3)} = (1-f)\chi^{(3)}$; it can be assumed to be constant since the electronic response in time domain is nearly instantaneous. It is convenient to define the ratio of these two susceptibilities as

$$\delta(\Omega) = \frac{\chi_R^{(3)}(\Omega)}{\chi_e^{(3)}} \tag{2.7}$$

In the absence of loss and for the case of no pump-depletion, the pump equation is

$$\frac{dA_1}{dz} = i\gamma_e[1+\delta(0)]P_{10}A_1 \tag{2.8}$$

where γ_e is the fibre nonlinearity coefficient, which accounts only for the electronic nonlinearity. A_k is the complex amplitude of the fields. The solution of Eq. (**2.8**) is

$$A_1(z) = A_1(0)\exp(i\gamma_e[1+\delta(0)]P_{10}z) \tag{2.9}$$

When the pump is propagating in isolation its power cannot change, and this implies that $\delta(0)$ must be real.

Including the loss, the pump power is reduced only by the fibre loss and therefore varies as $P_1(z) = P_{10}e^{-\alpha z}$. The pump-field equation then becomes

$$\frac{dA_1}{dz} = \left(-\frac{\alpha}{2} + i\gamma P_1\right)A_1 = \left[-\frac{\alpha}{2} + i\gamma P_{10}e^{-\alpha z}\right]A_1 \tag{2.10}$$

which has the solution:

$$A_1(z) = \sqrt{P_{10}}\exp\left(-\frac{\alpha z}{2} + i\gamma P_{10}L_{\text{eff}}\right). \tag{2.11}$$

The signal equation can be written as:

$$\frac{dA_3}{dz} = -\frac{\alpha}{2}A_3 + 2i\gamma_{33}P_{10}\exp(-\alpha z)\,A_3 \tag{2.12}$$

$$+i\gamma_{34}P_{10}\exp\left(-\alpha z - i\Delta\beta z + 2i\gamma P_{10}L_{eff}\right)A_4{}^*$$

where $\gamma = \gamma_e[1+\delta(0)]$, $\gamma_{33} = \gamma_e[2+\delta(0)+\delta(\Omega)]/2$, $\gamma_{34} = \gamma_e[1+\delta(\Omega)]$, $\gamma_{44} = \gamma_e[2+\delta(0)+\delta(-\Omega)]/2$ and $\gamma_{43} = \gamma_e[1+\delta(-\Omega)]$. Same kind of equation holds for the idler.

These equations have the general form as:

$$\frac{dA_k}{dz} = -\frac{\alpha}{2}A_k + 2i\gamma_{kk}P_{10}\exp(-\alpha z)A_k + i\gamma_{kl}P_{10}\exp\left(-\alpha z - i\Delta\beta z + 2i\gamma P_{10}L_{eff}\right)A_l{}^* \quad 2.13$$

Equation (**2.13**) can be rewritten in the form:

$$\frac{dA_k}{dz} = ip_kA_k + ir_k\exp\left(i\int_0^z q_k d\xi\right)A_l^* \quad 2.14$$

with

$$p_k = \frac{i\alpha}{2} + 2\gamma_{kk}P_{10}e^{-\alpha z}$$

$$q_k = i\alpha - \Delta\beta + 2\gamma P_{10}e^{-\alpha z}$$

$$r_k = \gamma_{kl}P_{10}$$

Letting $A_k = B_k exp\left(i\int_0^z p_k d\xi\right)$, we obtain

$$\frac{dB_k}{dz} = ir_k exp\left(-i\int_0^z \kappa_k d\xi\right)B_l{}^* \quad 2.15$$

where

$$\kappa_k = p_k + p_l{}^* - q_k = -i\alpha + \Delta\beta + (\gamma_{kl} + \gamma_{lk}{}^*)P_{10}e^{-\alpha z}$$

and

$$\acute{\kappa_k} = -\alpha(\gamma_{kl} + \gamma_{lk}{}^*)P_{10}e^{-\alpha z}.$$

Prime stands for derivative with respect to *z*.

We then take the derivative of Eq. (**2.15**) and eliminate B_l^*, which yields:

$$\frac{d^2B_k}{dz^2} + i\kappa_k \frac{dB_k}{dz} - r_k r_l^* exp\left[i\int_0^z (q_k - q_l^*)d\xi\right] B_k = 0 \qquad 2.16$$

a second-order differential equation for B_k.

Making use of the transformation $B_k = C_k exp\left(-\frac{i}{2}\int_0^z \kappa_k d\xi\right)$, which implies:

$$C_k = A_k exp\left[i\int_0^z \left(\frac{\kappa_k}{2} - p_k\right) d\xi\right] \qquad 2.17$$

we obtain

$$\frac{d^2C_k}{dz^2} - {g_k}^2(z)C_k = 0 \qquad 2.18$$

where

$${g_k}^2(z) = r_k r_l^* exp\left[i\int_0^z (q_k - q_l^*)d\xi\right] - \frac{{\kappa_k}^2}{4} + \frac{i\kappa_k'}{2} \qquad 2.19$$

Using the definitions above, we find

$${g_k}^2 = \frac{(\alpha + i\Delta\beta)^2}{4} - \frac{\Delta\beta(\gamma_{kl} + \gamma_{lk}^*)P_0 \exp(-\alpha z)}{2} - \frac{(\gamma_{kl} - \gamma_{lk}^*)^2 {P_0}^2 \exp(-2\alpha z)}{4} \qquad 2.20$$

It is seen that ${g_k}^2$ is of the form $g_k^2 = w + v_k \exp(-\alpha z) + u_k \exp(-2\alpha z)$, thus Eq.(**2.18**) can be written as

$$\frac{d^2C_k}{dz^2} - (w + v_k \exp(-\alpha z) + u_k \exp(-2\alpha z))C_k = 0 \qquad 2.21$$

Letting $x = \exp(-\alpha z)$, Eq.(**2.21**) is transformed to:

$$\frac{d^2C_k}{dx^2} + \frac{1}{x}\frac{dC_k}{dx} - \left(\frac{u_k}{\alpha^2} + \frac{v_k}{\alpha^2 x} + \frac{w}{\alpha^2 x^2}\right) C_k = 0 \qquad 2.22$$

Assuming $C_k = {}^{Y_k}/_{\sqrt{x}}$ yields

$$\frac{d^2Y_k}{dx^2} + \left[-\frac{u_k}{\alpha^2} - \frac{v_k}{\alpha^2 x} + \left(\frac{1}{4} - \frac{w}{\alpha^2}\right)\frac{1}{x^2}\right]Y_k = 0 \qquad 2.23$$

By letting $x = {}^{Z}/_{Z_0}$, where $Z_0 = Z(0)$ is a constant, we obtain

$$\frac{d^2Y_k}{dZ^2} + \left[-\frac{u_k}{\alpha^2 {Z_0}^2} - \frac{v_k}{\alpha^2 Z_0 Z} + \left(\frac{1}{4} - \frac{w}{\alpha^2}\right)\frac{1}{Z^2}\right]Y_k = 0 \qquad 2.24$$

Now with the following assumptions:

$$Z_0 = \frac{2u_k^{1/2}}{\alpha}, \eta = -\frac{v_k}{\alpha^2 Z}, \mu = \frac{w^{1/2}}{\alpha}$$

we obtain

$$\frac{d^2Y_k}{dZ^2} + \left[-\frac{1}{4} + \frac{\eta}{Z} + \left(\frac{1}{4} - \mu^2\right)\frac{1}{Z^2}\right]Y_k = 0 \qquad 2.25$$

Two independent solutions of Eq.(**2.25**) are:

$$Y_{k,1}(Z) = Z^{1/2+\mu} exp\left(-{}^{Z}/_{2}\right) F_1^1\left({}^{1}/_{2} - \eta + \mu, 1 + 2\mu; Z\right) \qquad 2.26$$

$$Y_{k,2}(Z) = Z^{1/2-\mu} exp\left(-{}^{Z}/_{2}\right) F_1^1\left({}^{1}/_{2} - \eta - \mu, 1 - 2\mu; Z\right)$$

, which are known as Whittaker's confluent hypergeometric functions. The two initial conditions, which we need to complete the solution, can be written as

$Y_k(Z_0) = C_k(0) = A_k(0)$, and

$$Y_k'(Z_0) = \frac{1}{Z_0}\left[\frac{1}{2}C_k(0) - \frac{1}{\alpha}C_k'(0)\right] = \qquad 2.27$$

$$\frac{1}{Z_0}\left[\frac{1}{2}A_k(0) - \frac{1}{\alpha}\left(A_k(0)\left(\frac{\alpha + i\Delta\beta}{2} + \frac{i}{2}(\gamma_{kl} + \gamma_{lk}^*)P_0\right) - i\gamma_{kl}P_0 A_l^*(0)\right)\right]$$

Here the solution is complete; substituting Z with $Z_0\exp(-\alpha z)$ in $Y(Z)$ and finding $C_k(z)$ by using the assumption $C_k = {}^{Y_k}/_{\sqrt{x}}$ is straightforward. Making use of Eq. (**2.17**) we can find the main quantity of interest $A_k(z)$ depending only on z.

2.2. Impact of stimulated Brillouin scattering

Stimulated Brillouin scattering discussed briefly in section **1.4.2** is the source of a number of severe problems to the operation and performance of OPAs. Hence, it has been studied extensively in this area [**18**]-[**23**]. The first and foremost problem caused by SBS is that it prevents injection of strong pump fields, which play a crucial role in exploiting the benefits of OPAs. As SBS is a very high gain process, if not suppressed, it clamps the pump power at very low levels and reflects back virtually all the pump power. For instance, it would not let more than 200 mW of pump power to be injected into a 300 m of HNLF. This means that the maximum phase shift achievable would be Φ = 1.2 if we assume the nonlinearity coefficient of γ= 20 $W^{-1}km^{-1}$ for the HNLF. This amount of phase shift would produce a trivial maximum gain of only 4 dB. Thus it is clear that without effective suppression of SBS OPAs cannot operate.

Other problems caused by SBS are closely in relation with the complex nature of this process. In general, it has been well studied and known that the dynamics of SBS leads to very unpredictable results for the evolution of the pump and the Stokes wave. The situation is often referred to as a *chaotic* behaviour of SBS. This behaviour is known to be because of at least two separate reasons. Firstly, as we mentioned the growth of the acoustic wave and the Stokes wave continues to reach a steady-state, however, simulations and experiments show that the Stokes power does not approach this steady-state monotonically but exhibits relaxation oscillations [**24**]-[**26**]. This phenomenon has been studied as early as 1983 [**24**] where the period of the oscillations was shown to be $2T_r$, and $T_r = L/v_g$ is the transient time for a fibre length L. In [**26**] the observation of the relaxation oscillations was explained as follows. The large gain of the SBS process gives rise to a rapid growth of the Stokes power near the input end of the fibre, which depletes the pump. The gain is then reduced until the depleted portion of the pump arrives at the fibre end. The gain then builds up, and the process repeats itself. In the presence of optical feedback, from the cleaved ends of the fibre for example, these

oscillations can turn into stable oscillations [**24**]. Some people refer to this type of behaviour as "*bursty*" since the oscillations appear and disappear in a chaotic manner.

Another source of a chaotic behaviour, which is more related to four-wave mixing, is the strong coupling between two counterpropagating waves due to the so-called Brillouin-enhanced four-wave mixing process. In [**27**], it has been predicted that in the case of small phase mismatch, counterpropagating waves can be unstable to the growth of the side modes at the frequency of Brillouin. The counterpropagating wave can be generated due to spontaneous Brillouin scattering from the noise level or because of back reflected pump from the ends of the fibre. This phenomenon has been studied in other situations extensively in [**28**]-[**30**] all predicting chaotic fluctuations in the intensities of the pump and the signal. Therefore, SBS is known to be a parasitic process in OPA work, which deteriorates the performance of OPAs drastically if it is not sufficiently suppressed. As a result, it is required to check the back-reflected light to make sure that it is well below a certain amount. In other words, for example, when injecting 1 W of pump power into a fibre, whether the back reflected light is 1 mW (0 dBm) or 10 mW (10 dBm) makes a considerable difference in the error-free operation of the OPA, although it would not cause noticeable difference in the amount of the gain as the pump will be either 999 mW or 990 mW.

With regard to what we mentioned in the preceding, many measures have been sought to increase the threshold of SBS. One solution which is most widely used in the experiments with OPAs is to broaden the linewidth of the pump by means of phase or frequency modulation. When the spectrum of the pump is broadened, the magnitude of the frequency components decreases so that they do not generate significant SBS back reflection. It has been shown that if the linewidth of the pump is broadened to $\Delta\nu$ the SBS gain is reduced to [**31**]

$$g_B' = \frac{g_B}{1 + (\Delta\nu_B/\Delta\nu)^2} \qquad 2.28$$

where g_B is the SBS gain without pump broadening. Considering $\Delta\nu_B = 50$ MHz, if one uses $\Delta\nu = 5$ GHz, the gain and subsequently the threshold power will be reduced by a factor 100 (20 dB). It should be noted that although the linewidth broadening could also be performed by means of intensity modulation (IM), it is not suitable for OPAs projected to amplify communication signals, because the gain would also be modulated.

Several modulation schemes has been used for this method including phase modulation with a pseudo-random bit sequence (PRBS) [**32**] or the sum of several sinusoidal RF tones, which are adjusted at proper frequencies to maximise the increase of the SBS threshold [**18**]. In [**18**], a multi-level modulation scheme was used to obtain 70 dB of gain in a one-pump OPA. In that modulation scheme the total optical bandwidth occupied by the pump was 25 GHz offering a 24 dB increase in the SBS threshold. Efforts have been made to reduce the occupied bandwidth by means of utilizing more suitable electrical waveforms. In a very recent piece of work two novel bandwidth-efficient electrical waveforms, namely an RF noise source and an RF frequency-hopped chirp, have been shown to offer a much better performance [**33**]. Specifically, a 19 dB increase in the SBS threshold was reported by using an RF noise source with bandwidth of only 1.5 GHz. The phase modulation method offers the advantage that it is active, controllable and does not change the fibre permanently, nonetheless, it is associated with some problems such as the intensity noise that the pump acquires through the phase modulation, which degrades the quality of the pump and influences the signal as well as the gain. Moreover, the idler is broadened twice as much as the pump. This can be readily understood from the frequency relation between the pump (in a one-pump OPA) and the signal and the idler i.e. $2\omega_p = \omega_s + \omega_i$. If the pump frequency deviates from its value by $\delta\omega$ and the frequency of the signal remains constant, the spectrum of the idler will be broadened by $2\delta\omega$. Therefore, it can cause problems for wavelength converters if one is interested in using the idler. This problem in two-pump OPAs however can be resolved by means of phase-conjugate pump dithering [**34**].

In addition to the problems associated with the phase (frequency) dithering of the pump, the phase (frequency) modulation technique for SBS suppression requires a considerable amount of RF equipment and at least one phase modulator (PM), which is a costly device. Besides, the use of external PM introduces a considerable amount of loss of about 5 dB. As a result, other passive techniques have been sought to replace the phase dithering technique. A major group of these passive methods work on the basis of finding a way to impede the exponential growth of the acoustic wave. If the rapid growth of the acoustic wave is prevented somehow, it will then be possible to increase the SBS threshold.

Placing isolators within the fibre length is an immediate solution of this kind. It has been used first in [**35**] to provide 60 dB gain. Embedded air gaps, stress distribution, tapered cores are other solutions that have been proposed [**36**]-[**37**]. It is expected that the holey fibre technology (see Chapter **5**) would contribute to increasing the SBS threshold to a large extent. Specifically, using some material to fill the air gaps that are lossy for acoustic waves but not for optical waves and designing structures with reduced overlap between the acoustic and optical modes are some possibilities that have been considered.

Replacing silica with other materials is another way to increase the SBS threshold. For example bismuth-oxide fibres that have attracted a considerable amount of attention [**38**] are claimed to own a better figure of merit compared to silica. More specifically, while the SBS gain in bismuth-oxide is about 70 times larger than that of silica, the Kerr nonlinearity is about 1000 times more enhanced. This leads to a relatively better figure of merit in terms of SBS threshold. Some passive techniques such as core tapering have been also considered in conjunction with the use of such compound glass fibres to improve the SBS threshold even more [**39**].

Regarding the passive techniques introduced for treating the SBS issue, one should note that they all change the structure of the fibre, which means changes in all its properties including dispersion characteristics. As dispersive properties are of a great importance especially in OPA work, the practical use of such techniques is still questionable.

As the last noteworthy point regarding the SBS-induced issues in the OPAs, it should be noted that two-pumps OPA in addition to other advantages have an SBS threshold which is 3 dB higher than that in one-pump OPAs since the total power is divided between two pumps. At any rate, the SBS problem is one of the main concerns for practical and more importantly for commercial OPAs.

2.3. Polarisation Dependence

The dependence of the gain of OPAs on polarisation is one of the fundamental shortcomings of OPAs. It is fundamental in origin since the FWM process is highly polarisation dependent due to the necessity of conservation of angular momentum among the four (three) interacting waves [**25**]. In the derivation of the OPA equations in section **1.3.3** we made two assumptions: (i) the waves are all linearly polarised along

one axis; (ii) the waves maintain their SOP along the OPA fibre. In a real optical communication system the SOPs of the signals are completely random when entering the amplifier. Thus the first assumption is not satisfied in practical communication systems. The second assumption is also questionable since even if we launch the waves with a same linear SOP, they would not maintain their SOP since the fibres are not precisely isotropic or polarisation-maintaining. In addition, the nonlinear polarisation due to strong pumps will cause birefringence. The problem of non-isotropic fibres however is less of a problem since with the advent of HNLFs and availability of high pump powers the length of the fibre required for OPAs has been reduced to about 100 m, which in turn reduces the probability of undesired birefringence. In addition, the technology of constructing silica HNLFs has reached such a level of development to produce almost isotropic fibres although this can be easily violated since any physical stress can induce some amount of birefringence. A proper winding radius is very important in this regard.

In order to investigate the problem of the dependence of the OPA gain on the SOPs of the waves interacting in the FWM process, a full vector theory is required. Such a development in the theory is introduced in [**25**], [**31**]. The starting point for such an analysis is to consider the tensor form of the third-order nonlinear susceptibility $\chi^{(3)}$. Assuming $\chi^{(3)}_{xxxx}$ to be one of the three independent elements, other elements can be expressed as

$$\chi^{(3)}_{ijkl} = \frac{1}{3}\chi^{(3)}_{xxxx}\left(\delta_{ij}\delta_{kl} + \delta_{ik}\delta_{jl} + \delta_{il}\delta_{jk}\right) \tag{2.29}$$

where δ_{mn} is the Kronecker delta function and is 1 if $m = n$ and 0 otherwise.

The total electric field due to four waves can be written as

$$\vec{E} = \frac{1}{2}\sum_{i=1}^{4} \overrightarrow{E_i}(\boldsymbol{r})e^{j(\omega_i t)} + c.c. \tag{2.30}$$

In order to include the polarisation changes, each field can be represented by a Jones vector as follows

$$\overrightarrow{E_i}(\boldsymbol{r}) = F_i(x,y)|A_i\rangle \exp(j\beta_i) \tag{2.31}$$

where $F_i(x,y)$is the transverse profile of each field, which is assumed to be the same for the four fields. β_i is the propagation constant for the field at frequency ω_i.

The Jones vector of each field is composed of its complex amplitude and SOP such that $\langle A_i|A_i\rangle = |A_i|^2 = P_i$ and P_i is the optical power of the field. Following a procedure closely related to the one in section **1.3.3** and assuming SPM and XPM terms due to the signal and idler to be negligible as well as the FWM term in the equation of the pumps, a set of four equations is obtained describing the amplitude evolution of the fields in an isotropic medium as [**40**]

$$\frac{d|A_l\rangle}{dz} = \frac{2i\gamma}{3}\left(\langle A_l|A_l\rangle + \langle A_k|A_k\rangle + \frac{1}{2}|A_l^*\rangle\langle A_l^*| + |A_k\rangle\langle A_k| + |A_k^*\rangle\langle A_k^*|\right)|A_l\rangle \tag{2.32}$$

for $l = 1,2$ and $k = 3-l$ and

$$\frac{d|A_l\rangle}{dz} = (\langle A_1|A_1\rangle + |A_1\rangle\langle A_1| + |A_1^*\rangle\langle A_1^*| + \langle A_2|A_2\rangle + |A_2\rangle\langle A_2| + |A_2^*\rangle\langle A_2^*|)|A_l\rangle$$
$$+\frac{2i\gamma}{3}(|A_2\rangle\langle A_1^*| + |A_1\rangle\langle A_2^*| + \langle A_1^*|A_2\rangle)|A_k^*\rangle e^{-i\Delta\beta z} \tag{2.33}$$

for $l = 3,4$ and $k = 7-l$. Indices 1and 2 represent the pumps and 3 and 4 are used for the signal and the idler, respectively.

In the case of a single-pump configuration, the second pump should be assumed to be equal to zero i.e. $|A_2\rangle = 0$. Also, one should replace $|A_2\rangle$ with $|A_1\rangle$ and 2γ with γ in the signal and idler equations.

Due to the extremely complex nature of the above equations a numerical approach is essential in general to solve the equations for different cases. However, to investigate the FWM efficiency, one can ignore the effect of SPM and XPM since they only alter the phase-matching condition. Moreover, it is known that the angular momentum can itself be quantised by considering the spin of each photon [**41**]. Also the concept of Jones vector is directly applicable to photons. On this ground we can decompose the Jones vector of each field to the quantised up-spin and down-spin states as

$$|A_i\rangle = U_i|\uparrow\rangle + D_i|\downarrow\rangle \tag{2.34}$$

where $|\uparrow\rangle$ and $|\downarrow\rangle$ denote the right circular and left circular polarisation states and represent photons with an intrinsic angular momentum value of $+\hbar$ and $-\hbar$, respectively. The terms on the right-hand side of Eq. (**2.34**) represent respectively the field amplitudes in the up-spin and down-spin states. Using this expansion, one can obtain from Eq. (**2.33**) that the creation of idler in the two orthogonal states in the case of complete phase-matching is governed by the following two equations [**25**]:

$$\frac{dU_4}{dz} = \frac{4i\gamma}{3}[U_1U_2U_3^* + (U_1D_2 + D_1U_2)D_3^*]$$
$$\frac{dD_4}{dz} = \frac{4i\gamma}{3}[D_1D_2D_3^* + (U_1D_2 + D_1U_2)U_3^*] \qquad 2.35$$

The two equations obtained above are very instructive in the sense that they provide a descriptive way for investigating the creation of the idler for different cases. They show, for example, if the two pumps are copolarised and the signal is perpendicular to them the idler should be perpendicular as well. For two pumps right-circularly polarised a left circular signal cannot produce idler and vice versa.

The dependence of the gain on the relative polarisation states of the waves can also be easily understood from these equations. When the SOPs of the pumps are arbitrary, they contain both up-spin and down-spin components. Thus for a signal, which also has an arbitrary SOP, the creation of the idler can happen through all the six paths in the equations. Since the efficiency of each path is depending on the relative probability amplitude they can be different for different SOPs of the signal and thus lead to different amounts of gain.

Based on such reasoning, it is seen that there is no possibility to obtain a polarisation-independent mode for a one-pump OPA. In other words, it is impossible to balance the FWM efficiency experienced by up-spin and down-spin components of the signal. However, in the case of a two-pump OPA, such a situation is possible. If the pumps are left and right circularly polarised the terms containing U_1U_2 and D_1D_2 vanish. In that case the FWM process becomes polarisation-independent. A similar situation is possible with two linearly orthogonal pumps. This causes the second term in each equation to disappear, and hence, a polarisation-independent operation becomes possible. In this case, however, the amount of gain is very small.

The solution of the OPA equations for different cases of the pump and signal SOPs is cumbersome, however, it is useful to have the solutions for the case of isotropic fibres and parallel or orthogonal signal and pump(s). Based on this assumption, different cases can be identified such as XXX, XYX, ... for a one pump OPA and XYYX, XYXY,... for a two-pump OPA. For example, for orthogonal pump and signal in a one-pump OPA in which the pump is aligned to the x-axis and the signal to the y-axis we have

$$\frac{dA_1}{dz}\begin{pmatrix}1\\0\end{pmatrix} = \frac{2i\gamma}{3}\left(|A_1|^2 + \frac{1}{2}|A_1|^2\begin{pmatrix}1 & 0\\0 & 0\end{pmatrix}\right)A_1\begin{pmatrix}1\\0\end{pmatrix} = i\gamma|A_1|^2A_1 \tag{2.36}$$

$$\begin{aligned}\frac{dA_3}{dz}\begin{pmatrix}0\\1\end{pmatrix} &= \frac{i\gamma}{3}\left(2|A_1|^2 + |A_1|^2\begin{pmatrix}2 & 0\\0 & 0\end{pmatrix} + |A_1|^2\begin{pmatrix}2 & 0\\0 & 0\end{pmatrix}\right)A_3\begin{pmatrix}0\\1\end{pmatrix}\\ &\quad + \frac{i\gamma}{3}\left(A_1{}^2\begin{pmatrix}1 & 0\\0 & 0\end{pmatrix} + A_1{}^2\begin{pmatrix}1 & 0\\0 & 0\end{pmatrix} + A_1{}^2\right)A_4^*\begin{pmatrix}0\\1\end{pmatrix}e^{-i\Delta\beta z}\\ &= \frac{2i\gamma}{3}P_1A_3 + \frac{i\gamma}{3}A_1{}^2A_4^*e^{-i\Delta\beta z}\end{aligned} \tag{2.37}$$

A similar expression holds for the idler. Comparing these equations with the equations obtained in section **1.3.3** for the case of parallel pump and signal, it is seen that the pump equation is the same as the pump is only influenced by its own SPM (neglecting all other terms). The signal equation is however modified. The modification is as if the effective value of γ is changed to $\gamma/3$. Therefore, one can verify that for example the maximum gain coefficient will be reduced to $g_{\max} = \gamma P/3$ instead of γP and also $\Delta\beta_{NL} = -2\gamma P/3$ instead of $2\gamma P$. This means that the maximum attainable gain and the frequency at which the maximum gain is provided will change. Figure 2.5 compares a sample gain spectra of a one-pump OPA for orthogonal and parallel SOPs of the pump and signal when all other parameters are identical.

One can calculate the modifications required for other types of OPAs accordingly [**31**].

Table 2.1 and Table **2.2** summarise such modifications. In the case of LRL for a one-pump OPA, $g_{\max} = 0$ indicating that no gain will be available as concluded from the discussion in the preceding. The same situation holds for a two-pump OPA with LRRL polarisation assignments for the fields.

Table 2.1 Parameters $g_{\max}/\gamma P$ and $\Delta\beta_{NL}/\gamma P$ for one-pump OPAs

OPA type spi	$g_{\max}/\gamma P$	$\Delta\beta_{NL}/\gamma P$
XXX	1	2
YXY	1/3	−2/3
RRR	2/3	4/3
LRL	0	4/3

Table 2.2 Parameters $\boldsymbol{g_{\max}/2\gamma\sqrt{P_1P_2}}$ and $\boldsymbol{\Delta\beta_{NL}/\gamma(P_1+P_2)}$ for two-pump OPAs

OPA type sppi	$g_{\max}/\gamma P$	$\Delta\beta_{NL}/\gamma P$
XXXX	1	1
YXXY	1/3	−5/3
XXYY	1/3	1
YXYX	1/3	1
RRRR	2/3	2/3
LRRL	0	2/3
RRLL	2/3	2/3
LRLR	2/3	2/3

Among the OPA types named in the above tables, those involving linear polarisation states are quite easy to construct since firstly, obtaining linear polarisation states is straightforward from the output of the laser sources and secondly, fibres normally exhibit linear birefringence if they are not precisely isotropic, and hence it is much easier to align the waves with linear principal states of polarisation (PSPs) of such fibres. Therefore, linearly polarised waves can propagate over a long distance. The situation is much more difficult for launching circular polarisation. In fact, circular polarisation states cannot be preserved for more than a few centimetres. This has

prevented demonstration of LRLR OPA to date. However, the use of spun fibres [**42**] may permit the use of circular polarisation states, since the PSPs of such fibres are

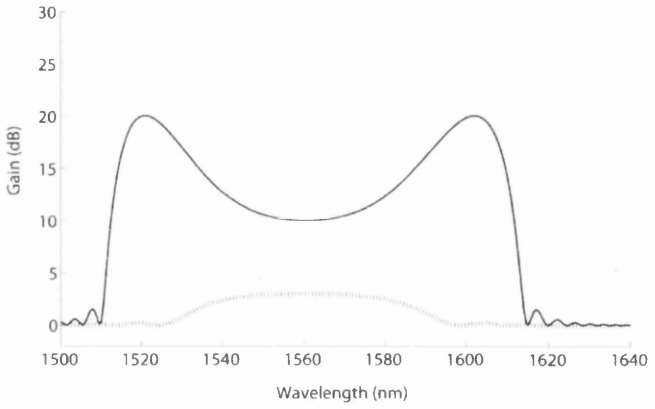

circular.

2.3.1. Effect of birefringence

To the discussion introduced so far, one could add the effect of either constant and intentional birefringence or that of the residual unintentional one. A large constant birefringence is normally intentionally induced in the process of fabrication to provide a mean for preserving linear SOPs over large lengths and mitigate the influence of random residual birefringence. This generates two distinct polarisation axes and the linear waves aligned to these axes maintain their SOPs over a long distance. The use of such fibres in OPA work has been limited. A most important case of their usage is the

Figure 2.5. A sample gain spectra for a one-pump OPA and parallel (solid) and orthogonal (dashed) pump-signal SOPs.

case of a one-pump OPA with orthogonal pump and signal. This is discussed in more details in section **3.2.2**.

The random birefringence which is present in fibres causes the evolution of the SOPs of the waves and hence can affect the performance of OPAs. Due to randomness of such birefringence a stochastic model together with an averaging process is often adopted for assessment of OPA performance. Such an approach has been examined in the evaluation of the SPM that occurs in long fibres [**43**]. Assuming a uniform distribution over the Poincare sphere, it has been shown that a random birefringence can be accounted for by using a value for γ, which is $\gamma' = {}^{8}/_{9}\,\gamma$. A similar approach shows the same effect in the case of one-pump and two-pump OPAs in which all the waves are

assumed collinearly polarised. However, it is in general very difficult to verify such an effect experimentally because the value of γ itself is not measured and reported with such a precision so that its original value and 8/9 portion of it could be distinguished experimentally. This explains why in general the scalar theory developed for OPAs is pretty sufficient in the correct modelling of the results of experiments with OPAs. The 8/9 correction factor is not however applicable for all types of OPAs, and one must consider other values.

The evolution of the SOPs in the OPAs caused by random birefringence can be separated in two parts [**25**]. One part accounts for the rotation of the SOP that occurs for all the waves in a same way and the other type accounts for the drift of the SOPs of the pumps, signal and idler from each other. The latter depends on the frequency. While for small frequency shifts and small amount of birefringence, it is justified to neglect the frequency dependence [**31**], for very broadband OPAs this can lead to erroneous results. In fact, in [**16**] it has been shown that for broadband OPAs with more than 200 nm bandwidth, the SOP can drift considerably. In that work, it is discussed that optimizing the signal SOP once at 1520 nm and another time at 1640 nm leads to different gain spectra.

2.3.2. Polarisation independent OPAs

With regard to the preceding, it is seen that the polarisation issue is of a great importance in the performance of OPAs. Especially, the high dependence of the gain of OPAs on the SOP of the input signal has been raising serious questions about their usefulness in communication systems. For this reason, a number of schemes have been proposed so far to overcome this issue. Using orthogonal pumps in a two-pump arrangement, polarisation-independent demonstrations have been reported [**44**]-[**47**].

In [**48**], a scheme is proposed to obtain a polarisation insensitive one-pump OPA in a highly-birefringent fibre. In this scheme the pump is launched at 45° to the principal axes of the fibre and thus is split equally into two parts on the principal axes. Simulations show a polarisation-independent gain with deviations smaller than 0.1 dB. However, in order to cancel the phase delay introduced, the fibre must be cut and re-spliced after a 90° rotation. This is a difficult task to perform without special instruments. Therefore, experimental verifications of this technique have not been reported to date.

Polarisation diversity is another scheme that has been proposed and demonstrated experimentally for both one- and two-pump OPAs to solve the problem of polarisation-dependent gain [**49**]-[**50**]. In this scheme, the pump(s) are launched with a 45° angle into a polarisation beam splitter (PBS). The signal is also passed through the same PBS. The two separated polarisation components of the pumps and signal are then launched into the fibre in opposite directions so that there is no interaction between them. As the orthogonal components of the pump(s) have equal powers, they provide an equal amount of gain to the two components of the signal. The components of the signal are then recombined through the PBS to form the final amplified signal. Although this method has been found to work properly with satisfactory results, the PBS introduces some loss. A drawback of this method is that the gain is about 6-dB below the counterpart OPA with a unidirectional arrangement regardless of the loss of the PBS [**49**].

Summary

This chapter reviews the main problems facing the OPAs currently. Beside technical and engineering work required to bring OPAs to the state of practically deployment in the telecommunication systems, the problems discussed in this chapter should be addressed and resolved.

The most fundamental difficulty with OPAs is that they are intrinsically polarization-dependent. In other words the amount of the gain of OPAs depends on the SOP of the incoming signal. This is due to the fact the FWM process is itself polarization-dependent. In this regard, the birefringence of the highly-nonlinear fibre used for OPA becomes an important issue to be considered.

Other problems include the impact of SBS and the Raman gain. SBS prevents the injection of high pump power into the HNLF, which is essential for obtaining broadband amplification with good amount of gain. Thus some techniques are required to suppress the SBS. SBS is also a parasitic process causing problems to the OPAs. The active method of phase-modulation of the pump is the most widely-used and successful technique, which provides about 20 dB suppression depending on the frequency of the modulation. It introduces problems for wavelength convertors as the idler is broadened as well twice the amount of the pump broadening.

The Raman gain is another problem that transforms the shape of the gain spectrum of the OPAs and prevents acquiring the expected gain spectrum. This becomes more influential in the case of broadband OPAs with gain bandwidth in excess of 100 nm.

References

[1] K. J. Blow and D. Wood, "Theoretical description of transient stimulated Raman scattering in optical fibers," *IEEE J. Quantum Electron.*, vol. 25, pp. 2665–2673, 1989.

[2] E. A. Golovchenko, P. V. Mamyshev, A. N. Pilipetskii, and E. N. Dianov, "Mutual influence of the parametric effects and SRS in optical fibers," *IEEE J. Quantum Electron.*, vol. 26, pp. 1815-1820, 1990.

[3] P. N. Morgan and J.M. Liu, "Parametric four-photon mixing followed by stimulated Raman scattering with optical pulses in birefringent optical fibers," *IEEE J. Quantum Electron.*, vol. 27, pp. 1011–1021, 1991.

[4] E. Golovchenko and A. Pilipetskii, "Unified analysis of four-photon mixing, modulational instability, and stimulated Raman scattering under various polarization conditions in fibers," *J. Opt. Soc. Amer. B.*, vol. 11, pp. 92–101, 1994.

[5] S. Trillo and S. Wabnitz, "Parametric and Raman amplification in birefringent fibers," *J. Opt. Soc. Amer. B.*, vol. 9, pp. 1061–1082, 1992.

[6] P. Dinda, G. Millot, and S. Wabnitz, ''Polarization switching and suppression of stimulated Raman scattering in birefringent optical fibers," *J. Opt. Soc. Am. B.*, vol. 15, pp. 1433-1441, 1998.

[7] C. Lin, L. G. Cohen, R. H. Stolen, G. W. Tasker, and W. G. French, "Near-infrared sources in the 1-1.3 μm region by efficient stimulated Raman emission in glass fibers," *Opt. Commun.*, vol. 20, pp. 426–428, 1977.

[8] P. Tchofo, E. Sève, G. Millot, T. Sylvestre, H. Maillote and E. Lantz, "Raman-assisted three-wave-mixing of non-phase-matched waves in optical fibers: application to wide range frequency conversion," *Opt. Commun.*, vol. 192, pp. 107-121, 2001.

[9] D. Chestnut, C. de Matos, and J. Taylor, "Raman-assisted fiber optical parametric amplifier and wavelength converter in highly nonlinear fiber," *J. Opt. Soc. Am. B.*, vol. 19, pp. 1901-1904 2002.

[10] C. de Matos, D. Chestnut, P. Reeves-Hall, and J. Taylor, "Continuous-wave-pumped Raman-assisted fiber optical parametric amplifier and wavelength converter in conventional dispersion-shifted fiber," *Opt. Lett.*, vol. 26, pp. 1583-1585, 2001.

[11] M. Matsumoto and K. Sanuki, "Performance improvement of DPSK signal transmission by a phase-preserving amplitude limiter," *Opt. Express.*, vol. 15, pp. 8094-8103, 2007.

[12] F. Vanholsbeeck, P. Emplit, and S. Coen, "Complete experimental characterization of the influence of parametric four-wave mixing on stimulated Raman gain," *Opt. Lett.*, vol. 28, pp. 1960-1962, 2003.

[13] A. Hsieh, S. Murdoch, S. Coen, R. Leonhardt, and J. Harvey, "Influence of Raman susceptibility on optical parametric amplification in optical fibers," *Opt. Lett.*, vol. 32, pp. 521-523, 2007.

[14] J. Chavez Boggio, J. Windmiller, M. Knutzen, R. Jiang, C. Bres, N. Alic, B. Stossel, K. Rottwitt, and S. Radic, "730-nm optical parametric conversion from near- to short-wave infrared band," *Opt. Express.*, vol. 16, pp. 5435-5443, 2008.

[15] J. M. C. Boggio, S. Moro, E. Myslivets, J. R. Windmiller, N. Alic, and S. Radic," 155-nm Continuous-Wave Two-Pump Parametric Amplification," *IEEE Photon. Technol. Lett.*, vol. 21, pp. 612-614, 2009.

[16] M. Jamshidifar, A. Vedadi, M. E. Marhic, "Continuous-wave one-pump OPA with 270 nm gain bandwidth," in *European Conference on Optical Communication (ECOC)*, Vienna, Austria, 20-24 September 2009, paper 1.1.4.

[17] A. Willinger, E. Shumakher, and G. Eisenstein, "On the Roles of Polarization and Raman-Assisted Phase Matching in Narrowband Fiber Parametric Amplifiers," *J. Lightwave Technol.*, vol. 26, pp. 2260-2268, 2008.

[18] T. Torounidis, P. A. Andrekson, and B. E. Olsson, "Fiber-Optical Parametric Amplifier with 70-dB Gain," IEEE *Photon. Technol. Lett.*, vol. 18, pp. 1194–1196, 2006.

[19] D. A. Fishman, and J. A. Nagel, "Degradations Due to Stimulated Brillouin Scattering in Multigigabit Intensity-Modulated Fiber- Optic Systems," *J. Lightwave Technol.*, vol. 11, pp. 1721–1728, 1993.

[20] R. Engelbrecht, M. Mueller, and B. Schmauss, "SBS shaping and suppression by arbitrary strain distributions realized by a fiber coiling machine," in *IEEE/LEOS Winter To*picals *Meeting Series.*, Innsbruck, 12-14 Jan. 2009, paper WC1.3.

[21] J. M. C. Boggio, J. D. Marconi, and H. L. Fragnito, "Experimental and numerical investigation of the SBS threshold increase in an optical fiber by applying strain distributions," *J. Lightwave Technol.*, vol. 11, pp. 3808–3814, 2005.

[22] J. M. Chavez Boggio, F. A. Callegari, A. Guimaraes, J. D. Marconi, and H. L. Fragnito, "Q Penalties due to Pump Phase Modulation in FOPAs," in *Optical Fiber Communication Conference (OFC)*, Anaheim, CA, 6-11 March 2005, paper OWN4.

[23] A. Mussot, M. Le Parquier, and P. Szriftgiser, "Thermal noise for SBS suppression in fiber optical parametric amplifiers," *Opt. Commun.*, vol. 283, pp. 2607–2610, 2010.

[24] I. Bar-Joseph, A. Friesem, E. Lichtman, and R. Waarts, "Steady and relaxation oscillations of stimulated Brillouin scattering in single-mode optical fibers," *J. Opt. Soc. Am.*, vol. B 2, pp. 1606-1611, 1985.

[25] G.P.Agrawal, *Nonlinear Fiber Optics*.4th Ed. United States Of America: Academic press, 2007.

[26] R. V. Johnson, and J. H. Marburger, "Relaxation oscillation in stimulated Raman and Brillouin scattering," *Phys. Rev. A.*, vol. 4, pp. 1175-1182, 1971.

[27] Boris Ya Zel'dovich, and V V Shkunov, " Characteristics of stimulated scattering in opposite pump beams," *Sov. J. Quantum Electron.*, vol. 12, pp. 223- 225, 1982.

[28] A. L. Gaeta, R. W Boyd, J. R. Ackerhalt, and P. W Milonni, "Instabilities and chaos in the polarization of counter-propagatinglight fields," *Phys. Rev. Lett.*, vol. 58, pp. 2432-2435, 1987.

[29] R. G. Harrison, J. S. Uppal, A. Johnstone, and J. V. Moloney, "Evidence of chaotic stimulated Brillouin scattering in optical fibers," *Phys. Rev. Lett.*, vol. 65, pp. 167-170, 1990.

[30] A. Gaeta, M. Skeldon, R. Boyd, and P. Narum, "Observation of instabilities of laser beams counterpropagating through a Brillouin medium," *J. Opt. Soc. Am. B.*, vol. 6, pp. 1709-1713, 1989.

[31] M. E. Marhic, *Fiber Optical Parametric Amplifiers, Oscillators and Related Devices*. United Kingdom: Cambridge University Press, 2008.

[32] S. Radic, and C. J. McKinstrie, "Two-Pump Fiber Parametric Amplifiers," *Technol Opt. Fiber.*, vol. 9, pp. 7–23, 2003.

[33] J. Coles, B. Kuo, N. Alic, S. Moro, C. Bres, J. Boggio, P. Andrekson, M. Karlsson, and S. Radic, "Bandwidth-efficient phase modulation techniques for Stimulated Brillouin Scattering suppression in fiber optic parametric amplifiers," *Opt. Express.*, vol. 18, pp. 18138-18150, 2010.

[34] K. K. Y. Wong, M. E. Marhic, and L. G. Kazovsky, "Phase-conjugate pump dithering for high-quality idler generation in a fiber optical parametric amplifier," *IEEE Photon. Technol. Lett.*, vol. 15, pp. 33–550, 2003.

[35] K. K. Y. Wong, K. Shimizu, K. Uesaka, G. Kalogerakis, M. E. Marhic, and L. G. Kazovsky, "Continuous-wave fiber optical parametric amplifier with 60-db gain using a novel two-segment design," *IEEE Photon. Technol. Lett.*, vol. 15, pp. 1707–1709, 2003.

[36] J. Hansryd, F. Dross, M. Westlund, P. A. Andrekson, and S. N. Knudsen, "Increase of the SBS Threshold in a Short Highly Nonlinear Fiber by Applying a Temperature Distribution," *J. Lightwave Technol.*, vol. 19, pp. 1691–1697, 2001.

[37] J. D. Marconi, J. M. Chavez Boggio, and H. L. Fragnito, "Narrow Linewidth Wavelength Converter with 70 nm of Signal Tuning Band Using Strain Distribution to Suppress SBS," in *European Conference on Optical Communications (ECOC)*, 25-29 September, Glasgow, Scotland, UK , Paper Mo4.5.6.

[38] F. Poletti, P. Petropoulos, N. G. Broderick, and D. J. Richardson, "Design of Highly Nonlinear Bismuth-Oxide Holey Fibres with Zero Dispersion and Enhanced Brillouin Suppression", *In European Conference on Optical Communications (ECOC)*, 24-28 September, Cannes, France, Paper Tu4.3.2.

[39] F. Poletti, K. Furusawa, Z. Yusoff, N. Broderick, and D. Richardson, "Nonlinear tapered holey fibers with high stimulated Brillouin scattering threshold and controlled dispersion," *J. Opt. Soc. Am.*, vol. *B.*, vol. 24, pp. 2185-2194 , 2007.

[40] Q. Lin and G. Agrawal, "Vector theory of four-wave mixing: polarization effects in fiber-optic parametric amplifiers," *J. Opt. Soc. Am. B.*, vol. 21, pp. 1216-1224, 2004.

[41] L. Mandel and E. Wolf, "Quantization of the free electromagnetic field", in *Optical Coherence and Quantum Optics*," New York: Cambridge University Press, 1995, pp. 456-522.

[42] M.E. Marhic, K.K. Y. Wong, and L.G. Kazovsky "Fibre optical parametric amplifiers with circularly-polarised pumps," *IEEE Electron. Lett.*, vol. 39, pp. 350- 351, 2003.

[43] S. Chernikov and J. Taylor, "Measurement of normalization factor of n2 for random polarization in optical fibers," *Opt. Lett.*, Vol. 21, pp. 1559-1561, 1996.

[44] R. M. Jopson, and R. E. Tench, "Polarization-independent phase conjugation of lightwave signals," *IEEE Electron. Lett.*, Vol. 29, pp. 2216, 1993.

[45] K. Inoue, "Polarization independent wavelength conversion using fiber four-wave mixing with two orthogonal pump lights of different frequencies," *J. Lightwave Technol.*, vol. 12, pp. 1916, 1994.

[46] K. K. Y. Wong, M. E. Marhic, K. Uesaka, and L. G. Kazovsky, "Polarization-independent and flat-gain CW two-pump fiber optical parametric amplifier and wavelength converter," in *Optical Fiber Conference*, 2002, Anaheim, Paper TuS5.

[47] . K. Y. Wong, M. E. Marhic, K. Uesaka, and L. G. Kazovsky, "Polarization-Independent Two-Pump Fiber Optical Parametric Amplifier", IEEE Photon. Technol. Lett. Vol. 14, pp. 911, 2002.

[48] F. Yaman, Q. Lin, and G. Agrawal, "A Novel Design for Polarization-Independent Single-Pump Fiber-Optic Parametric Amplifiers," in *Conference on Lasers and Electro-Optics/Quantum Electronics and Laser Science Conference and Photonic Applications Systems Technologies*, 2006, Paper JWB59.

[49] K. Y. Wong, M. E. Marhic, K. Uesaka, and L. G. Kazovsky, "Polarization-Independent Ono-Pump Fiber Optical Parametric Amplifier", *IEEE Photon. Technol. Lett.* Vol. 14, pp. 1506, 2002.

[50] G. Kalogerakis, M. E. Marhic, and L. G. Kazovsky, "Polarization-Independent Two-Pump Fiber Optical Parametric Amplifier with Polarization Diversity Technique", in *Optical Fiber Conference (OFC)*, 2006, Anaheim, Paper OWT4.

Chapter 3. Gain and bandwidth

The amount of the gain provided and the bandwidth over which the gain is available are the two factors of the prime importance in characterisation of any amplifier. Fibre optical parametric amplifiers are most attractive because of their ability to provide very wide bandwidth and large gain. In telecommunication systems due to other considerations 20 dB of gain for in-line amplifiers is a quite customary value, which corresponds to about 100 km transmission distance between successive amplifiers. Erbium-doped fibre amplifiers can easily provide this amount of gain over the bandwidth of normally less that 32 nm. Reaching this amount of gain in OPAs is also straightforward, but the bandwidth can be much larger than that of EDFAs. Moreover, in OPAs like as in RAs this gain and bandwidth is accessible around a centre wavelength, which can be determined almost arbitrarily provided that the right fibre and pump source are available.

The bandwidth of OPAs is often referred to as to be "man-made"; that is the bandwidth can be tailored to a great extent by the designer in response to the specific system requirements rather than being dictated by the material intrinsic properties as in EDFAs. In addition, the complex nature of the dependence of the bandwidth in OPAs on the dispersion properties of the fibre, birefringence, nonlinearity and the pump power leads to some interesting possibilities such as narrow-band gain regions at a distant location from the pump.

The gain spectrum of OPAs also shows several interesting properties. The possibility of obtaining very high small-signal gain or large conversion efficiency in transferring the pump power to the signal and the idler are among them.

In this chapter we will review some of the most important aspects of gain and bandwidth in OPAs separately, and present the results of two of our experiments; one

reported a record gain of 60 dB in a two-pump OPA and the other one reported a record bandwidth of 270 nm in a one-pump arrangement.

3.1. Gain

In section **1.3.3**, the signal gain expression of a two-pump OPA in a no pump depletion regime was found to be:

$$G_s(z) = \left|\frac{r}{g}\sinh(gz)\right|^2 + 1 \qquad 3.1$$

where, $g^2 = r^2 - \left(\frac{\kappa}{2}\right)^2$ is the parametric gain coefficient.

No pump depletion regime is the case of most interest, as in actual amplification of telecommunication signals a linear gain is required.

As is apparent from Eq. (**3.1**), the gain is maximal when $g = g_{\max} = r^2$ and that occurs when the nonlinear phase shift cancels the phase mismatch due to dispersion i.e. $\kappa = \Delta\beta + \Delta\beta_{NL} = 0$. When the gain is large, the maximum gain can be found as $G_{s,max}(z) \approx e^{2rz}/4$. Expressing the gain in decibels, we obtain $G_{s,max}^{dB}(z) \approx 17.2(\gamma\sqrt{P_1P_2}z) - 6$. For a fixed total pump power P_0=P_1+P_2, the gain is maximum for P_1= P_2= P_0/2; then

$$G_{s,\max}^{dB}(z) \approx 8.64\Phi - 6 \qquad 3.2$$

where $\Phi = \gamma P_0 z$ is a measure of the pump nonlinear phase shift. The above equation is applicable where Φ is large i.e. for high gain situation.

The expression of Eq. (**3.2**) is a beneficial expression as it allows us to estimate the maximum gain of an OPA quickly. It is worth noting that the maximum gain is only a function of the product $\gamma P_0 z$. Therefore, the fibre nonlinearity, length and pump power could be determined to give a particular gain.

The gain expression in Eq. (**3.1**) reveals that the small-signal gain spectrum of an OPA is governed by three quantities: r, $\Delta\beta$ and $\Delta\beta_{NL}$. The wavevector mismatch $\Delta\beta$ is dictated by the dispersion profile of the fibre. It has a crucial role in determining the shape of the gain spectrum as will be reviewed in the next section. The nonlinear wavevector mismatch determines at which wavelength $\kappa = 0$, and hence where maximum gain can

be expected. r and $\Delta\beta_{NL}$ can be determined by the knowledge from pump power and γ only.

The gain expression in Eq. (**3.1**) is applicable to one-pump OPAs with a slight modification. For a two-pump OPA with $P_1 = P_2 = P_0/2$ we have $g_{max} = \gamma P_0$ and $\Delta\beta_{NL} = \gamma P_0$. These quantities should be modified for one-pump OPA as $g_{max} = \gamma P_1$ and $\Delta\beta_{NL} = 2\gamma P_1$. The consequence of this is that for a one-pump OPA and a two-pump OPA with the same total pump power the maximum gain is the same, but it is obtained for different values of $\Delta\beta = -\Delta\beta_{NL}$.

Although the gain expression and maximum gain is the same for equal pump power, one- and two-pump OPAs generally have different gain spectra because of different expressions for $\Delta\beta$ and $\Delta\beta_{NL}$ as we will review in the succeeding sections.

3.1.1. High-gain OPAs

As mentioned, it is possible to obtain very large values for small-signal gain in OPAs. High gain amplifiers could find applications as bright ASE noise sources, preamplifiers, or in free space optical communication systems [**1**], [**2**]. The possibility of obtaining high gain values in OPAs is due to one of their unique features, which is that the parametric gain is unidirectional, which reduces the possibility of parasitic lasing caused by residual reflections of splices and components. It also cancels the backward propagation of amplified spontaneous emission. This feature is missing in EDFAs and, as a result, for EDFAs there has been proposed a fundamental limitation on the gain of about 57-70 dB [**3**].

According to Eq. (**3.2**) the maximum gain obtainable in a one- or two-pump OPA can be related directly to fibre nonlinearity coefficient, pump power and fibre length. For a given type of fibre (fixed γ) one must have a large value of the product P_0L in order to have high gain; hence one needs a long fibre and/or high pump power. For a typical HNLF with $\gamma = 15$ W^{-1} km^{-1}, one needs $P_0L = 0.5$ W km to obtain 60 dB of gain; this can for example be achieved with $L = 0.5$ km and $P_0 = 1$ W. In pulsed-pump experiments, it is easy to obtain a high amount of pump power, and SBS does not impose problems on injecting pump power into the fibre. However, if the amplifier is

designed for amplification of real communication signals it must be operated with a CW pump, and then SBS becomes an issue.

When the gain is high, some factors enter which limit G via pump depletion. This occurs when the output power of the signal and/or the OPA ASE is a significant fraction of P_0. Therefore, to minimize pump depletion, and increase maximum gain, it is helpful to use a large P_0. Since ASE total power scales with the amplifier bandwidth, saturation will occur sooner for a wideband amplifier.

Several experiments were conducted to obtain high gain values in OPAs as soon as silica-based HNLFs became available. For one-pump CW case, which is much easier to operate, it started with an experiment in [**4**] in which 49 dB of gain was reported. In that experiment the optical filter, which is normally put after the high-power EDFA to reject the ASE, was removed to provide more power injected into the fibre. The gain was then improved in [**5**] to 60 dB by making use of a novel idea for SBS suppression. In that experiment, an isolator was used in combination with pump phase modulation, where the phase modulation was performed by means of two cascaded phase modulators. The fibre length was 1 km and γ was 17 $W^{-1}km^{-1}$. The isolator put half-way in the fibre length stops back-reflected light from SBS. Consequently, the SBS threshold is increased by a factor 2, which in turn leads to increased gain by nearly a factor 2. The record gain of 70 dB in a one-pump OPA was reported three years later in [**2**] with a pump power of 1.9 W within a composition of three fibre segments with total length of 500 m. The measure taken for SBS suppression in that experiment was also interesting, in which two phase modulators were used in series. The first PM was driven by a 10 GHz sinusoid with the second PM driven by the sum of four different RF tones. The outcome was 243 new frequency components spread over a 25 GHz range. The increase in the SBS threshold was 24 dB. The gain in that experiment was found to be limited by SBS on the amplified signal and by saturation due to ASE.

The ASE of such high gain amplifiers can be used as ASE noise sources as mentioned before. The interesting feature of such ASE is that it is propagating in one direction and can be very bright. For example in [**2**] the ASE brightness was found to be 180 mW/nm. Moreover, in one-pump OPAs, the ASE is highly polarized as the gain is provided mainly in the same polarization as that of pump.

Two-pump OPAs are more difficult to operate, due to the increased complexity. One additional issue arising in the two-pump arrangement compared to the one-pump case is that for pump spacings reaching tens of nanometres, significant Raman interaction can take place between the pumps, requiring the use of unequal pump input powers in order to optimize the gain spectrum. With suitable pump adjustments, two-pump OPAs have the advantage over one-pump OPAs of providing broad and flat gain profiles. This however, leads to increased ASE, which can cause pump depletion more easily. To date, the highest gain reported for a CW two-pump OPA with parallel pumps is about 42 dB [**6**]-[**8**].

In the following, the results of an experiment are presented, in which we obtained a record gain for a two-pump OPA of about 60 dB over nearly 30 nm.

3.1.1.1. Experiment description[1]

The experimental setup for the two-pump OPA is shown in Figure 3.1 Two tunable lasers (TL1-TL2) with wavelength $\lambda_1$in the L-band and λ_2 in the C-band, respectively, are used as pumps. The two pumps are combined by a wavelength demultiplexer (WDM1) and passed through the PM which is used for SBS suppression purpose. The PM is driven by four RF sinusoids. The four tones had the frequecies 101 kHz, 300 kHz, 908 kHz, and 2.71 MHz giving the best possible SBS suppression of about 21 dB. Two polarization controllers (PC1-PC2) align the polarization of the pumps to the PM. The pumps are then separated by WDM2 and amplified by two high-power output amplifiers (EDFA1-EDFA2) to reach the desired pump powers P_1 and P_2. The polarization controller before EDFA2 (PC3) is used to adjust the polarization of one of the pumps parallel to the other in order to maximize the gain in the OPA. The ASE from each of the EDFAs is filtered out by a bandpass filter centred at the according pump wavelength. The pumps are then combined by WDM3 and injected into the HNLF through a 20 dB coupler. One power-meter is placed after the coupler to monitor the injected power into the fibre.

A tunable laser (TL3) acts as the signal, which is injected by the 20 dB coupler into the HNLF. The HNLF output is attenuated through a 10dB coupler and finally analyzed on an optical spectrum analyzer (OSA).

[1] This experiment was performed by me from design to data collection and analysis with Dr. Armand Vedadi's help in the setup. Prof. M. E. Marhic provided the overall supervision.

In this experiment, the sensitivity of the OSA was set to -65 dBm and the resolution bandwidth was 0.01 nm. The gain measured is the On/Off gain. It means that the power of the signal was read in decibels once when the pumps were on and another time with the pumps turned off. The difference between the two values is considered as the On/Off gain. Although the On/Off gain is not the actual gain of the amplifier (the output-to-input gain), this is a quite widely used term when talking about the OPAs gain.

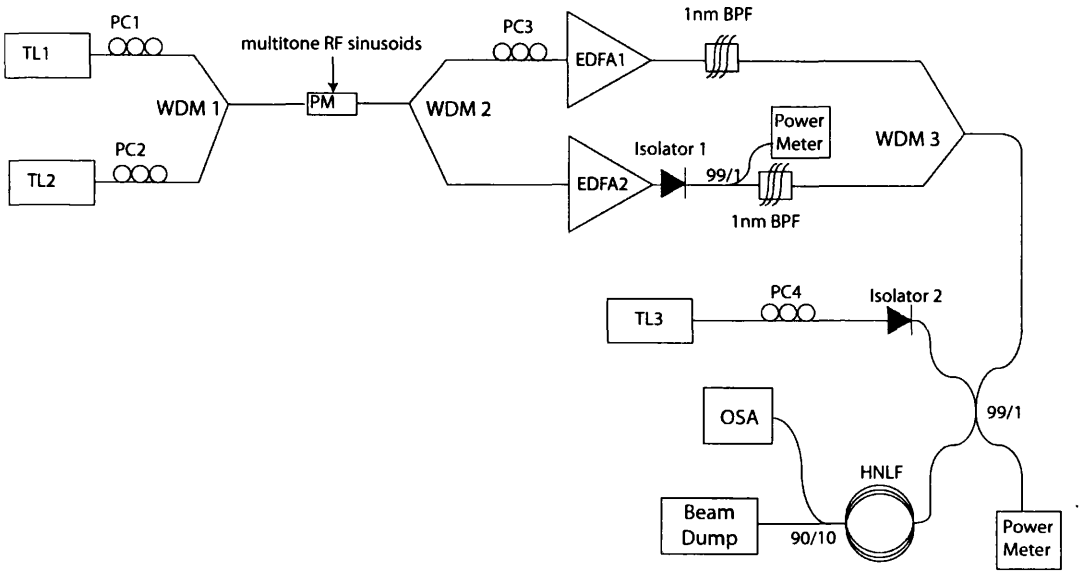

Figure 3.1. The experimental setup of the high-gain two-pump OPA.

3.1.1.2. Results and discussion

In Figure 3.2 different experimental gain spectra are shown for a pump spacing of 62nm. The total injected pump power is 32 dBm (1580mW). Different approaches aiming at a maximum and flat gain in the OPA were taken. As mentioned earlier, in a two-pump OPA with large pump spacing of tens of nanometres, a significant Raman interaction could take place between the two pumps i.e. energy from the pump at the shorter wavelength is transferred to the other pump resulting in unequal pump powers at the OPA output. This causes the gain spectra to lose flatness and the gain to drop. This situation is seen in Figure 3.2 **(a)**. When the pump input powers are equal (circle curve) the gain spectra shows a valley and the gain is between 50-55 dB. However, by

adjusting the pump powers gain flatness was improved to better than 2.5 dB of variation around 55 dB over 50 nm of bandwidth (Figure 3.2 **(a)** square curve).

Another issue that arises for the OPAs with such high gains (more than 55 dB) is that the signal power reaches comparable values to the pump powers resulting in pump depletion and saturation. In addition, the signal itself reaches SBS threshold. SBS due to signal, of course, prevents signal growing and affects the gain. We reduced the signal input power from -37 dBm to -40 dBm to obtain more gain so that the SBS and saturation effects could be weakened. A further 2 dB improvement in gain was achieved, as shown by the triangle curve in Figure 3.2 **(a)**.

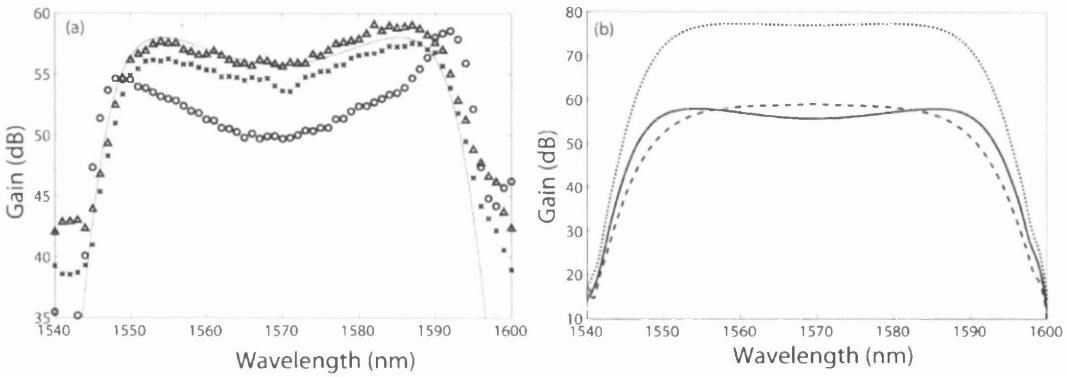

Figure 3.2. (a) Experimental gain spectra with λ_1 = 1601nm and λ_2 = 1539nm with P1=P2=790mW (circles), P1=330mW and P2=1230mW (star), and P1=330mW and P2=1230mW with lower signal input power (triangle). (b) Analytical gain spectra for P1=P2=790mW (dotted line), P1=330mW and P2=1230mW (dashed line) and P1=P2=610mW (continuous line).

To gain more insight, we have plotted the analytical gain for the two-pump OPA as given in [**1**]. For the experimental power, Figure 3.2 **(b)** shows that the theoretical gain is much higher than the experimental one. With unequal power, the gain values are consistent; however the gain shape is not well reproduced. These differences are accounted for by the fact that Raman is not taken into account. With lower equal pump powers, we notice that the theoretical gain curve fits well the experimental one with unequal pump powers. This shows that by using different pump powers at the HNLF input, one can counterbalance the influence of Raman on flat gain.

These results also suggest that even at low signal input power, strong pump depletion occurs because of the parametric ASE. One solution to mitigate that effect is to reduce the bandwidth, as shown in Figure 3.3 where the pumps were placed at λ_1= 1544.8nm

and $\lambda_2 = 1594.5$nm. The gain is greater 58dB over 30nm of bandwidth and reaches over 60dB over 5.5nm of bandwidth.

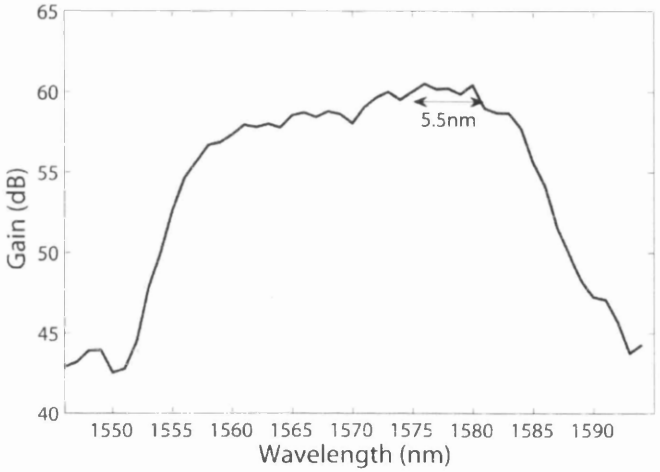

Figure 3.3. The experimental gain spectra of the high-gain OPA. The gain is above 60 dB over 5.5 nm.

3.1.2. High conversion efficiency and complete pump depletion

In addition to providing linear gain to signals, fibre OPAs can have other useful functionality such as wavelength conversion. In wavelength conversion, in contrast to linear amplification, the aim is to strongly deplete the pump power to the signal and the idler in order to obtain strong light sources at the wavelength of the signal and that of the idler.

The desirability of obtaining high power light sources at wavelengths where proper laser source and amplifiers are missing is clear. Employing wavelength conversion in OPAs, pump sources have been obtained at some exotic wavelengths such as 1490 nm in [**8**] and 1640 nm in [**9**]. It is interesting that those sources have been used in constructing other OPAs with extremely broad gain bandwidth [**9**].

In order to describe the evolution of the fields in OPAs under the pump depletion regime, the set of coupled equations presented in section **1.3.3** must be solved again assuming that pump powers may vary with distance owing to depletion. Since it is then possible that the signal and idler powers will become comparable with the pump powers, it is not possible to neglect any terms in the equations. We have the set of equations as:

$$-i\frac{dA_l}{dZ} = |A_l|^2 A_l + 2\sum_{j\neq l=1}^{4} |A_j|^2 A_l + 2\,A_m A_n A_k{}^* e^{i\varepsilon\Delta\beta Z/\gamma}, \quad l = 1-4 \tag{3.3}$$

The solution of this set of equations was obtained first in [**10**]. Here, we present formulation of [**1**] and eliminating the intermediate steps present the results.

If we define θ_k as the phase of A_k so that $A_k = \sqrt{P_k}e^{i\theta_k}$ where P_k is the optical power of the k[th] wave and multiply Eq. (**3.3**) by $A_l{}^*$, we obtain

$$-i\frac{dA_l}{dZ}A_l{}^* = P_l(2P_0 - P_l) + 2\sqrt{P_1P_2P_3P_4}e^{i\varepsilon\theta} \tag{3.4}$$

where $\theta = \Delta\beta z + \theta_3 + \theta_4 - \theta_1 - \theta_2$. Equation (**3.4**) leads to

$$\frac{dA_l}{dZ}A_l{}^* + \frac{dA_l{}^*}{dZ}A_l = \frac{dP_l}{dZ} = 2i\sqrt{P_1P_2P_3P_4}\left(e^{i\varepsilon\theta} - e^{-i\varepsilon\theta}\right) = -4\varepsilon\sqrt{P_1P_2P_3P_4}\sin\theta \tag{3.5}$$

Then we have

$$\frac{dP_1}{dZ} = \frac{dP_2}{dZ} = -\frac{dP_3}{dZ} = -\frac{dP_4}{dZ} = -4\sqrt{P_1P_2P_3P_4}\sin\theta \tag{3.6}$$

From Eq. (**3.6**) it can be concluded that the powers of four waves increase or decrease by a same amount x i.e.

$$P_1 = P_1(0) - x, \qquad P_2 = P_2(0) - x$$
$$P_3 = P_3(0) + x, \qquad P_4 = P_4(0) + x$$

This conclusion is consistent with the fundamental principle that in OPAs pumps lose energy at the same time when the signal and idler absorb exactly that amount of energy.

If we use x as an unknown it can be shown that x(Z) satisfies the differential equation [**1**]

$$dZ = \frac{dx}{2\sqrt{h(x)}} \tag{3.7}$$

where

$$h(x) = 4(P_{10} - x)(P_{20} - x)(P_{30} + x)(P_{40} + x)$$

$$-\frac{1}{4}\left[K_2 - \left(\frac{\Delta\beta}{\gamma} + \Delta P_0\right)x + 2x^2\right]^2 \quad 3.8$$

and $K_2 = 4\sqrt{(P_{10}P_{20}P_{30}P_{40})}\cos(\theta_{30} + \theta_{40} - \theta_{10} - \theta_{20})$.

Equation (**3.7**) has a solution, which is expressible in terms of Jacobian elliptic functions. It is obtained in terms of the four roots of $h(x)$.

In the pump depletion regime the concept of gain is not applicable any longer and in turn conversion efficiency is a relevant quantity, which is basically defined as the ratio of the desired output power to the total input power. The total input power is the sum of the power of pump and signal, while the desired output power is that of the idler:

$$\eta_{\text{eff}} = \frac{P_4}{P_{10} + P_{30}} \quad 3.9$$

3.2. Bandwidth

In this section, we aim to review different aspects of the optical gain spectrum in OPAs as the most important characteristics of an amplifier. In order to do so we will need to investigate the dependence of the gain as expressed in Eq. (**3.1**) on the different parameters i.e. pump power, fibre nonlinearity and the dispersion properties of the fibre, which determine the wavevector mismatch $\Delta\beta$. However, before studying the shape of the gain spectrum it is worth to emphasise the key fact about OPAs that the gain spectrum is extended by increasing the pump power. This was perhaps the most appealing feature of OPAs that created the motivation for extensive investigations of them historically [**11**]. In order to see this we quote a simple yet smart explanation from [**1**]. The maximum gain is obtained when phase mismatch is zero i.e. $= \Delta\beta + \Delta\beta_{NL} = 0$; it is $G_{\text{i,max}}(z) = |\sinh(rz)|^2$. If the signal frequency is changed, the gain drops by an amount that depends only on the parametric gain coefficient g. For instance, for a 3 dB reduction in gain, g needs to be reduced to some value $g' = \delta r < r$. Thus $\Delta\beta$ must change to $\Delta\beta' = 2r\sqrt{1-\delta^2} - \Delta\beta_{\text{NL}}$. Since r and $\Delta\beta_{\text{NL}}$ are proportional to the pump power, $\Delta\beta$

should scale as the pump power as well. As a result, the 3 dB bandwidth of the OPA, expressed in terms of $\Delta\beta$, scales as the pump power. We note that although this reasoning shows generally the possibility of obtaining large bandwidths by increasing the pump power, it is for the case where the fibre and hence the fibre nonlinearity coefficient is assumed to be determined. In other words, the same results can be obtained by increasing γ, provided the dispersion properties remain the same, as the nonlinear phase mismatch is γP.

We now turn our attention to the obtainable gain spectra in OPAs for different cases and try to highlight those topics I looked into more closely during my studies. As it is mentioned before, we pay more attention to the linear gain.

3.2.1. One-pump OPA

In order to investigate the possible shapes of the gain spectrum for one-pump OPAs, it is customary to expand the wavevector mismatch $\Delta\beta$ as a Taylor power series about the pump frequency ω_1:

$$\begin{aligned}\Delta\beta &= \beta(\omega_3) + \beta(\omega_4) - 2\beta(\omega_1)\\ &= \beta(\omega_1) + \sum_{m=1}^{\infty} \frac{\beta^{(m)}}{m!}(\omega_3 - \omega_1)^m\\ &+\beta(\omega_1) + \sum_{m=1}^{\infty} \frac{\beta^{(m)}}{m!}(\omega_4 - \omega_1)^m - 2\beta(\omega_1)\end{aligned}$$

$$= \beta^{(2)}(\omega_3 - \omega_1)^2 + \frac{\beta^{(4)}}{12}(\omega_3 - \omega_1)^4 + \cdots \qquad 3.10$$

In the above equation, $\beta^{(m)}$ denotes the m^{th} derivative of $\beta(\omega)$ evaluated at $\omega_1$and we have considered that $\omega_3 - \omega_1 = -(\omega_4 - \omega_1)$. It is seen that $\Delta\beta$ depends only on the even-order dispersion parameters and not directly on the odd-order ones. Particularly, it means $\Delta\beta$ does not depend on dispersion slope directly.

As seen from Eq. (**3.10**), $\Delta\beta$ is an even function of the pump-signal frequency detuning, which we show by $\Delta\omega_s = \omega_3 - \omega_1$. It means that g, $G_3(z)$ and $G_4(z)$ are all even functions of $\Delta\omega_s$. Hence, the signal and idler gain spectra are symmetric with respect to the centre frequency, albeit if the effect of linear birefringence and Raman gain are not

included. Also the symmetry is lost if one plots gain spectrum versus wavelength difference $\Delta\lambda_s = \lambda_3 - \lambda_1$, which is more preferable in experimental work.

The power series of the Eq. (**3.10**) is useful when it can be truncated after the first few terms so that $\Delta\beta$ is expressed in terms of a polynomial and can be used for studying and optimizing the gain spectrum. The right number of the terms to be kept should be determined with regard to the specific situation of interest. The simplest form is of course when we keep only the first term and write $\Delta\beta = \beta^{(2)}(\Delta\omega_s)^2$, which is suitable for the case when (i) the pump is not too close to ZDW (where by definition $\beta^{(2)} = 0$) and (ii) the frequency detuning is not very large. Here we can conclude another key fact in obtaining large bandwidth in a single-pump OPA. If the value of $\beta^{(2)}$ or equivalently the dispersion parameter D, which is defined as $D = -(2\pi c/\lambda^2)\beta^{(2)}$, is large, small frequency difference between the pump and signal will lead to large $\Delta\beta$, and thus a small gain bandwidth. Therefore, we will want to place the pump very close to λ_0; in practice, this means within a few nanometres. Although one may think that it would be then desirable to make the pump wavelength and the zero-dispersion wavelength to coincide, in which case the next surviving term would be the fourth-order dispersion, i.e. $\Delta\beta = \beta^{(4)}(\Delta\omega_s)^4/12$, in practice it turns out that keeping a small but non-zero value for $\beta^{(2)}$ is helpful in optimizing the spectrum shape. In practice $\beta^{(2)}$ is adjustable almost arbitrarily by adjusting the λ_1 about λ_0. In that region we have $\beta^{(2)} \approx \beta^{(3)}(\omega_1 - \omega_0)$.

With regard to what we mentioned above, we are led to approximate $\Delta\beta$ with two terms as:

$$\Delta\beta = \beta^{(2)}(\Delta\omega_s)^2 + \frac{\beta^{(4)}}{12}(\Delta\omega_s)^4 \qquad 3.11$$

3.2.1.1. Numerical simulations

Having approximated the wavevector mismatch with a suitable polynomial, we can simulate the gain spectrum of an OPA for specific fibre parameters. It is clear that such a simulation would be considering the ideal case only and other effects such as the Raman gain, fibre birefringence and the longitudinal variations of λ_0 must be included appropriately.

In addition, the above mentioned analysis is suitable for simulating the parametric behaviour in such fibres for which the dispersion properties including λ_0 and dispersion

parameters up to 4th order are firstly measurable with a good precision and secondly are adjustable to an acceptable extent. It is currently the situation for silica-based dispersion-shifted fibres (DSFs) and HNLFs. The manufacturing technology for these fibres is advanced and possibilities and limitations are known.

Due to the complex dependence of the gain spectrum of OPAs on dispersion and the large number of variables, the study of possible gain spectra is often confusing. Hence, it is only possible to examine some general properties of obtainable gain spectra unless the properties of the fibre in hand are determined. Provided that λ_0 and $\beta^{(3)}$ are in an appropriate range so that $\beta^{(2)}$ is adjustable, the sign of $\beta^{(4)}$ becomes the factor that determines the general gain shape. Figure **3.4** and Figure **3.5** show the gain spectra for a fibre with realistic parameters and $\beta^{(4)} < 0$ and $\beta^{(4)} > 0$, respectively. The sign of $\beta^{(4)}$ can be readily determined by adjusting the pump wavelength on both side of λ_0 and observing the gain shape.

In [**12**] a method has been proposed by which one can determine the ratio $\beta^{(4)} / \beta^{(3)}$. Since $\beta^{(3)}$ can be determined by other methods, one can then measure $\beta^{(4)}$. In a newly proposed method in [**13**], the chromatic dispersion was determined with a simple arrangement based on FWM efficiency.

In Figure **3.5**, the possibility of obtaining a broad flat-top gain spectrum is interesting, and as such it has been studied in great detail [**14**]. However, this type of gain spectrum is extremely sensitive to pump wavelength (or alternatively to zero-dispersion wavelength), which makes it very difficult to achieve. We attempted to produce such a gain spectrum using a large number of different fibre segments from different fibre spools but unfortunately, it was not successful. Small positive $\beta^{(4)}$ is also very desirable to obtain large bandwidth and has been the subject of some research to tailor $\beta^{(4)}$ both in sign and magnitude. In [**15**] a wavelength conversion range of 193 nm is reported in a fibre with small $\beta^{(4)}$. Such a fibre was also used in [**16**] to obtain 730 nm of gain bandwidth, with pulsed-pump with peak power of the order of 80 W. The measured value for $\beta^{(4)}$ in that experiment was $1.4(\pm 0.4)\times 10^{-56}$ s^4/m.We were given a spool of fibre with a claimed low value for $\beta^{(4)}$ on the same order as in [**16**], which we did not manage to verify. This indicates that still these fibres are difficult to obtain.

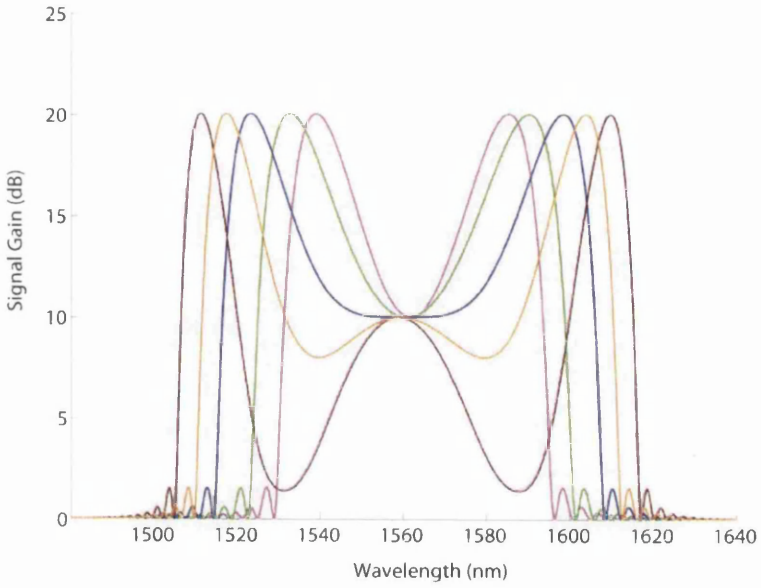

Figure 3.4. The theoretical gain spectrum of a one-pump OPA. The fibre has the parameters γ =15 $W^{-1}km^{-1}$, λ_0 = 1560nm, $\beta^{(3)} = 5.16\times10^{-41}$ s^3/m, $\beta^{(4)} = -5\times10^{-55}$ s^4/m, L = 200 m. The pump power is 1W and λ_p = 1562 nm (Pink), 1561 nm (Green), 1560 nm (Blue), 1559.5 nm (Orange) and 1559 nm (Brown).

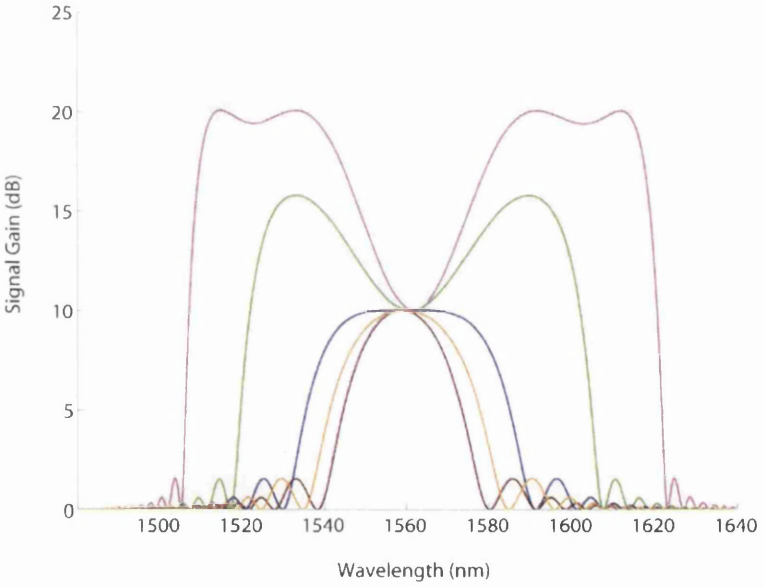

Figure 3.5. Theoretical gain spectrum of a one-pump OPA with identical parameters to Fig. 3.4 and positive $\beta^{(4)}$.

Procedure of the theoretical gain simulations

The theoretical gain simulations presented in figures (3.4)-(3.8) is performed with the Mat-Lab software taking the following steps. Determining the parameters of the fibre and the wavelength and the power of the pump, the linear wavevector mismatch $\Delta\boldsymbol{\beta}$ is

calculated using the appropriate equation, for example Eq.(**3.11**) or Eq.(**3.12**). The nonlinear wavevector mismatch is already in hand by using the equation$\Delta\boldsymbol{\beta_{NL}} = \boldsymbol{2\gamma PL}$. Using these two quantities parametric gain coefficient g is computable from Eq. (**1.36**) for the wavelength range of interest. Making use of the Eq.(**3.1**) the gain is also computable and the gain spectrum is plotted over the wavelength range determined.

3.2.1.2. Narrow-band tunable gain spectra

The complex dependence of gain on dispersion makes it possible to obtain another set of gain spectra, in which a tunable narrowband gain region is created instead of a continuous wideband gain. The word "tunable" refers to the adjustable centre wavelength of the narrowband gain region. This type of gain shape is produced for increased detuning of the pump wavelength from the zero-dispersion wavelength. By doing so the magnitude of $\beta^{(2)}$ increases, which leads to the gain spectrum to break into two separate parts (Figure **3.6** and Figure **3.7**). In principle, this can be done for both $\beta^{(4)} > 0$ and $\beta^{(4)} < 0$ cases, but the pump wavelength is required to be placed in the anomalous or normal dispersion region, respectively. Some proposed potential applications for this type of gain spectrum include selective wavelength conversion [**17**], filtering with gain, tunable narrowband amplification etc.

This regime was first investigated in [**18**]. The width of the narrow gain region is decreased by moving it further away from the pump. However, random longitudinal variation of λ_0 will cause the gain region to broaden and the peak gain to drop. Nevertheless, a relatively narrow gain can still be produced [**17**], [**18**].

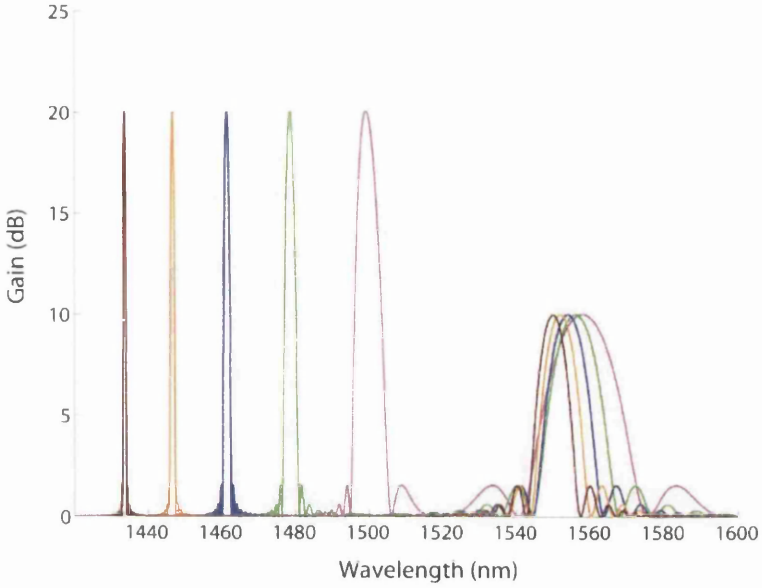

Figure 3.6. Gain spectrum of a one-pump OPA at distant region from the pump for negative $\beta^{(4)}$. The parameters are identical to Fig. 3.4 and λ_p = 1562 nm (Pink), 1564 nm (Green), 1566 nm (Blue), 1568 nm (Orange) and 1570 nm (Brown).

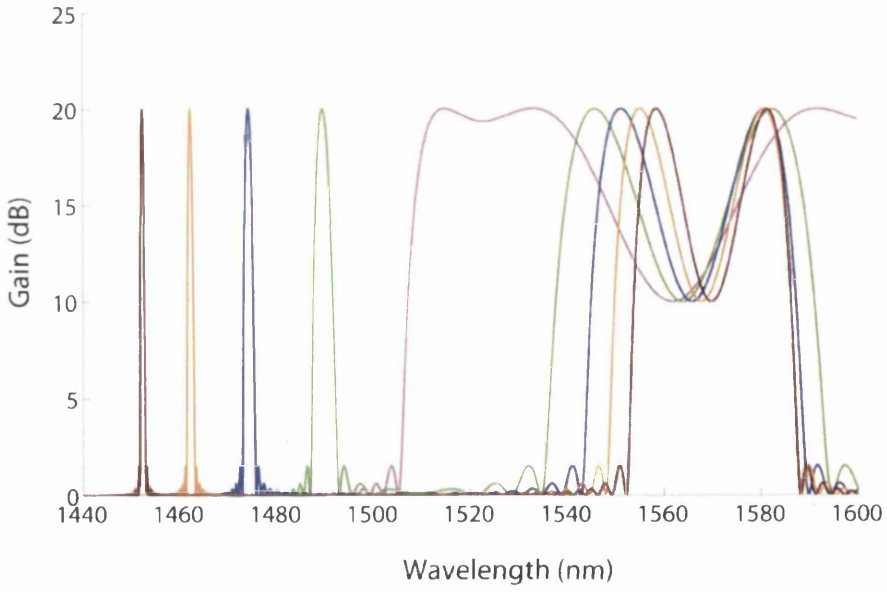

Figure 3.7. Gain spectrum of a one-pump OPA at distant region from the pump for positive $\beta^{(4)}$. The parameters are identical to Fig. 3.4 and λ_p = 1558 nm (Pink), 1556 nm (Green), 1554 nm (Blue), 1552 nm (Orange) and 1550 nm (Brown).

3.2.1.3. Gain flattening of one-pump OPAs

From the simulations and sample gain shapes presented so far, it is seen that it is often difficult to obtain a flat gain spectrum in one-pump OPAs. On the other hand, as seen from Figure **3.4** and Figure **3.5** there are two different types of gain spectra, more specifically, one group exhibits two symmetrical peaks and another has a single peak. It seems then logical to consider combining the two types of gain shapes by using two fibres with different ZDWs, for example, to obtain a flat gain. It should be noted that the total gain spectra is not simply the sum (in dB) of the two individual gain spectra. This is because OPAs are phase sensitive devices, and therefore, the gain in the second stage will be dependent on the phase of the fields emerging from the first section. Nonetheless, one still can assume that the same pump passes through two consecutive segments that have different ZDWs. This can be realised by splicing the two segments.

The idea could be extended to more than two segments so that one could suppress the ripples better. It has been shown that by using four segments a sufficiently flat gain is achievable [**19**]. The parameters in [**19**] were obtained by trial and error, however, one could in principle develop more systematic methods for optimisation the different parameters of the segments [**20**]. Although such a method for the design of flat-gain OPAs is attractive, no practical demonstration was reported until recently. The main reason is the difficulty of finding four segments with suitable ZDWs. However, by making use of the method introduced in [**21**] for obtaining a high-resolution dispersion map of the fibre, it has become possible to obtain flat gain spectra experimentally [**22**] using multi-section design.

3.2.2. Fibres with constant linear birefringence

In a one-pump OPA, the existence of a constant linear birefringence provides another means to produce narrow gain regions distant from the pump similar to what was mentioned in the previous section. Indeed, the possibility of creating such narrow gain regions with this approach was examined in some of the earliest OPA work in fibres [**1**] and was used to generate light at new wavelengths. In this arrangement, the pump and the signal are aligned with the axis of birefringence of the fibre.

In order to simulate and study the achievable gain spectrum, one should modify the expression of wavevector mismatch Eq. (**3.11**) to include the birefringence as:

$$\Delta\beta = \beta^{(2)}(\Delta\omega_s)^2 + \frac{\beta^{(4)}}{12}(\Delta\omega_s)^4 + 2\Delta n\frac{\omega_1}{c} \qquad 3.12$$

where, Δn is birefringence and the difference between the dispersion parameters of the two axes of birefringence is neglected. The sign of Δn is determined considering if the pump is aligned to slow or the fast axis and should be of the right sign for the intended phase matching to occur. The distance of the gain region from the pump, $\Delta\omega_g$, can be calculated by letting $\Delta\beta = 0$ in Eq.(**3.12**); this leads to

$$(\Delta\omega_g)^2 = \frac{6}{\beta^{(4)}}\left[-\beta^{(2)} \pm \sqrt{(\beta^{(2)})^2 - \frac{4\pi}{3}\frac{\beta^{(4)}\Delta n}{c\lambda_1}}\right] \qquad 3.13$$

It should be noted that the last term in Eq. (**3.12**) is much larger than the other terms when the frequency excursion is not large. Indeed, this is the reason behind why the gain regions are produced at a large distance from the pump and that they are narrow. To see this, let us assume that the birefringence is only $\Delta n = 10^{-5}$. Then the last term in the expression of $\Delta\beta$ for the pump wavelength λ_1=1550 nm is 80.07 m^{-1}. If we assume the values used in the previous section for the fibre parameters i.e. λ_0=1560 nm, $\beta^{(3)} = 5.15\times10^{-41}$ s^3m^{-1}, $\beta^{(4)} = -5\times10^{-55}$ s^4m^{-1} and $\gamma = 15$ $W^{-1}km^{-1}$, the first and the second terms for $\Delta\lambda_s = (\lambda_3 - \lambda_1) = 50$ nm are only 0.6610 m^{-1} and –0.1125 m^{-1}, respectively. It is seen that dispersion contribution to $\Delta\beta$ is very small compared to that of birefringence. Moreover, as in this arrangement the SOP of the signal and the pump are orthogonal the effective nonlinear coefficient would be $\gamma/3 = 5$ $W^{-1}km^{-1}$. Therefore, even if the pump power were 200 W the nonlinear phase mismatch would be only 2 m^{-1}. As a result, the frequency excursion, $\Delta\omega_s$, must be very large to counterbalance the mismatch from birefringence (the distance of the gain region will be large). Also considering that the gain in an OPA is only available for $-4\gamma P > \Delta\beta > 0$, when $\Delta\omega_s$ is a large value, small changes in signal frequency (wavelength) are sufficient for $\Delta\beta$ to fall out of that region. In other words, the slope of $\Delta\beta$ is large as $\Delta\beta$ passes through zero. Hence, the width of the gain region would be small. In addition, as we saw that even for very large pump powers the nonlinear phase mismatch is very small compared to birefringence, and as a result, the pump power has an incremental influence on the bandwidth. Figure **3.8**

shows the theoretical gain spectrum available using the figures mentioned above for the various parameters.

It is seen that by changing the sign of birefringence and dispersion quite different gain spectra are produced in terms of the location. The width remains small unless such a pump wavelength is chosen to have a finite $\beta^{(2)}$. Then it is possible to reduce the slope of $\Delta\beta$ and achieve a flat-top gain. The possibility of creating two gain peaks is also interesting. In addition, if it is desired to pull the gain region close to the pump, one should look for fibres with large dispersion slope.

Although the gain spectra introduced in this section are appealing, it is seen that in order to obtain such gains in HNLFs one needs a very high pump power, which indicates that pulsed pump must be used. In Chapter **5**, we will introduce experimental observation of such gain regions in a bismuth-oxide fibre, which has a much larger value for γ, and hence, the required pump power is much smaller. In addition, the very large dispersion in that type of fibre makes it possible to observe the gain regions at very smaller distances (about 30 nm) from the pump.

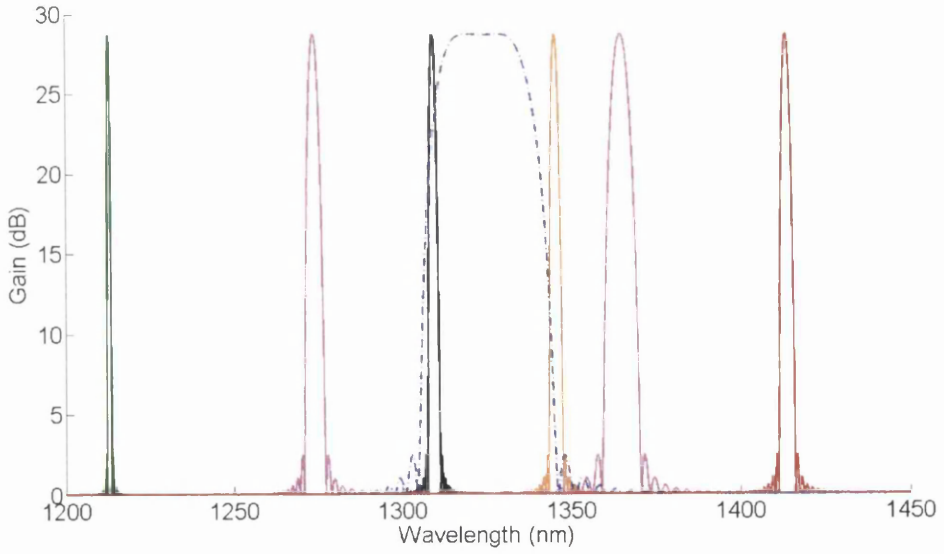

Figure 3.8. Theoretical gain spectra in the presence of birefringence. For black (λ_1=1550 nm) and orange (λ_1=1570 nm) curves $\Delta n = 10^{-5}$, $\beta^{(3)} = 5.15\times10^{-41}$ s^3m^{-1}. For green (λ_1=1550 nm) and brown (λ_1=1570 nm) curves $\Delta n = 10^{-5}$, $\beta^{(3)} = 5.15\times10^{-40}$ s^3m^{-1}. For pink (λ_1=1550 nm) and blue-dot-dash (λ_1=1551 nm) curves $\Delta n = -10^{-5}$, $\beta^{(3)} = 5.15\times10^{-40}$ s^3m^{-1}. P = 200 W, L = 3 m, $\beta^{(4)} = -5\times10^{-55}$ s^4m^{-1} and γ = 15 $W^{-1}km^{-1}$.

3.2.3. Influence of dispersion fluctuations on the gain spectra

In the discussions and examples of the preceding sections, we assumed that the ZDW is unchanging along the entire length of the fibre. In addition, from the examples it is understood that the gain spectra of an OPA can be greatly altered if the pump wavelength varies. In some conditions small variations as little as 0.1 nm can strongly affect the gain spectra. Therefore, it is not unexpected that if the pump wavelength is fixed but the ZDW of the fibre drifts by such an amount then the spectrum will be affected for the same reason, and the expected gain shape and bandwidth will not be achieved.

The ZDW of any optical fibre is not precisely uniform and varies randomly along its length. This is due to finite precision achievable in controlling variables such as refractive index profile, the quantity and homogeneity of dopant and more importantly the core diameter in the perform and draw process like any other physical process. The problem would be understood better if we note that only ± 0.03 % fluctuation in the core diameter translates to about 1 nm variation in the ZDW [**23**]. On the other hand, 0.03 % of the core diameter for HNLF (4 μm) is 1.2 nm. Silica is formed of a 6-fold ring molecular structure and the dimension of the rings is about 0.6 nm. Therefore, in order to control the ZDW within 1 nm, one needs to control the core diameter within the dimensions of molecular rings of silica! This implies that such undesired longitudinal variations will be unavoidably present in any fibre to some extent. Besides distortions of the gain spectrum induced by random fluctuations of the ZDW of the fibre and limitations in achieving the desired bandwidth, such impairment greatly exacerbates the problem of crosstalk in OPAs (Chapter **4**).

The problem of longitudinal variations of the ZDW and consequently the dispersion parameter was soon considered as a topic for thorough investigations. In 1998, Karlsson attempted to model the gain distortions by a random ZDW [**24**]. Farahmand et al revised and completed the model in 2004 [**25**]. In that model, two different cases were considered for the variations of ZDW; one assumed a continuous drift with a Gaussian distribution and in the other the ZDW was assumed constant over short pieces and the magnitude was chosen from a Poisson distribution. The evolution of the fields in the segments of the fibre was then calculated by means of a matrix approach, similar to what was mentioned in the context of gain flattening of one-pump OPAs, so that the

final fields could be obtained. Such a simulation revealed interesting results. The variation of the gain was shown to be insensitive to the model details. Moreover, the variations over a considerable length (compared with a defined correlation length) were shown to be most influential, while very fast fluctuations were proved not affective.

In addition to numerical simulations, experimental verification of the adverse influence of ZDW fluctuations were performed [**26**]. Also, many researchers became interested in mapping the ZDW or equivalently the dispersion parameter along the fibre length. In fact, dispersion mapping techniques were first considered and developed in order to resolve transmission problems and soliton propagation, among which the Mollenauer technique was the most successful [**27**]. However, most of those techniques had a low resolution and were suitable for conventional SMF, which has a relatively large dispersion at 1550 nm. In [**28**] a method was proposed to map ZDW of HNLFs with short lengths, which required a large amount of computational task. In [**21**], an elegant approach was proposed and implemented based on localized four-photon mixing. The method is capable of mapping the dispersion of the fibre with a one-metre resolution for HNLFs with small dispersion of the order 0.01 ps/nm/km. This method is the most powerful one to date but needs quiet a complex set up.

Despite all efforts to map dispersion fluctuations and to model their effect, no successful measure has been proposed to mitigate this problem except for some technique that only partly improve the situation, such as cutting the fibre in pieces and rearranging them [**29**]. Hence, it is a technical matter to be solved by fibre producers to deliver fibres with uniform dispersion properties.

3.3. Broadband OPAs and the problem of Raman gain

In the preceding sections, we discussed some very general and key aspects of the gain spectrum of OPAs and saw that OPAs can provide very broad gain bandwidth provided a fibre with right nonlinearity and dispersion characteristics and a high-power pump are available. The availability of such highly-nonlinear fibres and high-power EDFAs used to pump the OPAs are quite recent, and hence, demonstrating wideband OPAs specifically in the CW regime are interesting experiments. Previously, experiments with OPAs normally required pulsed pumps and very long lengths of conventional dispersion shifted fibres (DSFs).

Using a pulsed pump a one-pump OPA with bandwidth of 400 nm was reported in 2007 [**18**]. In the CW regime, OPAs with a gain between 10 and 13 dB over 100 nm were reported [**30**]. Boggio et al demonstrated two interesting OPAs in 2008 [**16**] and 2009 [**9**] showing the remarkable capability of OPAs. In [**16**], a one-pump OPA in the pulsed regime was demonstrated with 730 nm of bandwidth, extending from 1300 nm to 2030nm. It was achieved using a pump with 200 W of peak power. In [**9**] a two-pump OPA was reported with 155 nm of bandwidth, which was operating in the CW regime.

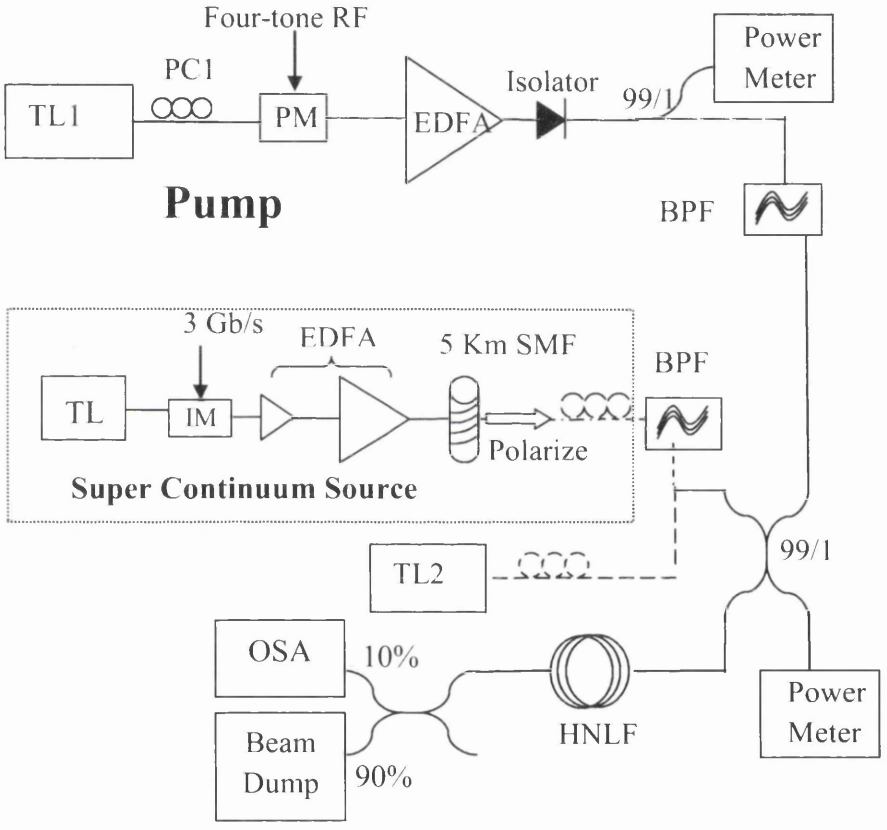

Figure 3.9. Experimental setup for the one-pump OPA. The inset shows the setup for supercontinuum generation.

These figures are more appealing if we consider that the achievable bandwidth of EDFAs is only about 32 nm. However, for such broadband OPAs the mutual interaction of Raman and parametric gain adversely affects the flatness of the gain spectrum and reduces their usefulness as briefly mentioned in section **2.1**.

In the following, we present our results on constructing a one-pump CW OPA with 230 nm of bandwidth, which we then increased up to 270 nm.

3.3.1. CW one-pump OPA with 270 nm bandwidth[2]

3.3.1.1. Experimental setup

The experiment set up is shown in Figure 3.9. For the pump a tunable-laser (TL1) is first phase-modulated in order to suppress the SBS. It is then amplified by a high-power EDFA with 10 W of CW output. A specific isolator capable of handling 10 W CW power is placed after the EDFA to protect it from any back-reflections. One percent of the pump is split for power monitoring. The ASE of the EDFA is rejected by a dual-stage band-pass filter (BPF) with 1 nm of pass band. The pump beam is then injected into the HNLF through a 20 dB coupler. The HNLF is 114-m long and has a nonlinear coefficient of 15 $W^{-1}km^{-1}$. The signal is obtained from another tunable-laser source (TL2) in the range of 1460-1640 nm. The output of the HNLF is separated into a high-power and a low-power branch. The high-power arm is terminated with a beam-dump. The other branch is directed into an OSA for analysis.

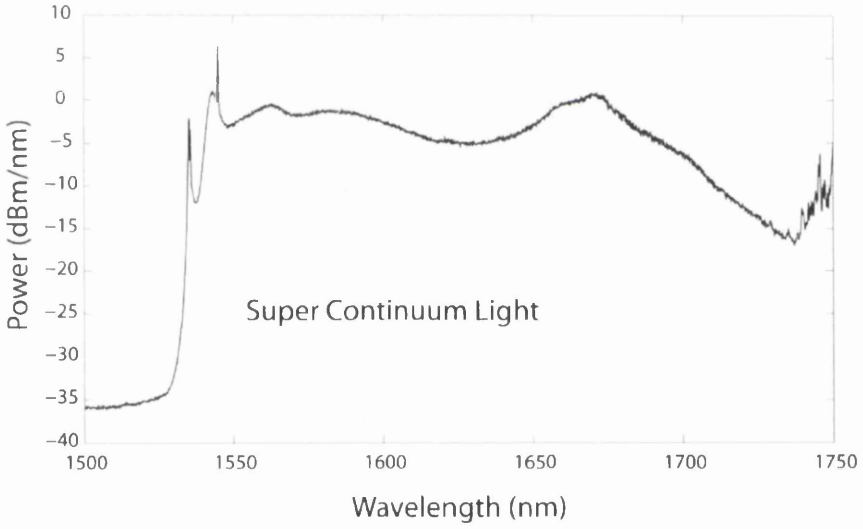

Figure 3.10. The continuum expanded from 1550 nm to 1750 nm. The intensity reaches 1 mW.

3.3.1.2. A simple light source for the wavelength range 1550 nm-1750 nm

The laser sources available in academic laboratories are usually commercially available sources, which extend from 1460 nm to 1640 nm. Due to this limitation, at least in the

[2] This experiment was fully performed by me. The initial idea was decided with the help from Dr. Armand Vedadi and Prof. M. E. Marhic.

context of OPAs to my knowledge, actual gain measurements beyond 1640 nm have never been performed.

In an attempt to obtain some source of light beyond 1640 nm, we tried generating a supercontinuum in a conventional single-mode fibre (SMF), which is inexpensively available. We prepared pulses with rectangular shape modulated at 10 GHz with 1/256 duty-cycle and amplified them to 20 W peak power. Injecting such pulses into a spool of SMF, which was 5 km long, we obtained a quite flat supercontinuum with acceptable brightness of about 0 dBm/nm (maximum). We filtered the output spectrum at different wavelengths and using a polariser, we obtained a useful polarised light, which we used for actual gain measurement beyond 1640 nm. The inset in Figure 3.9 shows the set-up and the output light spectrum is shown in Figure 3.10. For filtering we used the built-in grating filter existing in any optical spectrum analyser (OSA). One interesting possibility was to use a fibre coupler and change the set-up into an optical oscillator from which a very bright output could be obtained. However, due to very large loss of the filter this set-up was only useful for a narrow wavelength range between 1650 nm to 1675 nm.

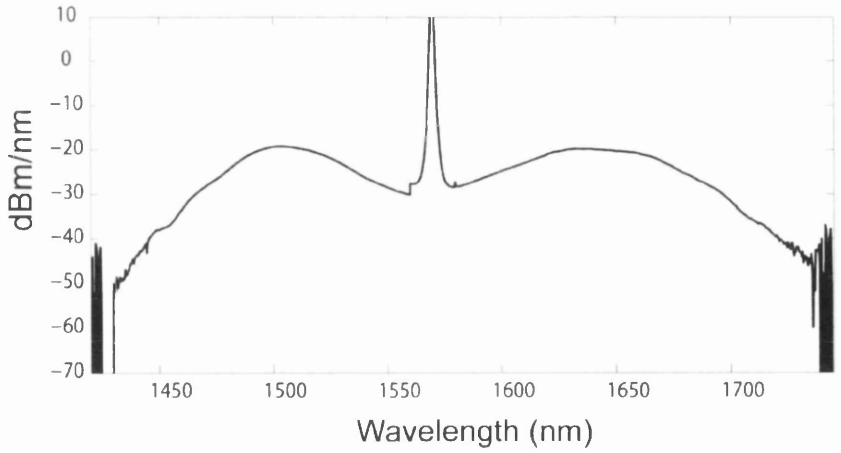

Figure 3.11. The optical spectrum of the ASE of the one-pump OPA. It expands over nearly 300 nm.

3.3.1.3. Results and discussion

Observing the ASE spectrum of an OPA is a convenient and simple step in optimizing the gain spectrum of the OPA, since it is an indication of where actual gain is available [**1**]. We first operated the OPA with no input signal. Figure 3.11 shows the ASE spectrum, which spans a wide range of nearly 300 nm. As it is seen, the spectrum is

wider on the Stokes side of the pump. This is mainly due to the asymmetry of the gain plot versus wavelength and partly because of the Raman gain.

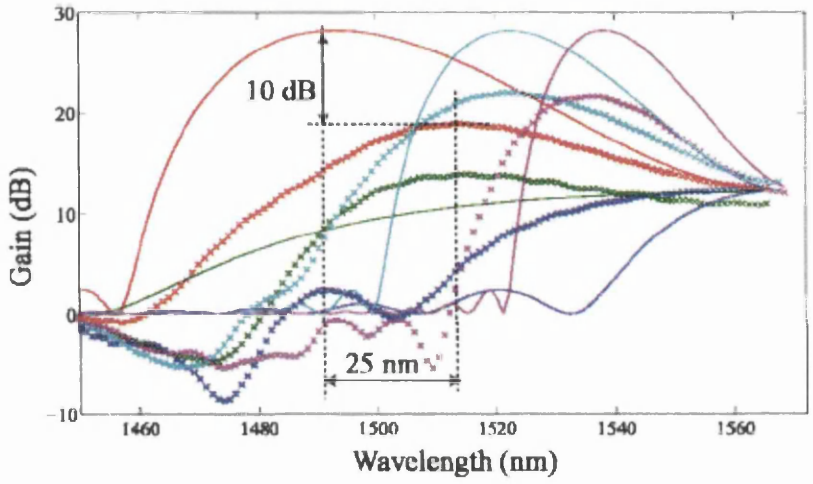

Figure 3.12. Experimental (star) and theoretical (solid) parametric gain spectra for λ_p = 1567 nm (blue), 1568 nm (Green), 1569 (Red), 1570 nm (Cyan) and 1572 nm (Purple).

We then recorded several gain spectra for different pump wavelengths, as shown in Figure 3.12. The theoretical parametric gain is also plotted for each wavelength. As it is seen the gain bandwidth never reaches the expected value and there is a large inconsistency between the theoretical and experimental curves. In addition, for large signal-pump detunings the measured gain drops below 0 dB. Since the parametric gain can never have a negative value, it is apparent that the negative gain is because of the Raman effect, which shows up as a loss. In other words, a signal placed at a large distance (about 100 nm) from the pump acts as a Raman pump for the pump of the OPA through the Raman effect. The net result of receiving energy via parametric gain and delivering energy through the Raman effect is a loss. Thus, the Raman gain adversely affects the expected gain bandwidth at the Stokes side as seen in this experiment. Considering the fact that the Raman effect would act in the opposite direction on the Stokes side, one would conclude it will add to the gain on that side. In that experiment we observed 230 nm of bandwidth. We performed numerical simulations including the Raman gain using the Raman susceptibility as seen in Figure 3.13. The simulations show a good agreement between the numerical and the experimental results.

As we mentioned in Chapter **2**, the Raman gain almost vanishes for the case where the signal and the pump have orthogonal SOPs, specifically for signal-pump detunings

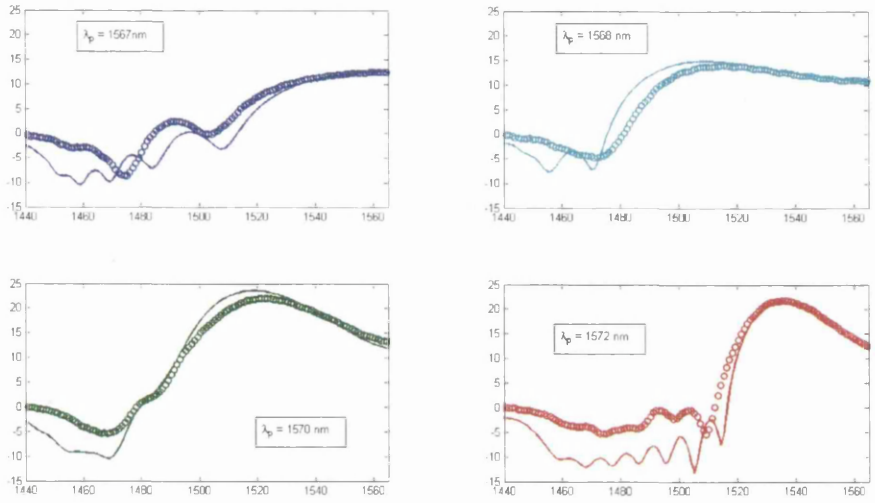

Figure 3.13. Experimental gain curve (circles) and numerical simulations (lines) including the Raman gain. Simulations match well with experimental results.

between 15 THz and 20 THz. On the other hand, the parametric gain exists for linear and orthogonal signal and pump SOPs, although it is very small. Guided by this intuition, we were led to try to cancel the negative gain seen in our experiments by altering the SOP of the signal which normally is adjusted to be parallel with that of the pump in OPA experiments to obtain the maximum gain. Our observations showed that by finely tuning the pump wavelength it was possible to bring the negative part of the gain spectrum above 0 dB. This resulted in a positive and actual gain over an additional 30 nm and yielded 270 nm of bandwidth. Figure **3.14** shows this situation, where the gain spectra are plotted for λ_0 = 1570.33 nm and for different signal SOPs. It is seen in solid curve, which corresponds to the SOP of the signal for which the gain at 1460 nm is maximum, that the gain at that wavelength can be positive. It is apparent that the amount of the gain in that region is not such to be considered as a genuine capability of the OPA. The aim is rather to show that it is possible to use the idea to add to the flatness of the gain spectra of very broadband amplifiers. The amount of the gain was not large in that region anyway since the phase-matching for parametric gain is not achieved. The other two curves correspond to the cases in which the SOP of the signal was adjusted to attain maximum gain at 1520 nm (doted curve) and 1640 nm (dot-dashed curve). It is seen that, as we mentioned in section **2.3.1** for very broadband

amplifiers, the drift of SOP can be significant due to the residual random birefringence of the fibre.

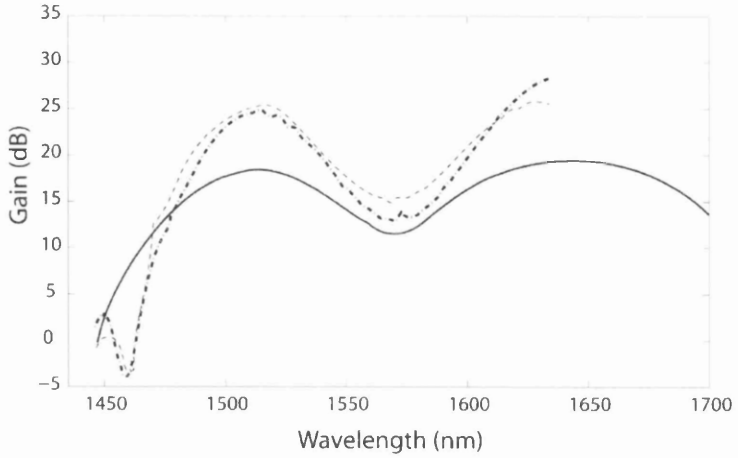

Figure 3.14. Experimental gain curve for λ_P = 1570.33 nm and different signal SOPs.

Summary

In this chapter, we discussed two important aspects of amplifiers, namely, the gain and the bandwidth in OPAs. We mentioned that OPAs are capable of providing very large amount of gain. OPAs with gain of 70 dB have been reported. A two-pump OPA with a record gain of about 60 dB over 30 nm and the experimental description was presented. OPAs are most attractive for being able to provide huge gain bandwidth besides the high gain.

The shape and bandwidth of gain spectrum of OPAs are dependent on various parameters i.e. pump power, fibre nonlinearity coefficient and dispersion properties of the fibre. The complicated dependency of the gain spectrum of OPAs on the wavevector mismatch, $\Delta\beta$, makes it possible to achieve very different gain spectra with OPAs. One interesting possibility is to generate very narrow gain regions at distant regions from the pump. This can be achieved by detuning the pump further and further away from the ZDW. Another means to do that is by making use of fibres with constant linear birefringence.

Different classes of gain spectra achievable in one-pump OPAs were introduced by presenting simulations.

Finally, the description of an experiment reporting a continuous-wave one-pump with a record bandwidth of 270 nm was presented. The problem of the Raman gain introduced and discussed in Chapter **2** is shown to be partially removable by deliberately misaligning the SOP of the signal and that of the pump.

It is experimental shown that although in this case the gain would not be maximum but the problem of the Raman gain can be weakened. This may be considered in very broadband OPAs to improve the smoothness of the gain spectrum.

References

[1] M. E. Marhic, *Fiber Optical Parametric Amplifiers, Oscillators and Related Devices*. United Kingdom: Cambridge University Press, 2008.

[2] T. Torounidis, P. A. Andrekson, B. E. Olsson, "Fiber-optical parametric amplifier with 70-dB gain," *IEEE Photon. Technol. Lett.*, vol. 18, pp. 1194-1196, 2006.

[3] S. L. Hansen, K. Dybdal, and C. C. Larsen, "Gain limit in erbium-doped fiber amplifiers due to internal Rayleigh scattering," *IEEE Photon. Technol. Lett.*, vol. 4, pp. 559–561, 1992.

[4] J. Hansryd, and P. A. Andrekson, "Broad-band continuous-wave-pumped fiber optical parametric amplifier with 49-dB gain and wavelength-conversion efficiency," *IEEE Photon. Technol. Lett.*, vol. 13, pp. 194–196, 2001.

[5] K. K. Y. Wong, K. Shimizu, K. Uesaka, G. Kalogerakis, M. E. Marhic, and L. G. Kazovsky, "Continuous-wave fiber optical parametric amplifier with 60-db gain using a novel two-segment design," *IEEE Photon. Technol. Lett.*, vol. 15, pp. 1707–1709, 2003.

[6] S. Radic, C. J. McKinstrie, R. M. Jopson, J. C. Centanni, Q. Lin, and G. P. Agrawal, "Record performance of parametric amplifier constructed with highly nonlinear fibre," *Electron. Lett.*, vol. 39, pp. 838–839, 2003.

[7] R. Jiang, N. Alic, C. McKinstrie, and S. Radic, "Two-pump parametric amplifier with 40dB of equalized continuous gain over 50nm," in *Optical Fiber Communication Conference (OFC)*, Anaheim, CA, 25-29 March 2007, paper OWB2.

[8] J. M. C. Boggio, C. Lundström, J. Yang, H. Sunnerud, and P. A. Andrekson, "Double-pumped FOPA with 40 dB flat gain over 81 nm bandwidth," in *European Conference on Optical Communication (ECOC)*, Brussels, 21-25 Sept.2008, Paper Tu.3B5.

[9] J. M. C. Boggio, S. Moro, E. Myslivets, J. R. Windmiller, N. Alic, and S. Radic, "155-nm continuous-wave two-pump parametric amplification," *IEEE Photon. Technol. Lett.*, vol. 21, 612–614, 2009.

[10] Y. Chen and A. Snyder, "Four-photon parametric mixing in optical fibers: effect of pump depletion," *Opt. Lett.*, vol. 14, pp. 87-89, 1989.

[11] J. Hansryd, P. A. Anderson, M. Westlund, J. Li, and P. Hedekvist, "Fiber-based optical parametric amplifiers and their applications," *IEEE J. Select.Topics Quantum Electron,* vol. 8, pp. 506–520, 2002.

[12] J. M. Chávez Boggio, and H. L. Fragnito, "Simple four-wave-mixing-based method for measuring the ratio between the third- and fourth-order dispersion in optical fibers," J. *Opt. Soc. Am. B.*, vol. 24, 2007.

[13] M. Hirano, and T. Sasaki ," Straightforward Chromatic Dispersion Measurement Based on Phase Mismatching FWM," in *Optical Fiber Communication Conference (OFC)*, Vienna, Austria, 20-24 Sept. 2009, paper 4.1.6.

[14] C. Floridia, M. L. Sundheimer, L. S. Menezes, and A. S. L. Gomes, "Optimization of spectrally flat and broadband single-pump fiber optic parametric amplifiers," *Opt. Commun.*, vol. 223, pp. 381-388, 2003.

[15] M. Hirano, T. Nakanishi, T. Okuno, and M. Onishi, "Broadband wavelength conversion over 193-nm by HNL-DSF improving higher-order dispersion performance," in *European Conference on Optical Communication (ECOC)*, Glasgow, U.K., 25-29 Sept. 2005, Paper Th 4AA.

[16] J. Chavez Boggio, J. Windmiller, M. Knutzen, R. Jiang, C. Bres, N. Alic, B. Stossel, K. Rottwitt, and S. Radic, "730-nm optical parametric conversion from near- to short-wave infrared band," *Opt. Express.*, vol. 16, pp. 5435-5443 , 2008.

[17] M. Hirano, T. Nakanishi, T. Okunko, and M. Onishi, "Selective FWM-based wavelength conversion realized by highly nonlinear fiber," in *European Conference on Optical Communication (ECOC)*, Cannes, France, Sep. 2006.

[18] M. E. Marhic, K. Y. K. Wong, and L. G. Kazovsky, "Wide-band tuning of the gain spectra of one-pump fiber optical parametric amplifiers," *IEEE. J. Sel. Topics Quantum Electron.,* vol. 10, pp. 1133–1141, 2004.

[19] L. Provino, A. Mussot, E. Lantz, T. Sylvestre, and H. Maillote, "Broad-band and flat parametric amplifiers with a multi-section dispersion-tailored nonlinear fiber arrangement," *J. Opt. Soc. Am. B.*, vol. 20, pp. 1532-1539, 2003.

[20] M. Gao, C. Jiang, W. Hu, and J. Wang, "Optimized design of two-pump fiber optical parametric amplifier with two-section nonlinear fibers using genetic algorithm," *Opt. Express.*, vol. 12, pp. 5603-5613, 2004.

[21] E. Myslivets, N. Alic, T. Nakanishi, T. Okuno, M. Hirano, M. Onishi and S. Radic, "High Resolution Measurement of Nearly Dispersionless Fiber by Localized Four Photon Mixing," in *Optical Fiber Communication Conference (OFC)*, San Diego, California, 24 Feb.2008, paper PDP11.

[22] S. Moro, E. Myslivets, J. R. Windmiller, N. Alic, J. M. Chavez Boggio, and S. Radic, "Synthesis of equalized broadband parametric gain by localized dispersion mapping," *IEEE Photon. Technol. Lett.*, vol.20, pp.1971-1973, 2008.

[23] T. Okuno, T. Nakanishi, M. Hirano, and M. Onishi, "Practical considerations for the application of highly nonlinear fibers," in *Optical Fiber Communication conference (OFC) and the national fiber optic engineers conference (NFOEC)*, Anaheim, CA, 25-29 March 2007, paper OTuJ1.

[24] M. Karlsson, "Four-wave mixing in fibers with randomly varying zero-dispersion wavelength," *J. Opt. Soc. Am. B.*, vol. 15, pp. 2269-2275, 1998.

[25] M. Farahmand and M. de Sterke, "Parametric amplification in presence of dispersion fluctuations," *Opt. Express.*, vol. 12, pp. 136-142, 2004.

[26] F. Yaman, Q. Lin, S. Radic and G. P. Agrawal , "Impact of dispersion fluctuations on dual-pump fiber-optic parametric amplifiers," *IEEE Photon. Technol. Lett.*, vol.16, pp.1292-1294, 2004.

[27] L. Mollenauer, P. Mamyshev, and M. Neubelt, "Method for facile and accurate measurement of optical fiber dispersion maps," *Opt. Lett.*, vol. 21, pp. 1724-1726, 1996.

[28] A. Mussot, E. Lantz, A. Durecu-Legrand, C. Simonneau, D. Bayart, T. Sylvestre, and H. Maillotte, "Zero-dispersion wavelength mapping in short single-mode optical fibers using parametric amplification," *IEEE Photon. Technol. Lett.*, vol. 18, pp. 22–24, 2006.

[29] K. Inoue, "Arrangement of fiber pieces for a wide wavelength conversion range by fiber four-wave mixing," *Opt. Lett.*, vol. 19, pp. 1189-1191, 1994.

[30] T. Torounidis, and P. Andrekson, "Broadband Single-Pumped Fiber-Optic Parametric Amplifiers", *IEEE Photon. Technol. Lett.* Vol. 19, pp. 650, 2007.

[31] G. P. Agrawal, *Nonlinear Fiber Optics*. 4th Ed. United States of America: Academic press, 2007.

Chapter 4. Nonlinear Crosstalk

"In telecommunications, crosstalk is any phenomenon by which a signal transmitted on one circuit or a channel of a transmission system creates an *undesired* effect in another circuit or channel [**1**]." As understood from this quotation, crosstalk is a very general concept in telecommunications, and of course is a source of difficulties. Almost every transmission technology suffers from some sort of crosstalk generated by different causes. In wired communication systems, crosstalk due to capacitive, inductive or conductive coupling causes leakage from one channel to another. In wireless systems, crosstalk appears by co-channel and adjacent-channel interference.

Optical communication systems are subject to crosstalk-induced issues as well. Indeed, the types and origins of crosstalk in optical communication systems are much more complicated. Crosstalk is more of a severe problem in WDM and DWDM systems where quite a large number of channels are transmitted over a single fibre, in the hope that they would arrive to receivers with minimal distortion. Nevertheless, in single carrier TDM systems crosstalk can still happen.

The most important kind of crosstalk in optical communications is due to energy transfer mechanisms from one electromagnetic wave to another mediated by various nonlinear processes named in the preceding chapters. They can be categorised under the general name of nonlinear crosstalk. However, apart from nonlinearity-induced crosstalk, even for perfectly linear systems, crosstalk can arise as a result of imperfections of optical components. This type of crosstalk is referred to as linear crosstalk and can be classified into two categories: heterowavelength and homowavelength crosstalk [**1**]. The cause of this type of crosstalk is the imperfect nature of various WDM components in the sense that they do not ideally separate and direct individual channels to the determined routes. Residual power leaked from other

channels at different wavelengths (heterowavelength crosstalk) or at identical wavelength (homowavelength crosstalk) is added to the power of a specific channel resulting in producing crosstalk and degradation of that channel.

Nonlinear crosstalk can originate from different phenomena, and thus it can be classified and studied with respect to its origin. Stimulated Raman scattering transfers energy from waves at higher frequencies to those at lower frequencies. As a result, high-frequency channels lose energy while low-frequency channels gain energy. The process transforms the modulation of the channels and thus causes crosstalk. More specifically, in the case of amplitude modulation the energy transfer takes place only when the energy delivering and receiving channels are at logical "1" states. It is then clear that the both interacting channels will obtain some unwanted modulation of amplitude. In the same manner, stimulated Brillouin scattering can give rise to some crosstalk. However, in the case of SBS, the very narrow gain spectrum of the interaction makes it quite easy to avoid the problems. Cross-phase modulation is another source of crosstalk in lightwave systems. The process can be readily understood by considering the nature of XPM. Other channels can alter the phase of the pulse of a channel. Phase shifts of random nature can then be converted to intensity variations via dispersion and make distortions in the original modulation of the channel [**1**], [**2**].

Although all the named sources of crosstalk are important enough to be considered when designing optical transmission systems, the most important source of crosstalk is the crosstalk arising from four-wave mixing. The waves generated by the FWM process between any two (degenerate) or three (non-degenerate) channels can coincide with other channels at the same wavelength and give rise to crosstalk.

In OPAs, specific conditions exacerbate the problem of FWM-induced crosstalk. Hence, this type of crosstalk has put serious doubts on the usefulness of OPAs in WDM systems. In the following sections of this chapter we review this issue and present some results we have obtained, which may tone down the negative comments on OPAs.

4.1. Four-wave mixing crosstalk in OPAs

Four-wave mixing crosstalk in WDM systems is a cause for concern as it can grow to large values and degrade the quality of signal (measured by SNR). However, what

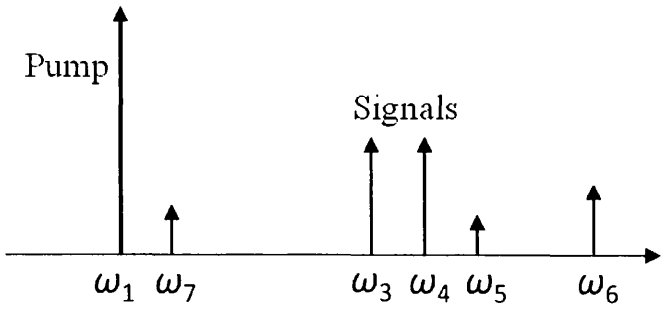

Figure 4.1. Spurious FWM in a one-pump arrangement: ω_5 is due to signal-signal interaction and ω_6 and ω_7 are due to pump-signal interaction. (After Ref [3]).

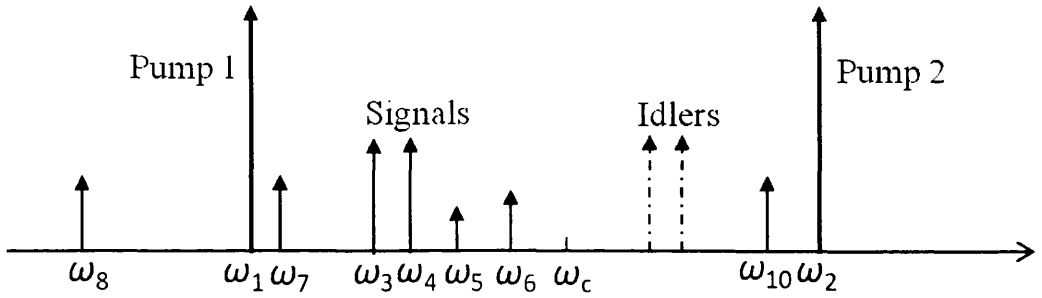

Figure 4.2. Spurious FWM in a two-pump arrangement: ω_{10} is the idler of ω_7 the FWM between the idlers and Pump2. (After Ref [3]).

makes the situation less harmful in transmission systems is: (i) the relatively low power levels of WDM channels limited by other factors such as Raman-induced crosstalk, SBS etc, (ii) the low γ values of conventional fibres deployed for transmission, which reduces the efficiency of FWM process, (iii) the large chromatic dispersion at communication window in those fibres, which prevents a good phase-matching between different channels, and hence the growth of spurious FWM terms.

However, it is clear that all these conditions are violated in the operation of an OPA used for actual amplification. In OPAs, the channels grow to high power levels by the definition of amplification. In addition, in order to have a good amount of gain and bandwidth one should choose highly-nonlinear fibre with large γ values and provide almost perfect phase-matching between the pump(s) and the signals by shifting the zero-dispersion wavelength of the fibre close to the region where channels are located.

Altogether, the situation for spurious FWM terms in OPAs is almost as suitable as for signals to grow, and thus become deleterious. Another aggravating factor in OPAs is the presence of strong pump waves and the generated idlers. Their undesired interactions with signals, among themselves, and even with spurious FWM terms to generate another set of FWM-generated terms add considerably to the complexity of the situation. Figure 4.1" and Figure 4.2" schematically show some of the spurious FWM in single- and dual-pump OPAs in which only two channels are present at the input.

For the one-pump case since every frequency component on one side of the pump has a counterpart on the other side, only that side of the pump where signals are placed is shown. In general, two kinds of FWM terms are distinguishable in the figure: the terms generated by FWM between signals, and those involving the pump. The first kind, which are also called second-order FWM [**3**], are of the form $\omega_5 = 2\omega_3 - \omega_4$. This type of spurious terms are most dangerous as: firstly, they fall right in the region where the channels are placed; secondly, they see the maximum parametric gain of the one-pump OPA, as it is assumed to occur in that region. Moreover, the number of such terms scales with the number N_s of channels as N_s^3. Therefore, the number of FWM terms of this kind grows rapidly with N_s leading to considerable crosstalk in WDM systems. The terms that involve the pump are called first-order terms and are either of the form $\omega_6 = \omega_3 + \omega_4 - \omega_1$ or $\omega_7 = \omega_1 + \omega_4 - \omega_3$. These terms are somewhat less dangerous, as the terms of first kind (ω_6) fall beyond the channels and those of the second kind (ω_7) are generated close to the pump where normally channels are not placed.

In a simplified theory presented in [**3**], the ratio of the power of the first- and second-order FWM terms to the signal output power in the one-pump case are approximated as:

$$XT_{ss} \stackrel{\text{def}}{=} \frac{P_5}{GP_{30}} = \frac{1}{4}\left(\frac{P_{4,\text{out}}}{P_{10}}\right)^2 \qquad 4.1$$

$$XT_{PS} \stackrel{\text{def}}{=} \frac{4P_6}{GP_{30}} = \frac{P_{4,\text{out}}}{P_{10}}, \qquad 4.2$$

where P_{10} is the pump power at the input, and P_{4out} is the signal power at the output. The terms XT_{SS} and XT_{PS} denote the signal-signal and pump-signal crosstalk respectively.

Although, the theory is a simplified view of the problem, it generally shows a good agreement with experiments and provides an approximate insight on the issue [**4**]. Any exact analytical theory is lacking, otherwise.

For the two-pump case, the generation of spurious FWM terms is somewhat more complex than in a one-pump OPA due to the location of the pumps with respect to the signals and idlers [**3**]. Although for signal-signal FWM, the situation and the sought countermeasures remain similar to the one-pump case, significant FWM terms appear from pump-signal FWM. Cases that are more specific include the generation of the terms like ω_8, ω_9 and ω_{10} (Figure 4.2"). The terms like $\omega_8 = 2\omega_1 - \omega_3$ fall outside the region between the two pumps, which is not the region of normal amplification in conventional two-pump OPAs. The terms of the form $\omega_9 = 2\omega_3 - \omega_2$ also fall far away from the pumps and hence do not introduce serious problems. Other terms are of the form $\omega_{10} = \omega_2 + \omega_3 - \omega_4$; ω_{10} is due to the idler associated with ω_7 and to FWM between the idlers corresponding to ω_3 and ω_4 and the pump at ω_2.

Many research groups who are active in the field of OPAs have investigated the different aspects of FWM-induced crosstalk in OPAs [**4**]-[**9**]. Due to the extremely complex nature of the FWM crosstalk problem, most of the investigations are based on experimental observations and/or numerical simulations. The complexity arises from the large number of the generated terms even for low channel numbers (N_s >3), which makes it impossible to approach the problem analytically.

In an attempt in [**10**], for the case of one-pump OPA with only two channels the closed form solution for the first-order crosstalk is shown to include 64-96 exponential terms. The number of terms for second-order crosstalk, which involves the pump, one signal or idler and one FWM term of first-order, is 520.

Investigations on the influence of the physical parameters of the fibre show an adverse impact of the zero-dispersion wavelength (ZDW) variations on the crosstalk. It is experimentally demonstrated in [**11**] that an increase in the variance of ZDW variations from 0.2 nm to 2 nm can increase the amount of crosstalk by an order of magnitude. It

is not then unexpected that reducing the fibre length while increasing the pump power to keep the gain at a desired level will improve the OPA performance greatly since the ZDW variations are more likely to be small in short fibres.

In [**12**], it is experimentally shown that FWM crosstalk in a one-pump OPA tends to be less problematic on the Stokes side of the gain bandwidth. This could be partially due to stimulated Raman scattering and the difference between the phase-matching because of the sign of $\beta^{(2)}$. Moreover, by properly positioning the signals with respect to the pump wavelength so that the pump is placed halfway between two grid carriers the situation can be improved.

Uneven channel spacing is known as another method of improving the crosstalk as then it is possible to make some FWM terms fall in between the channels and even out of the band in which channels are put [**12**], [**13**].

Other methods have been proposed based on the fact that the FWM process in general is polarisation dependent. In other words, the efficiency of FWM process drops dramatically when the SOPs of the waves involved are orthogonal. Some techniques in which channels have orthogonal polarisation states have been proposed and demonstrated with improved crosstalk [**14**].

4.2. Reduced FWM crosstalk in a short fibre OPA[3]

From the brief review of the FWM crosstalk issue in OPAs, one could conclude that the problem is of a fundamental nature. This means that although the introduced countermeasures can partially improve the performance of OPAs, there is not any solution to eliminate the problem. Hence, the only way to reduce the amount of crosstalk considerably is increasing the pump power and reducing the length of the fibre, which helps in two different ways: (i) the crosstalk scales approximately as L^2, and thus it is reduced by reducing the length (L), (ii) reduced length of the fibre decreases the range of ZDW variations. Increasing the pump power, of course, has another very important and desirable consequence, which is the increased bandwidth of the OPAs. In the following experiment, we verified this general approximate theory by

[3] This experiment was performed by with the help from Dr. Armand Vedadi in the initiation and the progress of the experiment. The split-step simulations were performed using a program provided by Prof. Michel Marhic.

reducing the fibre length from 340 m to 50 m. The obtained results also brought up hopes about OPAs as they confirmed that it would be possible to amplify a good number of channels before crosstalk poses limitations.

4.2.1. Experiment description

The experimental setup is shown in Figure 4.3. A tunable laser (TL1) is used as the

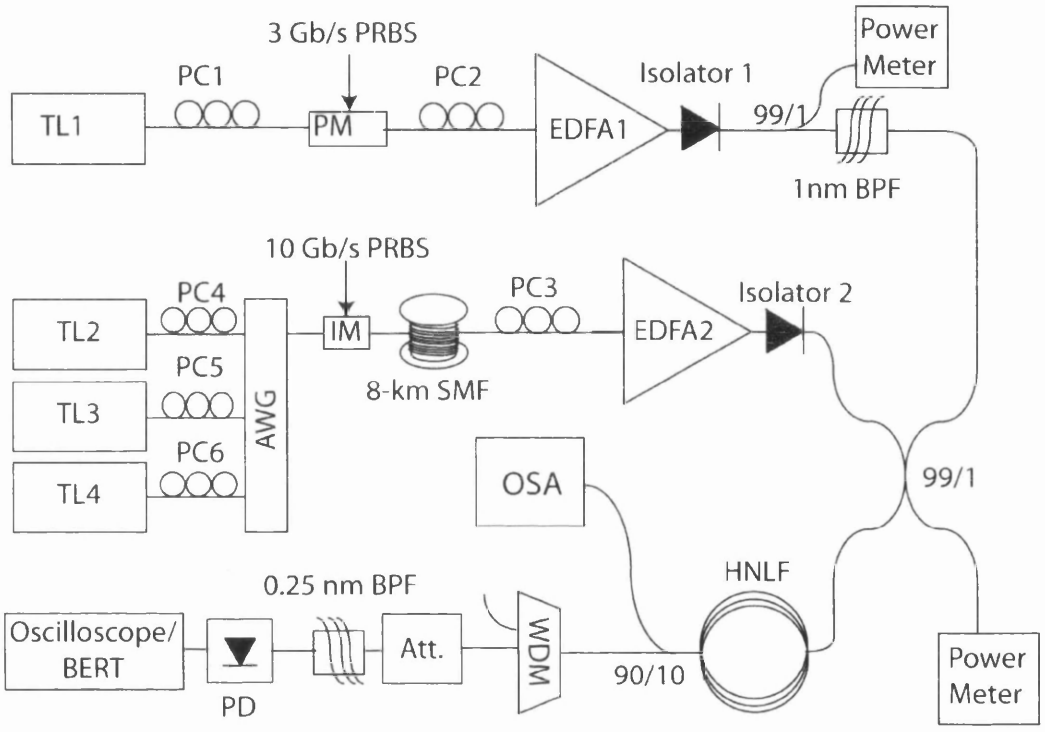

Figure 4.3. Experimental setup of the short one-pump fiber OPA. Three signals modulated at 10 Gb/s are decorrelated through the 8-km spool of SMF.

pump. It is phase-modulated by a phase modulator (PM) in order to suppress stimulated Brillouin scattering (SBS). The PM is driven by a 3 Gb/s pseudo-random bit sequence (PRBS). The pump is amplified using a 10-W erbium-doped fibre amplifier (EDFA1) to the desired power level. An isolator is placed after EDFA1 in order to attenuate any potential back-reflections. The ASE of EDFA1 is then filtered out by a tunable bandpass filter (BPF).

Three channels separated by 100 GHz serve as signals. They are generated by three tunable lasers (TL2-TL4) SOPs are controlled by separate polarization controllers (PC4-PC6).The signals are combined by the arrayed waveguide grating (AWG) and intensity-modulated by a 10 Gb/s PRBS. An 8-km long SMF is used to decorrelate the signals.

PC3 is used to align signal and pump SOPs. The signals are then amplified by EDFA 2 and, together with the pump, injected into the HNLF through a 99/1 coupler.

The HNLF output spectrum is analysed by an optical spectrum analyser (OSA) placed after the 10% branch of a 90/10 coupler. A C/L-band WDM coupler is placed in the other branch in order to divert the high-power pump into a beam dump. A variable attenuator and a narrow bandpass filter are used to attenuate and select the signal to be analysed by a bit-error rate tester (BERT).

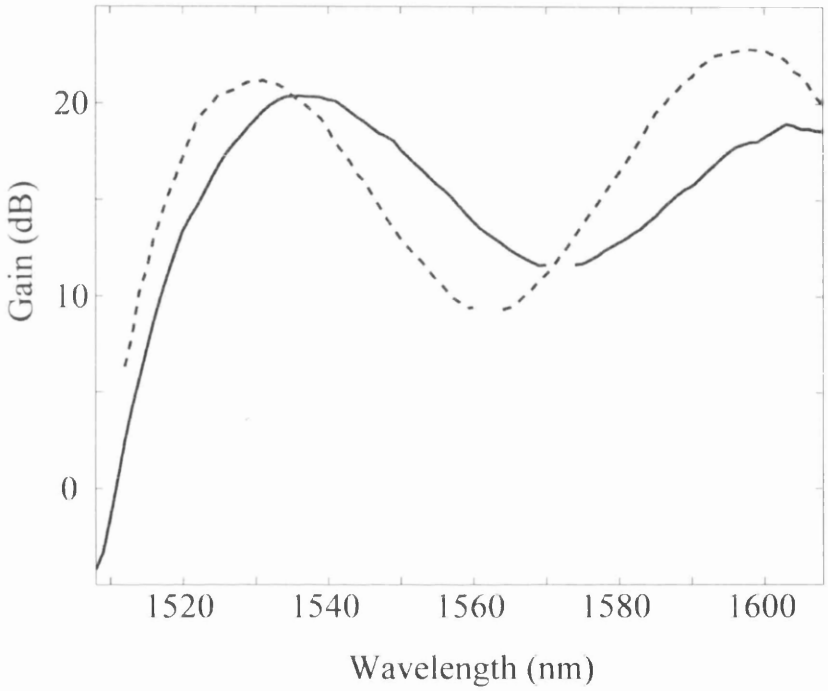

Figure 4.4. Gain spectra of the two OPAs. For 340-m fiber λ_P = 1562 nm (dashed) and for 50-m fiber λ_P = 1572 nm (solid line).

We use two pieces of HNLFs with 340 m and 50 m length. Both HNLFs have the same nonlinearity coefficient γ = 15 $W^{-1}.km^{-1}$ and dispersion slope D_S = 0.023 ps/nm^2-km, but slightly different ZDWs: 1561 (1566.5) nm for the 340-m (50-m) long HNLF. In both cases, the signals are positioned close to the maximum gain (exponential gain regime). For OPA1, the pump wavelength is 1562 nm and the pump power is 630 mW, which provides a gain slightly larger than 20 dB around 1531 nm. In order to have a precise comparison of signal-signal FWM crosstalk, the gain spectrum of OPA2 is adjusted to be similar to that of OPA1 (about their respective pump wavelengths), and the signals are also placed near maximum gain. This is achieved by using pump power

and pump wavelength in OPA2 of 4.6 W and 1572 nm, respectively, providing about 20 dB of gain around 1535 nm (see Figure 4.4). The signal wavelengths are 1530.2 nm, 1531 nm, and 1531.8 nm for OPA1, and 1534.2 nm, 1535 nm, and 1535.8 nm for OPA2.

4.2.2. Results and discussions

First we compare the crosstalk level in the amplifiers when two of the signals are present. As mentioned before the crosstalk is defined as the ratio of the power of a spurious FWM term to that of the signals. Figure 4.6 depicts the optical spectra showing the signals and the generated crosstalk components. As seen in the figure, while we have relatively substantial crosstalk (-19 dB on the left side and -27 dB on the right side) at the output of OPA1, a negligible amount of crosstalk is observed at the output of OPA2 even for a larger signal input power.

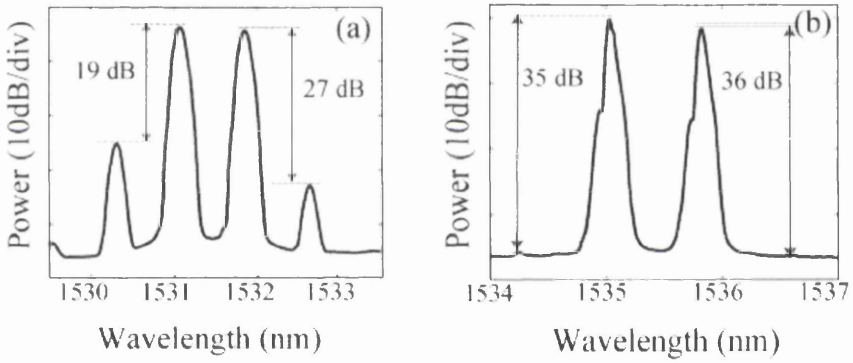

Figure 4.6. Output spectra of the (a) 340-m OPA and (b) 50-m OPA. Signal input power is -6.5 dBm for (a) and -5.8 dBm for (b).

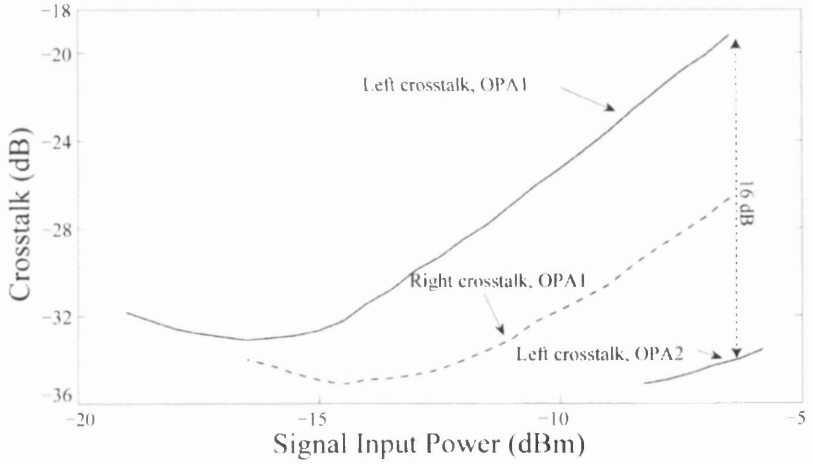

Figure 4.5. Left (solid line) and right (dashed line) crosstalk as a function of signal input power. For signal powers below -8 dBm, the crosstalk is too low to be measured for the 50-m OPA.

Figure 4.5 shows the amount of crosstalk corresponding to the two spurious FWM terms on the left and right sides of the two signals for the two OPAs as a function of signal input power. For large signal input powers a large amount of crosstalk is generated for the 340-m OPA, while it is almost down to the noise level for the 50-m OPA. A difference of about 16 dB between the spurious crosstalk terms in the two cases is obtained at an input power level of -6.5 dBm per signal.

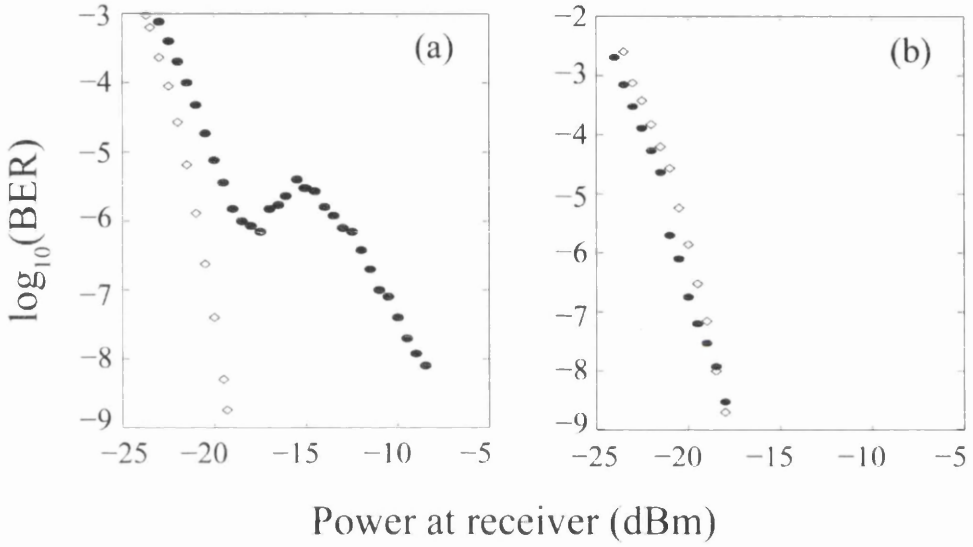

Figure 4.7. BER measurement results for the signal positioned on an FWM term generated by the other two signals. (a) 340-m OPA (power penalty is 16 dB). (b) 50-m OPA. (Diamond curve corresponds to back-to-back measurement.)

It is important to note that for -6.5 dBm of signal input power, the signal output power is approximately 13.5 dBm, which is very high by telecommunication standards. For a typical communication system the signal output power could be reduced by about an order of magnitude, and in that case the crosstalk in OPA2 would be too low to measure. This indicates that one could then add many more signals before nonlinear crosstalk would become a problem.

In order to compare the degradation suffered by a third signal falling on a FWM term generated by the two original signals, a bit-error rate (BER) measurement was performed for such a signal. Figure 4.7 shows the results for this measurement. While for OPA2 the third signal suffers almost no degradation, in the case of OPA1 the third signal coinciding with the crosstalk of the other two is substantially degraded. For a BER of 10^{-9}, which is typical of communication systems, the power penalty reaches 16 dB for OPA1.

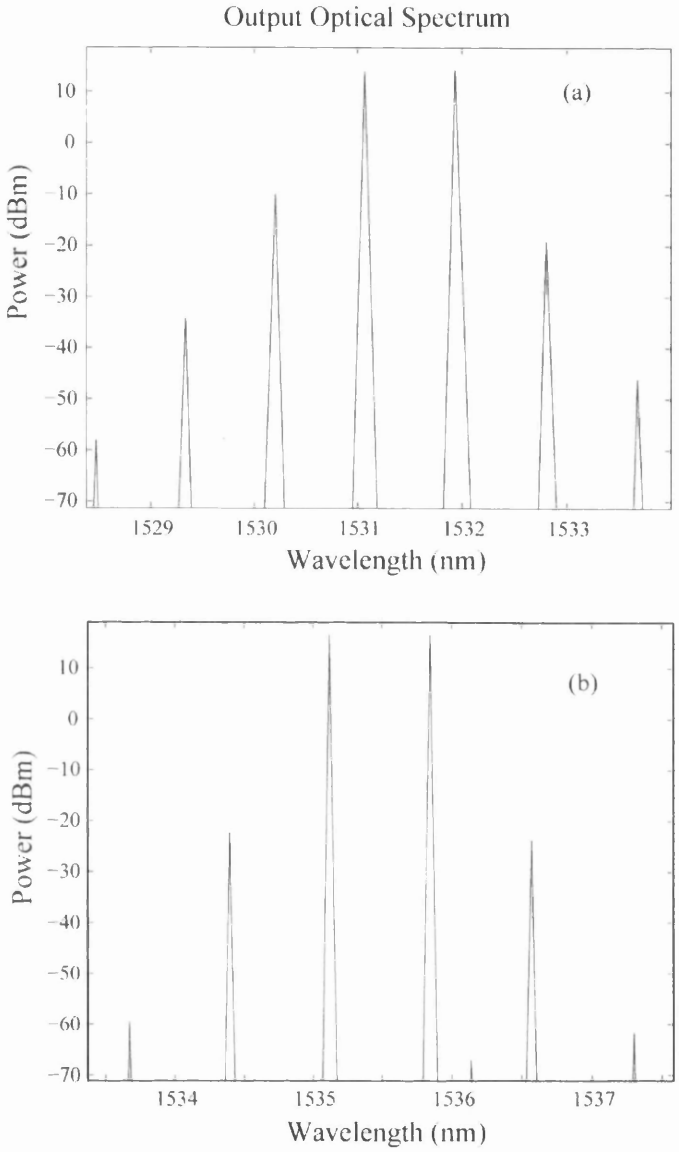

Figure 4.8. Numerical simulations results obtained using the SSMF. (a) 340-m fiber and (b) 50-m fiber.

In order to model the kind of crosstalk reductions expected by reducing the OPA length, we performed numerical simulations using the scalar split-step Fourier method (SSFM). We did not include Raman gain in the model, as the wavelength spacings between the signals and the pump are small compared to the Raman shift. We assumed that the fibre had constant dispersion properties along its length. We did not include ASE, as we wanted to clearly see the amplitudes of the various FWM terms. Results are shown in Figure 4.8 for a 340-m and a 50-m fibre, with the same maximum gain of about 20 dB and a signal input power of -6.5 dBm. As in the experiments, the pump locations were adjusted to have maximum gain at the same distance from the pump in both cases.

Figure 4.8**(a)** shows the output optical spectrum for conditions similar to the experiment performed with OPA1. We see that two FWM terms flank the two signals. The FWM term at the shorter (longer) wavelength is 24 (32) dB below the common power of the signals. Figure 4.8**(b)** shows results for the 50-m fibre. As expected, the crosstalk terms are significantly reduced: the term on the left (right) is now 36.2 (37.7) dB below the common power of the signals. The asymmetry between the FWM terms is in good accordance with the experiments. This can be attributed to the slightly different dispersion on either side of the signals. Although the model correctly predicts decrease of the crosstalk level, the amount of reduction does not scale as L^{-2}, which highlights the influence of the other FWM terms that are neglected in the simplified theory. Also, the crosstalk level reduction predicted by SSFM simulation is lower than the one observed experimentally. This can be attributed to a stronger dispersion variation in the longer fibre, which can lead to substantially larger crosstalk levels [**11**].

One important point to be considered in this experiment is that, since the three channels are decorrelated, the effect of XGM is included as well in assessing the signal quality, while some authors separate the effect of crosstalk and XGM by launching all channels with the same modulation [**15**]. Therefore, the error-free performance of the OPA in this experiment is obtained despite the combined influence of crosstalk and XGM, which is promising.

4.3. Pushing OPA to the boundaries of modern WDM systems

In the experiment described in the previous section, the results showed that with three channels amplified to the high power level of 13.5 dBm, there was no noticeable crosstalk. This promising result encouraged us to increase the number of channels to 8, 16 and eventually to the full capacity of our laboratory, 26 channels modulated at 43.7 Gb/s, which aggregated to a data rate in excess of 1 Tb/s. Prior to this, the highest reported data rate amplified in an OPA was 120 Gb/s [**15**], and as mentioned in that paper the effect of XGM was not taken into account. The results obtained were impressive as the overall power penalty was less than 1 dB indicating that combined with other unique features of OPAs, they can be considered as capable candidates for future high capacity systems. It is worth noting that in our experiment, the fibre was 114-m long and hence there was still considerable room for improvement by shortening

the fibre. However, due to limitations in time and resources this was postponed to a later time[4].

4.3.1. Experiment description

The performance of the OPA was evaluated using the back-to-back configuration shown in Figure **4.9**. The OPA was placed between the transmitter and receiver of a DWDM testbed and its performance was compared with a single-stage EDFA which has 17-dB flat gain and 25-dBm maximum output power.

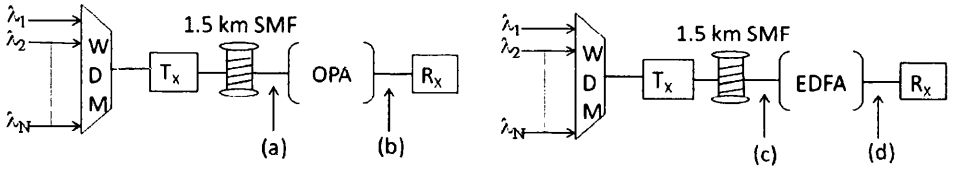

Figure 4.9. Evaluated system configuration (WDM: Wavelength Division Multiplexer, Tx: Transmitter, T-DCM: Tunable DCM, Rx: Receiver). (a) - (d) are measurement points.

The testbed contained 26 channels on the ITU grid with 100 GHz channel spacing starting from 1531.11 nm, with the channels at 1537.40 and 1538.19 nm missing. After multiplexing, the channels were modulated at 43.7 Gb/s by two $LiNbO_3$ Mach-Zehnder modulators. The first modulator was driven by a 2^{31}-1 pseudo-random bit sequence to generate a differential phase shift keyed (DPSK) signal. The second was driven by a half-rate clock creating RZ-DPSK modulation with 67% duty cycle. The channels were decorrelated through 1.5-km of SMF, and then launched into the EDFA or OPA. The OPA was a single-pump OPA with pump power of 35 dBm and wavelength 1572.5 nm. The gain medium was 114-m of HNLF with a 15 $W^{-1}km^{-1}$ nonlinear coefficient and 0.023 ps/nm^2-km dispersion slope. The gain curve of the OPA was tailored by tuning pump wavelength and power in order to obtain as flat a gain spectrum as possible in the transmission range. Figure **4.10** shows the gain spectrum of the OPA. Since the SOP of each channel was slightly different after passing through the decorrelating fibre, it was possible to further flatten the gain using a polarization controller so that all the channels

[4] The experiment described in this section was performed with the help of the transmission group supervised by Prof. Nick Doran. The testbed was installed and operated by Dr. Donald Govan. He also provided the instructions and guidance on transmission technical issues. Dr. Nayla El-dahdah helped greatly in data recording and manipulating.

experienced gain of at least 20 dB, with a 3dB tilt across the channels. The channel powers were levelled at the output of the amplifiers by adjusting the input channel powers. The total power at the OPA (EDFA) input was 1.5 dBm (-4.8 dBm). The signals were received using a tunable flat-top filter with a bandwidth of 0.6 nm to de-multiplex the selected channel, followed by a Mach-Zehnder delay interferometer and balanced photodiodes.

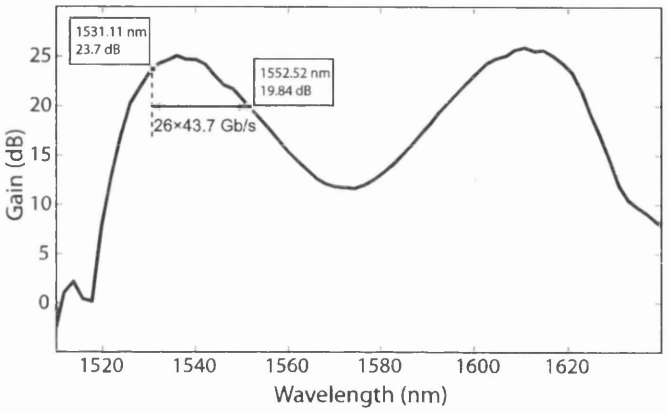

Figure 4.10. Gain Spectrum of the evaluated OPA; λ_P = 1572.5 nm, λ_0 = 1570 nm.

4.3.2. Results and discussions

The performance of the OPA was evaluated by measuring BER versus power and OSNR at the receiver input (points (b) and (d)). We first measured the back-to-back performance of the OPA. Next we substituted the OPA with the EDFA ensuring that the input and output OSNR measured at points (c) and (d) were equal to those measured at points (a) and (b), which required a reduction of the total input power using a variable optical attenuator.

The normalized optical spectrum of the transmitted channels at the output of the OPA and EDFA is shown in Figure **4.11**. It is seen from the spectrum that there is a tilt in the noise level across the band. This was measured by turning the channels off in pairs and is the same for OPA and EDFA. In the case of the OPA the tilt increases with total power or number of channels. Indeed, the OPA-induced noise is generated by nonlinear crosstalk due to four-wave mixing (FWM) which is greater at short wavelengths

because of stronger phase-matching. This is in agreement with simulation results obtained using the split-step Fourier method. Figure **4.12** shows the output spectrum obtained with the parameters used in our experiments, and four equal-power input signals. The results clearly verified that crosstalk level is higher for shorter wavelengths.

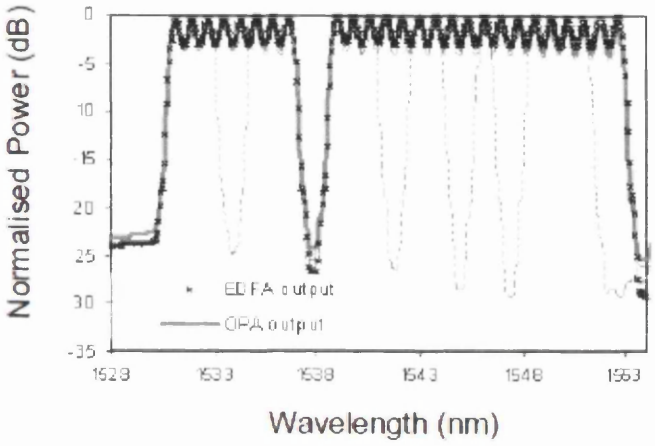

Figure 4.11. Normalized optical spectra of the data at EDFA output (x) and OPA output (solid line) with some channels off (dotted line), measured with 0.5-nm resolution bandwidth.

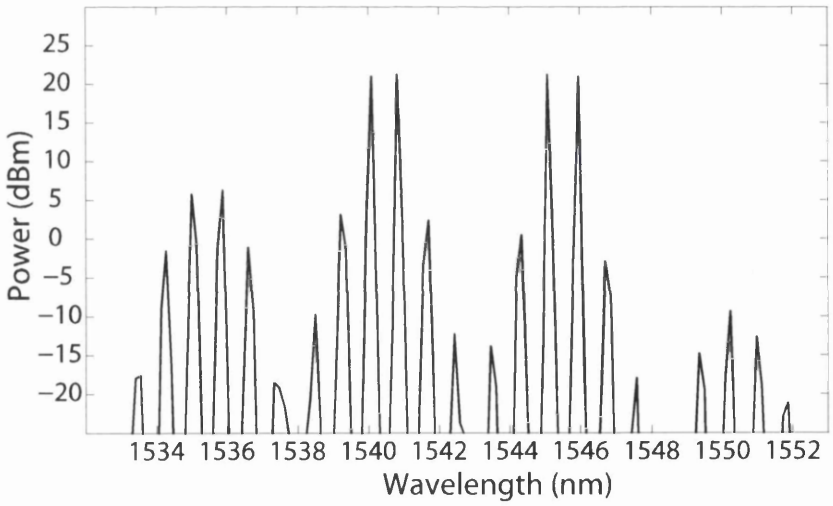

Figure 4.12. OPA output spectrum for four equal-power input signals, with wavelengths 1540, 1540.8, 1545 and 1545.8 nm.

With 34-dB input OSNR (0.5 nm resolution bandwidth) at points (a) and (c), the BER variations of channels 1, 4, 9, 12, 16, 20 and 26, measured at points (b) and (d) respectively, versus the received power, measured at points (b) and (d) respectively, are shown in Figure **4.13**. The accuracy on the received power level was 0.3 dB; therefore both cases exhibit similar performance variation with channel wavelength. The penalty on the received power was plotted against wavelength in Figure **4.14**. We found 0.7-dB average penalty across the channels. The origin of the measured penalty at the OPA output is partly due to the coherent nature of the induced noise. Indeed, we verified that the channels amplified by the OPA contain additional intrinsic noise, i.e. they have higher relative intensity noise (RIN). It originates from the pump and is independent of the signal's characteristics [**3**].

These results show that OPAs can be suitable amplifiers for DWDM systems. Future plans for evaluating OPAs include using them as a transmitter amplifier (booster) with a transmission line, to ensure that the nonlinear nature of the noise does not introduce any strong limitations.

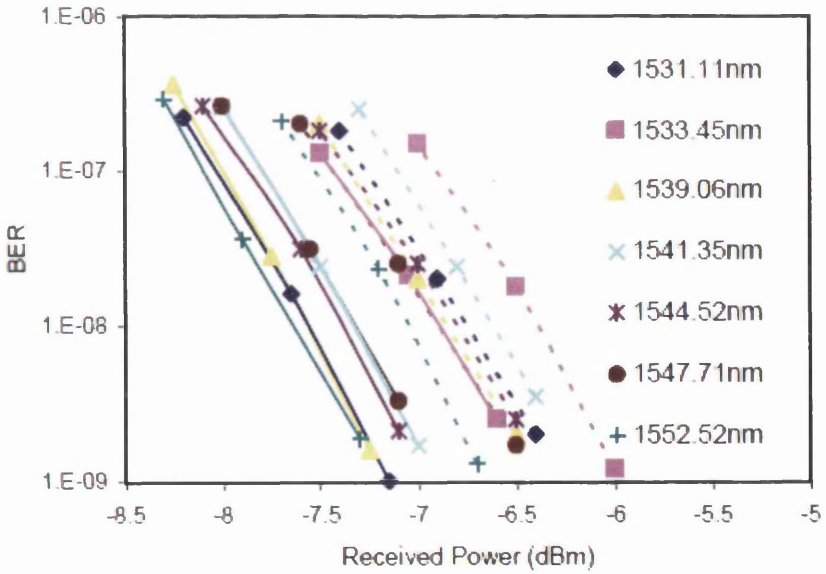

Figure 4.13. BER measurements vs. Received Power of the data amplified by EDFA (solid line) and OPA (dotted line) at channels 1 (diamond), 4 (square), 9 (triangle), 12 (x), 16 (star), 20 (circle) and 26 (+).

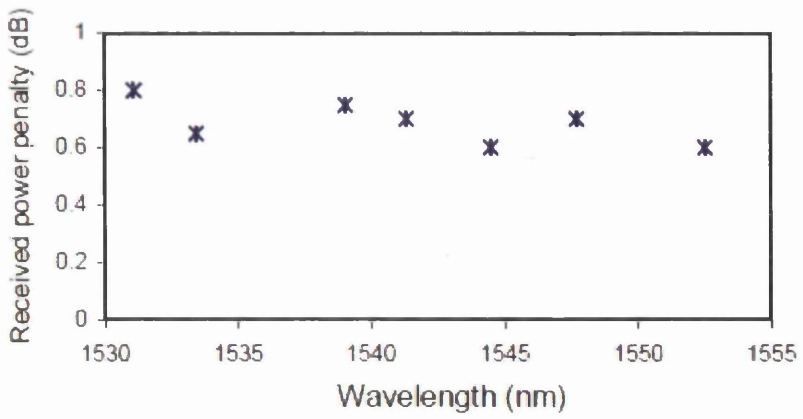

Figure 4.14. Received power penalty vs. wavelength of the channels 1, 4, 9, 12, 16, 20 and 26 amplified by OPA compared with EDFA.

Summary

This chapter of the thesis is on the main criticism on the OPAs, namely, nonlinear crosstalk. Since in the OPAs the phase-matching condition is good as a requirement for the broadband amplification, spurious waves due to FWM among the channels and between the channels and the pump are generated. These new waves fall on the channels deteriorating the performance of the OPAs. The number of such FWM terms can grow very rapidly by adding to the number of channels in WDM systems. This results in lack of any exact theoretical model to analyse the situation.

The only way to reduce the adverse impact of the nonlinear crosstalk is to reduce the fibre length while increasing the pump power to maintain the gain. Results for two experiments using this approach is presented, which seem promising. In one experiment the amount of crosstalk is shown to be reduced by 16 dB when reducing the fibre length from 340 m to 50 m.

In the other experiment, 24 channels modulated at 43.7 Gb/s are amplified with a short OPA with performance close to that of EDFAs showing that OPAs can find their position in modern high-speed telecommunication systems.

References

[1] G. P. Agrawal, *Fiber-optics communication systems*. 3rd Ed. United States of America: Willey, 2002.

[2] R. Ramaswami, K. N. Sivarijan, *Optical networks*. 2nd Ed. United States Of America: Morgan Kaufmann, 2002.

[3] M. E. Marhic, *Fiber Optical Parametric Amplifiers, Oscillators and Related Devices*. United Kingdom: Cambridge University Press, 2008.

[4] J. D. Marconi, J. M. Chavez Boggio, and H. L. Fragnito, "Crosstalk in double-pumped fibre optic parametric amplifiers for wavelength division multiplexing systems," *Opt. Comm.*, vol. 259, pp. 94–103, 2006.

[5] M. Jamshidifar, A. Vedadi, and M. E. Marhic, "Reduction of Four-Wave-Mixing Crosstalk in a Short Fibre-Optical Parametric Amplifier," *IEEE Photon. Technol. Lett.*, vol. 21, pp. 1244-1246, 2009.

[6] J. L. Blows, and P. Hu, "Cross-talk-induced limitations of two-pump optical fibre parametric amplifiers," *J. Opt. Soc. Amer. -B.*, vol. 21, pp. 989-995, 2004.

[7] P. Hu, and J. L. Blows, "Four-wave mixing crosstalk in optical fibre parametric amplifiers with orthogonal pumps", *Opt. Commun.* Vol. 250, pp. 421-427, 2005.

[8] T. Torounidis, H. Sunnerud, P. O. Hedekvist, and P. A. Andrekson, "Amplification of WDM signals in fiber-based optical parametric amplifiers," *IEEE Photon. Tech. Lett.*, vol. 15, pp. 1061-1063, 2003.

[9] J. Hansryd, P. A. Andrekson, M. Westlund, J. Li, and P. O. Hedekvist, "Fiber-based optical parametric amplifiers and their applications," *IEEE J. Sel. Topics Quantum Electron.*, vol. 8, pp. 506–520, 2002.

[10] M. Marhic, and J. Chavez Boggio, "Solutions for first- and second-order four-wave mixing cross talk in one-pump fiber optical parametric amplifiers," *J. Opt. Soc. Am. B.*, vol. 25, pp. 841-848, 2008.

[11] J. M. C. Boggio, F. A. Callegari, A. Guimarães, J. D. Marconi, and H. L. Fragnito, "Influence of zero dispersion wavelength variations on four-wave mixing in single-pumped parametric amplifiers," *Opt. Commun.*, vol. 242, pp. 471–478, 2004.

[12] A. Mussot, E. Lantz, A. Durécu -Legrand, C. Simonneau , D. Bayart, H. Maillotte, and T. Sylvestre , "Simple Method for Crosstalk Reduction in Fiber Optical Parametric Amplifiers," in *European Optical Communications conference (ECOC)*, Cannes, France, 24-28 Sept. 2006.

[13] F. Forghieri, R. Tkach, A. Chraplyvy, and D. Marcuse, "Reduction of four-wave mixing crosstalk in WDM systems using unequally spaced channels," *IEEE Photon. Technol. Lett.*, vol. 6, pp. 754–756, 1994.

[14] K. K. Y. Wong, G.-W. Lu, and L. K. Chen, "Polarization-interleaved WDM signals in a fiber optical parametric amplifier with orthogonal pumps," *Opt. Exp.*, vol. 15, pp. 56-61, 2007.

[15] J. M. Chavez Boggio, E. A. M. Fagotto, M. E. Marhic, F. A. Callegari, and H. L. Fragnito, "Amplification of 12 × 10 Gb/s WDM signals with negligible FWM crosstalk in a double-pumped fiber optical parametric amplifier," *Opt. Comm.*, vol. 280, pp. 468-471, 2007.

Chapter 5. Highly-nonlinear fibres

Since nonlinear optical signal processing introduced itself as a key technology for next generation optical communication systems, an enormous amount of research activity has been dedicated over the past decade to develop new techniques, applications and devices aiming all optical signal processing by making use of nonlinearities. The ultrafast operation, transparency and desirability of elimination of optical-electrical-optical conversion are the main motivations for all-optical processing [**1**]. For this purpose, a wide range of photonic devices based on silicon-waveguides [**2**] exploiting second-order nonlinearity, metamaterials [**3**], photonic crystal devices [**4**] have been realised.

In this context, one attractive possibility is to perform the nonlinear optical processing within the fibre, which has the immediate desirable feature of keeping light inside the fibre and combine processing with transmission. It also makes it possible to perform different processing steps simultaneously within a single device. Since nonlinearities in optical fibre arise from third-order nonlinearity, which has a very fast and almost instantaneous response, fibre-based devices can be very fast, thus able to perform processing in ultra fast communications.

One of the key features that make optical fibres such an attractive medium for nonlinear interactions is that one can almost arbitrarily choose the length over which the interaction can take place. This feature combined with dense light concentration, which leads to high nonlinear coefficients, yields strong nonlinear interactions.

However, associated with long fibres are some serious issues such as instability. Therefore, it is very desirable to construct fibres with large nonlinearity coefficients to

reduce the length of the fibre required. To this end, many techniques have been proposed and a large number of different materials have been investigated.

In this chapter, we first briefly review some of the promising technologies that have been successful in construction of such highly-nonlinear fibres together with recent advances in this area. As the focus of this thesis is on fibre optical parametric amplification, we then present our results on an investigation of a recently-introduced type of highly nonlinear fibre based on bismuth-oxide, and its suitability for real OPA work.

5.1. New technologies for development of highly-nonlinear fibres

For any type of nonlinear work in optical fibres, in order to have strong nonlinear interactions the fibre should exhibit strong nonlinear properties. As it is mentioned in section**1.2**, the extent of nonlinearity in a fibre is measured by nonlinear coefficient γ, which has direct dependence on the nonlinear refractive index n_2 of the core material and inverse dependence on the effective area of the fibre. Therefore, logically, any attempt to increase the nonlinearity of a fibre should address either one or both approaches of replacing the core material with materials with large intrinsic nonlinear refractive index n_2 or designing waveguide structures with small effective area. Moreover, in nonlinear work and specifically in OPAs, dispersion properties of the fibre play a crucial role in identifying suitable fibres as well. In other words, high nonlinear coefficient is not solely enough for a fibre to be suitable for OPAs, and thus tailored dispersion properties of a fibre is of the same importance as high nonlinearity.

In the following, we briefly review advances in highly-nonlinear fibre technology in both directions in separate parts.

5.1.1. Silica-based step-index highly-nonlinear fibres

The dispersion-shifted step-index fibres were the first modification of conventional low-loss silica-based fibres, which provided suitable ground for nonlinear work in fibres. The fact that the ZDW of these fibres was shifted to the telecommunication window together with their low loss made them attractive; however, the nonlinearity coefficient was very small and about 2 $W^{-1}km^{-1}$. Although many interesting OPA experiments have been conducted with pulsed-pump at very high peak powers with this category of fibres,

they are not suitable for actual amplification purpose of telecommunication channels; where the pump must be CW.

Dispersion-shifted highly nonlinear fibres (DS-HNLF or simply HNLF) are a modified version of conventional DSF for which the core size is shrunk to provide smaller A_{eff}. The effective area of this kind of fibre was reduced to about 10 μm^2. Also, in order to maintain single-mode operation in the C-band manufacturers have increased the germania content of the core up to about 3%. The germania dopant (GeO_2) of about 30 mol% increases the n_2 of the core to about 5–6×10^{-20} m^2W^{-1} which is originally 2.2×10^{-20} m^2W^{-1} [5], [6]. The core dopant increases the attenuation coefficient to 0.5-2 dB/km; however, it is still incremental. The effective length with these values for attenuation coefficient can be found to be a couple of kilometres. Thus the product of γPL can be almost arbitrarily chosen to provide any desired amount of gain even with moderate figures for pump power. The combination of small core diameter and increased germania dopant leads to γ values increased by an order of magnitude; γ values of about 25 $W^{-1}km^{-1}$ has been reported while the more typical figure is 15 $W^{-1}km^{-1}$.

Although the γ value for silica-based HNLFs is an order of magnitude greater than that of conventional DSF, they are limited to 25-30 $W^{-1}km^{-1}$. On the other hand, several fibre designs have been realised with extraordinary values for γ in excess of 1000 $W^{-1}km^{-1}$. Nonetheless, silica-based HNLFs remain the main and most important type of highly nonlinear fibre for several reasons. They are built up of silica, which is quite easy to find and inexpensive. They can be easily fusion spliced to other types of silica fibres with low splice-losses of less than 0.5 dB. Moreover, the technology is mature so that most of the properties of these fibres such as ZDW and dispersion properties can be tailored in accordance with specific needs, while other technologies are at the research stages.

5.1.2. Tapered fibres

In order to reduce the core diameter of silica fibres, a simple approach known as tapering was employed as early as 1993 [**7**]. In this approach, starting from a typical communication fibre with a cladding diameter of 125 μm, the fibre is heated up past the softening point and is pulled slowly from both ends so that the diameter is shrunk to 1-2 μm. For heating, either a flame torch or a CO_2 laser is used [**8**]. By making use of this

method, fibres with diameters as small as 1 μm or less can be made. It should be noted that when the diameter of the cladding becomes so small, essentially, whatever remains from the original core plays no role in confining the light. Confinement occurs due to the large index difference between the cladding and the surrounding air [**9**].

In the tapered region, the V-parameter is such that the single mode operation criterion is not satisfied and thus the light is conveyed in multiple modes. However, when the transition from the original fibre to the tapered part is very gradual the energy of the light is redistributed over the modes in such a way that losses are low. Also when exiting the tapered part, the light is again confined in a single mode automatically. Therefore, the tapered fibres have a remarkable property that coupling in and out of 1-μm-diameter region is not particularly difficult [**9**].

Although large values for nonlinearity coefficient are achievable with tapered fibres, since they are fragile and barely can be made in lengths more than a few tens of centimetres, they are not used extensively in nonlinear applications. Moreover, their dispersion properties are strongly dependent on the core size, which makes it difficult to obtain uniform and proper dispersion properties.

5.1.3. Microstructured optical fibres

In attempt to develop new fibre structures aiming at high, a new class of fibres has been introduced recently under the general name of microstructured optical fibres (MOFs) [10], [11]. The word *"Microstructured"* refers to the structuring of an arrangement of air holes with micrometer dimension surrounding the core in this type of fibre. This means a constellation of air holes surrounds the core and act as cladding. For this reason, such fibres are also referred to as Holey Fibres (HFs). The immediate advantage of this design is that in principle these fibres can be constructed from a single material; nonetheless, there have been a number of other unique features exploited in these fibres so far such as surprisingly high nonlinearity when combined with the use of some novel materials, which have attracted a massive amount of research interest in this area.

Generally the confinement of light in MOFs occurs by means of two distinct mechanisms, namely, photonic bandgap effect, which is produced by a two-dimensional periodic arrangement of the air holes [**10**] and by the total internal reflection effect

which is the result of decreased effective refractive index of cladding region because of air holes [**12**].

The analysis of modal and dispersive properties of microstructured fibres is quite a difficult task because the refractive index of the cladding can not be considered homogenous [**8**], and an elaborate numerical approach is often required. However, by suitably changing the size, shape and special arrangement of the holes, most fibre properties can be tailored. Two specific parameters, which influence the fibre properties, are the air-hole diameter d and the hole-to-hole spacing Λ and the ratios d / Λ and λ / Λ.

The overall dispersion is governed not only by the material dispersion, but also by the waveguide dispersion. The contribution of the waveguide is relatively small in conventional step-index fibres except near zero-dispersion wavelength (ZDW), and the main effect of that is to shift the ZDW towards longer wavelengths [**8**]. However, the waveguide dispersion, dependent on the parameters mentioned above, can be very strong in HFs. A unique feature of HFs is that by properly tailoring the dispersion of the waveguide it is possible to pull the ZDW into the regions below 1.27 μm, which is impossible in step-index design. Another interesting feature of HFs is that it is possible in principle to have holey-fibres supporting only the fundamental mode at all wavelengths if $d / \Lambda < 0.45$; such a fibre is referred to as an endlessly single-mode fibre [**9**]. Although other remarkable features have been exploited in HFs such as dispersion-flattening over a wide range, which can be particularly important in OPAs, they suffer from large amount of attenuation resulting from confinement loss [**13**]. Another complication is the fairly strong dependence of γ on the wavelength, which can be a serious problem for wide-band OPAs.

5.1.4. Novel materials

As mentioned in the introduction, one of the two approaches to increase the nonlinearity coefficient is to search for materials with a high intrinsic nonlinear refractive index n_2. The nonlinear refractive index of silica is relatively small, and thus a variety of other materials have been sought to replace silica. These include materials such as lead silicates, chalcogenide, tellurium oxide and bismuth oxide.

An empirical relation between the nonlinear and the linear refractive indices suggests that they scale directly [**14**]. This is because they both depend on the density of the material. This relation is shown in Figure **5.1** for a variety of glasses [**15**]. As it is seen, silica is on the lower end, while glasses doped with heavy-metal-oxide are on opposite side. Some glasses are almost 1000 fold more nonlinear than silica.

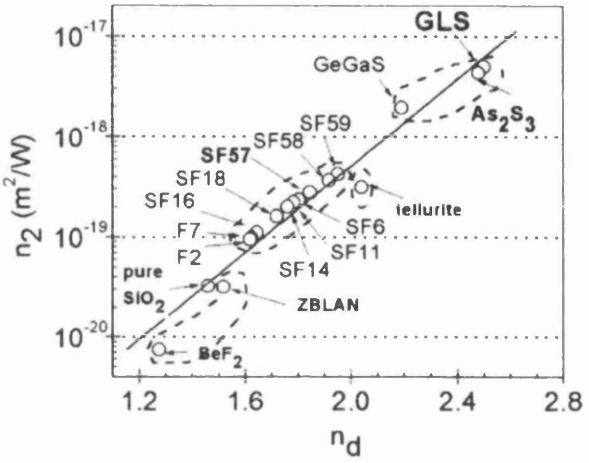

Figure 5.1. Relation between linear refractive index (n_d) and nonlinear refractive index (n_2). (After Ref [15]).

In designing optical fibres using novel materials named above, finding materials with appropriate optical and mechanical properties for cladding is an issue. Thus, normally these fibres are designed to have HF structure, where air is the cladding. It is by combining the small-core HF structure and the high intrinsic nonlinear refractive index that extraordinary values of the order of 1000 $W^{-1}km^{-1}$ are achieved for γ [**15**], [**16**].

Although the advent of optical fibres with extremely large nonlinearity coefficient opens a new horizon for nonlinear applications, there are issues to be addressed in designing such fibres. They normally exhibit large attenuation of the order of 2 dB/m. They also exhibit very large dispersion in the C-band, which limits the use of such fibres. However, research aiming at optimised designs is ongoing. The recent report of a new fibre with a W-type design based on lead-silicates, which has γ as high as 840 $W^{-1}km^{-1}$ and dispersion of about -5 ps/km/nm is a promising example of such improvements [**17**].

5.2. Bismuth-oxide highly-nonlinear fibre

Optical fibres based on bismuth oxide (Bi_2O_3) have attracted considerable attention in the production of highly-nonlinear fibres [**18**]-[**20**]. The nonlinear refractive index of $n_2 \approx 1.1\times10^{-18}$ m^2/W for Bi_2O_3 is greater by a factor of 70 compared with that of silica [**8**]. Starting with a value of 64 W^{-1}km^{-1} for the nonlinear coefficient in 2002 [**18**], it was increased to values as high as 1360 W^{-1}km^{-1} for a step-index design in [**19**] and continued to values of the order of 6000 W^{-1}km^{-1} in sub-wavelength regime and HF design in [**21**]. Many interesting experiments have been conducted using highly-nonlinear optical fibres based on bismuth-oxide (Bi-HNLF) to exploit the promising prospects of such fibres. In [**22**] only 2 cm of a Bi-HNLF was used to generate smooth supercontinuum over a range of 600 nm. Wavelength conversion over 10 nm in the CW regime was reported in [**20**] using a 40-cm segment of Bi-HNLF. In that experiment no SBS suppression was required. Indeed Bi-HNLF are claimed to have a higher SBS threshold in comparison with silica (see section **5.2.2**). Since, like other types of optical fibres based on novel materials, bismuth oxide suffers from a large material dispersion in the communication range, a HF structure has been adopted to overcome this difficulty. In [**23**] a value of -9.9 ps/nm/km at 1550 nm was reported whereas it is normally in the range of -250 ps/nm/km. It permitted wavelength conversion over 32 nm with -20 dB conversion efficiency.

The propagation loss and loss of fusion-splicing such fibres to conventional silica-based fibres are other issues associated with non silica fibres such of Bi-HNLF.

In this section we present the results of our investigations on a sample Bi-HNLF from Asahi Glass Corporation. We will discuss our findings about practical issues we encountered in attempt to make use of the Bi-HNLF in constructing CW OPAs. Although the SBS threshold of Bi-HNLF is higher than that of silica, unless the dispersion properties of those fibres are not improved considerably their use will be limited for fibre OPAs.

5.2.1. Practical considerations

In order to be useful in optical communications, like many other nonlinear optical processing techniques and applications, optical parametric amplification needs to be in the CW regime. On the other hand, in order for effective nonlinear interactions to take

place intense electrical fields are required. Hence, OPAs need very strong pump fields to have considerable gain. Operating fibre-based devices with high-power CW light introduces some issues and requires precautions. Bismuth-based fibres suffer from two kinds of losses, which could be detrimental with regard to the preceding: propagation loss and splice loss.

5.2.1.1. Propagation loss

Bismuth-based fibres exhibit large propagation loss which is intrinsic to the material i.e. bismuth-oxide, and despite efforts put on reducing the loss [**24**], available Bi-HNLFs still have a high loss of about 2 dB/m, which was the case for the sample at our disposal. With such a high loss the effective length of the fibre is reduced to a few meters. Although it is claimed that the high nonlinear coefficient, γ, can counterbalance this difficulty, from a practical point of view high loss means large power absorption in the fibre. For instance, when injecting 2 W of CW pump power a loss of 2 dB/m means that almost 750 mW of power is dissipated in the first meter of the fibre. Considering impurities in the fibre and other latent issues this could cause problems. In our experiments the fibre started to change colour to brown at different points, indicating possible hot spots. Also a fibre fuse occurred in the first meter of the length of the fibre. As a preventive measure the fibre was immersed in cool water; this prevented the discoloration observed otherwise.

5.2.1.2. Splice loss

Fusion splicing of bismuth-oxide fibres to silica-based fibres has been investigated [**25**], [**26**]. Although it is now possible to splice the two kinds of fibres using specialized splicers and specific splice parameters, there is a loss of about 1.5 dB associated with such splices. As with propagation loss, this results in two problems: waste of pump power, which is costly to provide, and CW power dissipation. The latter problem is more severe in this case, as power is dissipated locally rather than in a distributed manner along the fibre.

In addition, due to the difference between the refractive indices there are reflections from the splice points. These contribute to the splice loss, and also cause observable lasing effects, likely due to insufficiently SBS suppression, for high pump powers. These two issues can cause severe problems. In our experiments we observed fibre fuses

ignited at the splice points and burnt splices a number of times; these were attributed to the above-mentioned facts.

5.2.2. SBS figure of merit

Bi-HNLFs have been reported to have enhanced SBS characteristics [**27**]-[**29**] i.e. increased SBS threshold compared to silica-based fibres. However the extent of the improvement has to be assessed carefully to have a correct insight into their suitability for OPA work. In [**28**] it was reported that CW pump power as high as 31.5 dBm was injected into a 5.64 m-long piece of Bi-HNLF without using any pump broadening, and phase-sensitive gain (PSG) of about 31 dB was reported. If confirmed this could be a significant improvement compared to the use of silica-based HNLFs, for which pump broadening by several gigahertz is required in order to obtain significant CW gain. However, one should note that in [**28**] two closely-spaced pumps were used, and simulations show that strong four-wave mixing occurred. As a result, at the fibre output the pump power is spread nearly evenly over a dozen frequencies [**30**]. A consequence of this is that the initial pump powers decay much faster along the fibre than in the absence of FWM, and so the SBS threshold increases.

A new figure of merit was introduced in [**29**], defined as $\gamma P_{th} L$, where P_{th} is the SBS threshold power. Under this definition, the figure of merit for Bi-HNLF turns out to be around 1.05, which is twice as large as for conventional silica-based HNLF. As a consequence one could in principle obtain with Bi-HNLF a gain (in decibels) about twice as large as with silica-based HNLF, if the dispersion parameters of Bi-HNLF were such that phase-matching could be optimum.

Our investigations show that for a single pump the SBS threshold in Bi-HNLF was reached for power levels as low as 340 mW when no pump broadening was applied (Figure **5.2**). This agrees with the figures of merit reported in [**29**]. However this power is insufficient for obtaining useful parametric gain. In order to do so, the pump power must be increased further, and therefore significant pump broadening must still be applied, in contrast to [**28**]. We had to use pump phase modulation by means of a 300-MHz PRBS in order to obtain only 6 dB of parametric gain (Section **5.2.3**).

It is worth noting that Bi-HNLF is considerably birefringent (Section **5.2.4**); and that the SBS threshold in a birefringent fibre depends on the SOP of the pump. Indeed the SBS

threshold can vary by a factor of 2 (3 dB) when the SOP of the pump moves from linear polarization aligned with one of the principal axes to linear polarization at 45° with respect to the principal axes [**31**]; we have made use of this fact in our experiments to find the principal axes (Section **5.2.5**). Although this fact could modify figure of merit by a factor of 2, as far as OPAs are considered, this will not introduce a substantial change. The reason behind this is that the best situation for injecting more power with a fixed amount of SBS suppression would be the worst case in terms of OPA gain.

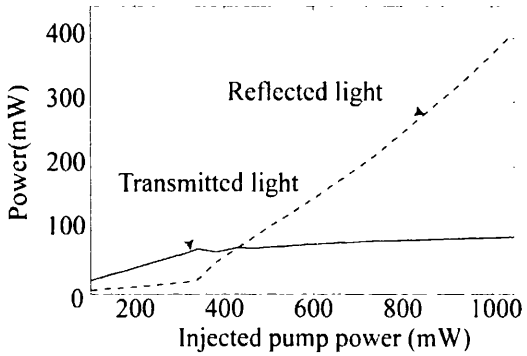

Figure 5.2. Transmitted light and back-reflected light due to SBS for a 3 m long Bi-HNLF.

5.2.3. One-pump OPA: gain close to the pump

In this section, we describe our implementation of a CW OPA with a 3-m long Bi-HNLF. As mentioned in the preceding, a significant amount of spectrum-broadening was needed to obtain 6 dB of gain. Moreover, the gain bandwidth at half maximum was only about 3.5 nm due to the high dispersion in the C-band.

Since loss is significant in Bi-HNLF, one cannot ignore the loss in obtaining closed-form solutions for OPAs. Thus in the simulations we have included the effect of loss which leads to solutions in terms of Bessel functions [**9**].

Moreover, the Raman shift of bismuth is about 30 nm as shown in Figure **5.6**. Hence, for broadband amplification or any other application which extends to this region Raman gain should be considered in addition to loss. We have developed, for the first time to our knowledge, a closed-form solution for OPAs equations including the effect of Raman gain and fibre attenuation based on hypergeometric functions, applicable to such situations (see section **2.1.1**).

5.2.3.1. Experiment description[5]

The experimental setup of the Bi-HNLF OPA is shown in Figure **5.3**. For the pump, a tunable laser (TL1) was first phase-modulated by a 2^{31}-1 PRBS and then amplified by a 33.5 dBm EDFA. The frequency of the PRBS generator could be tuned from 50 MHz up to 3 GHz. A high power isolator was placed after the EDFA to protect it from any potential SBS back reflection. The signal was generated by another tunable laser source (TL2). A polarization controller (PC2) was used to align the signal SOP with that of the pump. The fibre was a 3-m long Bi-HNLF, with loss coefficient $\alpha = 2$ dB/m, chromatic dispersion coefficient D =−240 ps.nm^{-1}.km^{-1} and nonlinearity coefficient $\gamma = 1$ W^{-1}m^{-1}. Pump and signal were injected into the Bi-HNLF through a 99/1 coupler. The splice between the SMF pigtail and the Bi-HNLF introduced a subsequent 2.6 dB loss after the coupler. In order to acquire the OPA output spectra, we used an optical spectrum analyzer (OSA) with 0.01 nm resolution. The pump wavelength was tuned to λ_P=1560.7 nm. The signal wavelength was swept from 1556.4 nm to 1564.8 nm. The injected signal power was −15.5 dBm.

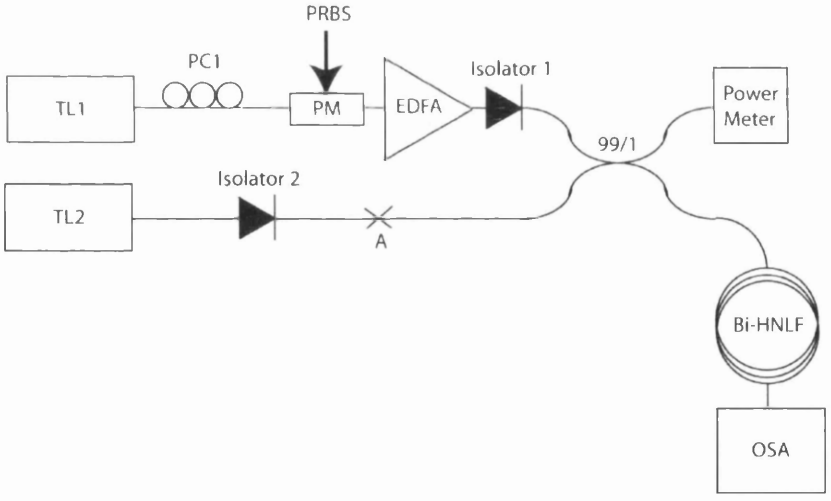

Figure 5.3. Experimental setup for OPA gain measurement in Bi-HNLF. PM: Phase Modulator; 300 MHz of phase modulation is applied to obtain 6 dB of gain near the pump.

[5] This experiment was performed by the joint work of me and Dr. Armand Vedadi.

5.2.3.2. Results and discussions

At maximum EDFA output power, we verified that SBS was sufficiently suppressed for PRBS phase modulation frequency higher than 300 MHz. The injected pump power at the Bi-HNLF input was 30.2 dBm (1.05 W). Figure **5.4** shows the optical spectrum at the Bi-HNLF output for a signal located at 1559.6 nm, when the pump is turned OFF (dashed line) and ON (solid line). The generation of the idler is clearly seen, as well as a few decibels of ON/OFF gain for the signal. Moreover, we observe the generation of symmetrical OPA amplified noise at the pedestal of the pump. By sweeping the signal wavelength, we measured the ON/OFF gain over approximately a 10 nm bandwidth. The results are shown in Figure **5.5**.

The OPA gain spectrum exhibits almost 6 dB ON/OFF gain close to the pump. Because of the high negative dispersion, optimum phase-matching is not achieved. Hence the maximum gain is attained very close to the pump and then it decreases symmetrically. The bandwidth at half maximum was 3.5 nm.

In Figure **5.5** the theoretical gain spectrum obtained by including loss in the OPA equations is plotted in solid line, showing excellent agreement with experimental results. The tilt in the experimental gain spectrum is attributed to birefringence.

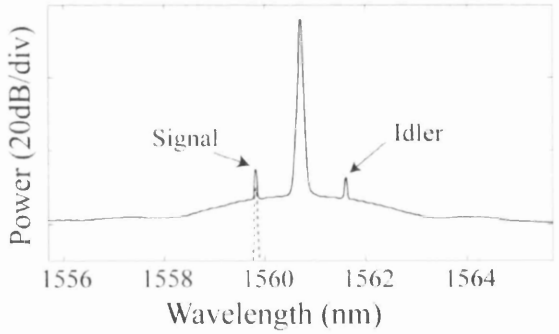

Figure 5.4. Output spectrum of the signal with no OPA pump (dashed), Output spectrum of OPA pump, amplified signal and idler (solid).

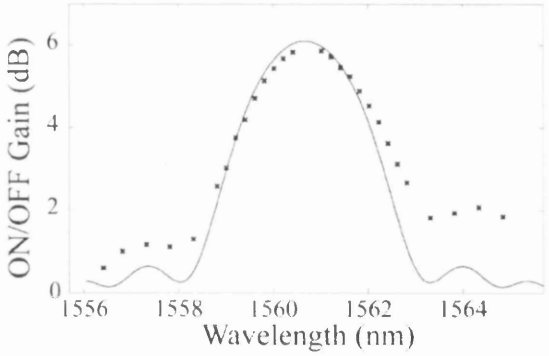

Figure 5.5. Experimental OPA gain (dotted) and theoretical gain curve including loss (solid); the tilt is due to birefringence.

5.2.4. Fibres with constant birefringence and parametric gain with vectorial phase-matching

It was recently found that Bi-HNLFs exhibit a significant amount of constant linear birefringence [**32**]. In [**32**] the amount of birefringence was found to be $\Delta n = 5.1 \times 10^{-6}$. Also the ZDW of current Bi-HNLF lies in the vicinity of 2 microns and thus these fibres show high normal dispersion i.e. GVD of the order of −240 $ps.nm^{-1}.km^{-1}$ in the 1550 nm window. The complex dependence of the gain shape of OPAs on dispersion and phase-matching conditions makes it possible to achieve very different forms for the gain spectra [**9**]. One interesting possibility is to obtain very narrow gain regions far from the pump (Figure **5.6**). This could take place for two different scenarios: (i) when the fourth-order dispersion of the fibre is negative i.e. $\beta^{(4)} < 0$ and GVD is normal and large; (ii) when the fibre is linearly birefringent. In the latter case phase-matching is achieved for orthogonal pump and signal SOPs, while in the former case these SOPs have to be parallel for maximum gain. In Bi-HNLF the observation of such gain regions was reported in [**32**] and [**33**]. In [**33**] this gain was attributed to dispersion, while in [**32**] it was attributed to birefringence.

Injecting a pulsed pump with high power (>10 W) we observed such vectorial modulation-instability (MI) peaks (Figure **5.6**). Since explaining the results solely with dispersion led to impossibly large figures for the dispersion parameters we concluded that these MI peaks are due to birefringence, as in [**32**]. Moreover, we were able to greatly change the amplitude of the peaks, and even eliminate them, by slightly altering the pump SOP. This was another confirmation that the MI peaks originated from birefringence, since otherwise they would not be dependent on the pump SOP.

The phase-matching condition for vectorial modulation-instability described here can be written as:

$$\kappa = \beta^{(2)}\Delta\omega^2 + 2\Delta n\frac{\omega_P}{c} + \frac{2}{3}\gamma P = 0 \qquad 5.1$$

, where γ is the fiber nonlinear coefficient, $\beta^{(2)}$ is the GVD parameter at the pump wavelength and Δn is the linear birefringence. In normal dispersion regime Δn must have negative sign i.e. the SOP of the pump should fall on slow axis. The term $\frac{2}{3}\gamma P$ is the nonlinear phase mismatch. For pump power below 20W, this term is much smaller than both birefringence and dispersion term, and hence its contribution to the phase-matching condition is negligible. Therefore, the location of the MI peaks depends mainly on the position of the pump and not on pump power. Rigorous investigations also suggest that the width of the peaks does not change considerably with pump power or wavelength.

The birefringence can be calculated from the distance between the MI peaks and the pump (30 nm) and the fibre dispersion coefficient [**9**], [**34**]. For our fibre we found that $\Delta n = 2 \times 10^{-5}$, approximately four times larger than for the fibre used in [**32**].

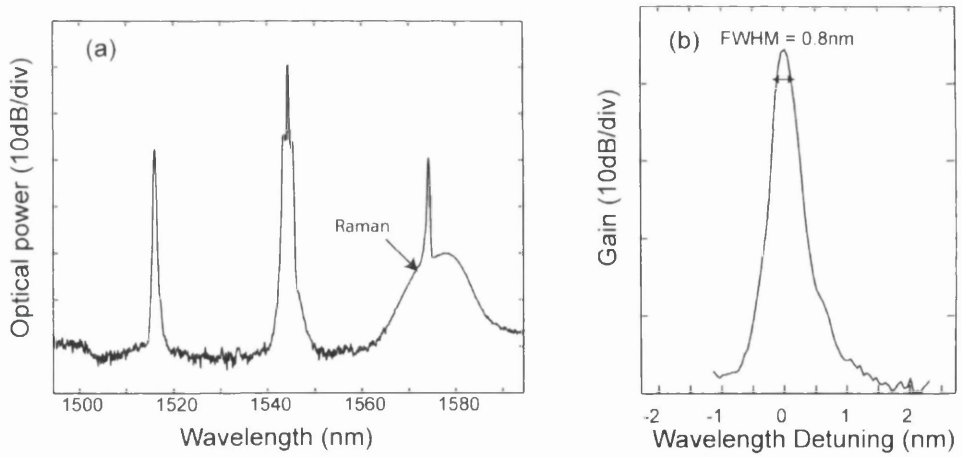

Figure 5.6. (a) ASE spectrum showing the Vectorial Modulation Instability with an input pump power of 18 W; Raman shift is about 30 nm. (b) Shape of the expected gain spectrum (Anti-Stokes side); FWHM is about 0.8 nm.

5.2.5. A novel scheme for active wavelength demultiplexing with gain

The width of the gain regions described in the previous section was measured to be about 100GHz (0.8 nm). In addition, the location of the peaks is controllable by tuning

the pump wavelength. This feature is interesting for filtering (demultiplexing) applications in WDM networks where channels are located 100 GHz apart. Hereinafter, we present an innovative scheme for wavelength demultiplexing exploiting this feature. We report on demultiplexing WDM channels modulated at 10 Gb/s and located on a 100 GHz grid with a power penalty of less than 2 dB using this scheme [**35**]. To the best of our knowledge, this is the first time that a filtering device concurrently providing gain is reported.

In order to demultiplex asynchronous telecommunication signals, the pump needs to be CW. Since the phase-matching used here is achieved for orthogonal SOPs of pump and signal, there is an effective reduction of γ by 2/3 (Eq. (**5.1**)); hence an even higher pump power than in section **5.2.3** is required to exploit this gain mechanism.

5.2.5.1. Experiment description[6]

The experimental setup is shown in Figure **5.7**. For the pump, a tuneable laser (TL1) is phase-modulated by a 3 Gb/s PRBS to suppress SBS. It is then amplified by EDFA1 to 4.5 W and its ASE is filtered out by a bandpass filter (BPF), before being coupled with the WDM channels through a 99/1 coupler into the 2.9-m long Bi-HNLF. The splice loss between the pigtail and the Bi-HNLF is 2 dB. Thus the injected pump power was around 2.5 W. To our knowledge, this is the highest CW power launched into a Bi-HNLF.

Three tunable lasers with wavelengths λ_1=1530.2 nm, λ_2=1531 nm and λ_3=1531.8 nm are used as WDM channels 1, 2 and 3. They are combined through an arrayed waveguide grating (AWG) and intensity modulated by a 10 Gb/s PRBS. The channels are subsequently decorrelated by an 8-km spool of SMF-28 before being amplified. The mean power per channel at the Bi-HNLF input is -12 dBm.

In order to obtain maximum gain, it is essential to align the pump SOP with the Bi-HNLF fast polarization axis and the signal SOP with the slow one. To this end, the GPIB-controlled polarization controller PC2 is used to sweep the pump SOP over the whole Poincare sphere while measuring the SBS power coming from the circulator when no phase modulation is applied (Figure 5.8(**a**)). The two locations for which the SBS power is maximized correspond to the locations of the two axes of birefringence.

[6] This experiment was performed with joint work of me and Dr. Armand Vedadi. The initial idea and the overall supervision was provided by Prof. Michel Marhic.

For each of these pump SOPs, the signal SOP was swept via PC3 (Figure 5.8**(b)** and **(c)**). By optimizing the idler power, the correct pump and signal SOPs could be determined and set. To select channel 1, 2 or 3, λ_p was set at 1558.8 nm, 1559.7 nm or 1560.5 nm, respectively.

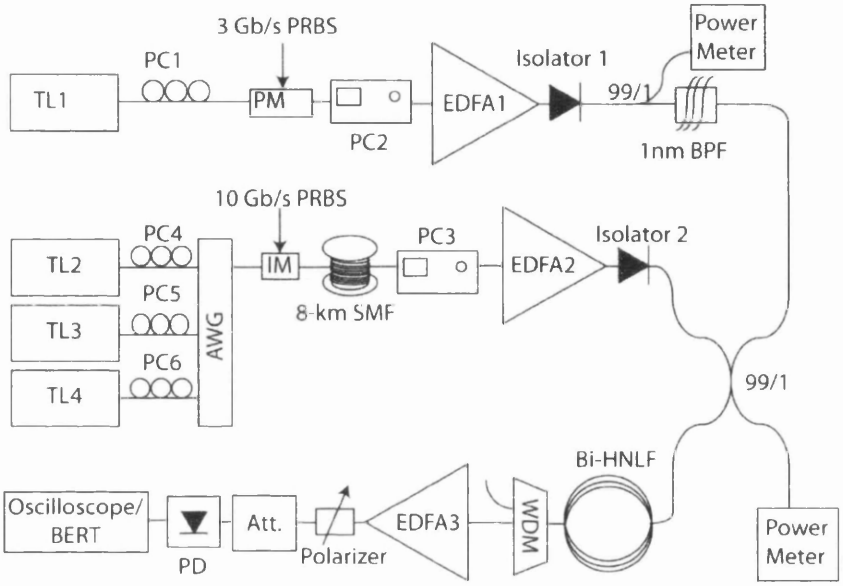

Figure 5.7. Experimental setup for novel tunable wavelength demultiplexing scheme with gain; three 10 Gb/s channels are demultiplexed with power penalty of less than 2 dB.

5.2.5.2. Results and discussions

Figure **5.9(a)** shows the WDM channels spectrum at the Bi-HNF output when the pump is OFF and ON with λ_p = 1559.7 nm. When the pump is ON, we observe that channel 2 is amplified by 6 dB. Moreover, the other two channels are slightly attenuated because of Raman loss. Overall, channel 2 is selected with a crosstalk of less than -6.5 dB. Through the parametric gain process, the signal data is also copied onto a generated idler wave, which is located at a wavelength symmetric with respect to the pump. The demultiplexing of the idler is even more efficient with a crosstalk of less than -20dB, as Figure **5.9(b)** shows.

To assess the error penalty, we placed a C/L band WDM coupler at the Bi-HNLF output to filter out the pump and signal and keep only the idler. The idler is then amplified by

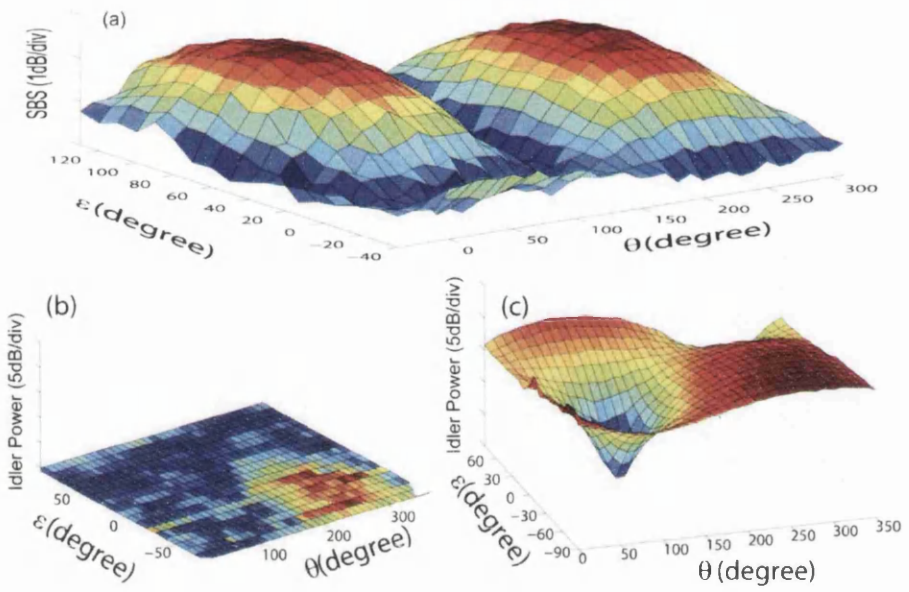

Figure 5.8. (a) Back reflected power due to SBS for different Poincare sphere coordinates of PC2; it varies by a factor of 2 (3 dB). (b, c) Idler power for Poincare sphere coordinates of PC3 when the pump polarization is on (b) the slow or (c) fast axis.

an L-band EDFA that also removes any remaining pump. A polarizer is placed to filter out the Raman-induced ASE, which is polarized like the pump. Finally an attenuator is placed before the photodetector receiver. Signal quality was assessed through eye diagram and bit error rate (BER) measurements. Figure **5.10(a)**, **(b)** and **(c)** show the eye diagrams for idler channels 1, 2 and 3, respectively. No significant distortion is observed and the eyes remain clearly open. Figure **5.11** shows the BER plots for channels 1, 2 and 3. The OSNR of the input signals was 24.5 dBm. We see that the demultiplexer operates with low penalty at bit-error rates well below the FEC limit. For example for channel 1, which exhibits the best performance, a penalty of about 2dB is obtained for BER = 10^{-9}. The difference in performance between channels can be attributed to the shape of the gain spectrum (Figure **5.6(b)**). Indeed, the channels located in the vicinity of the demultiplexed channel experience a residual gain as seen in Figure **5.9**. Hence, channel 2 which has two channels in its vicinity exhibits the worst performance. Also Figure **5.6(b)** shows that the gain spectrum exhibits a tail on the side closest to the pump location. This explains the improved performance of channel 1, over channel 3. Indeed, the steep decrease of the gain at higher wavelengths reduces the interference of channel 2 for channel 1 compared to channel 3.

Note that because both signal and idler SOPs are orthogonal to the pump, one could straightforwardly remove the pump by using a high-contrast polarizer and extract both signal and idler at the same time.

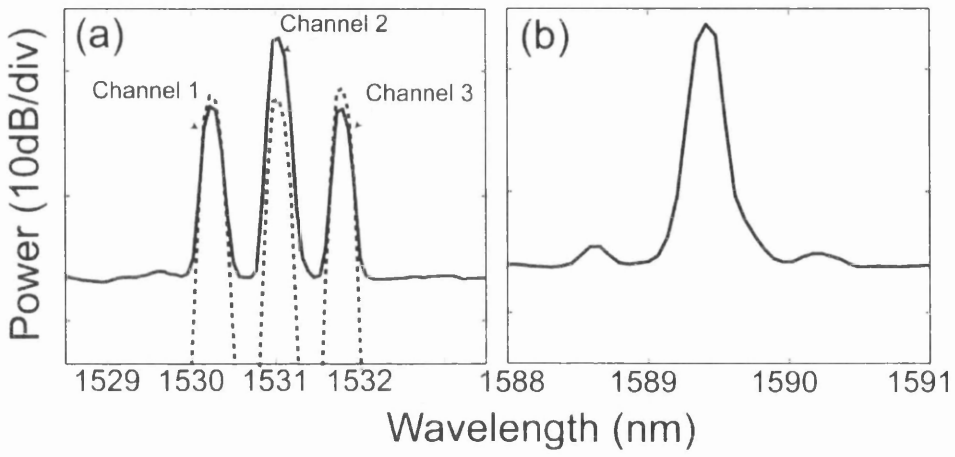

Figure 5.9. (a) WDM channels spectrum with pump OFF (dashed line) and ON (solid line). (b) Idler spectrum.

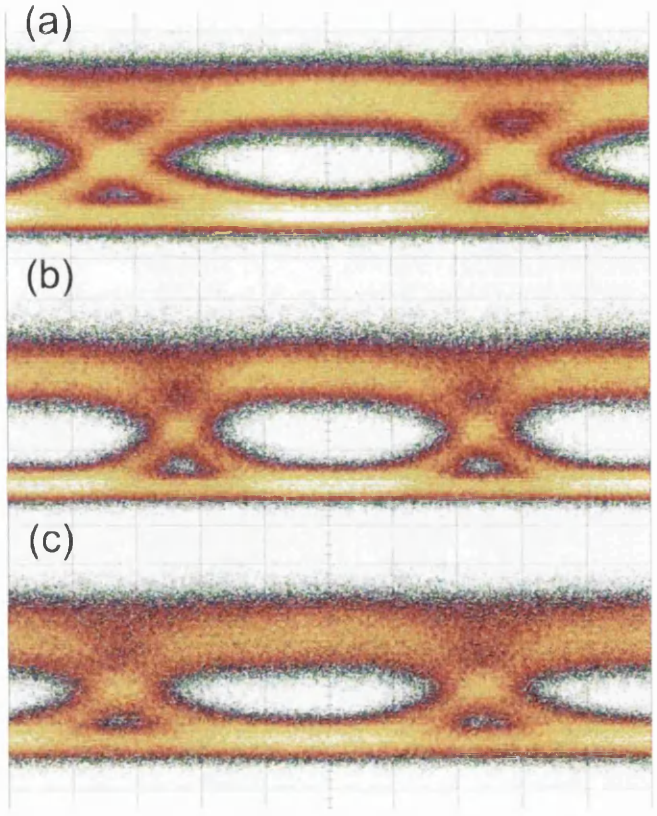

Figure 5.10. (a), (b) and (c) Eye diagrams for channels 1, 2 and 3.

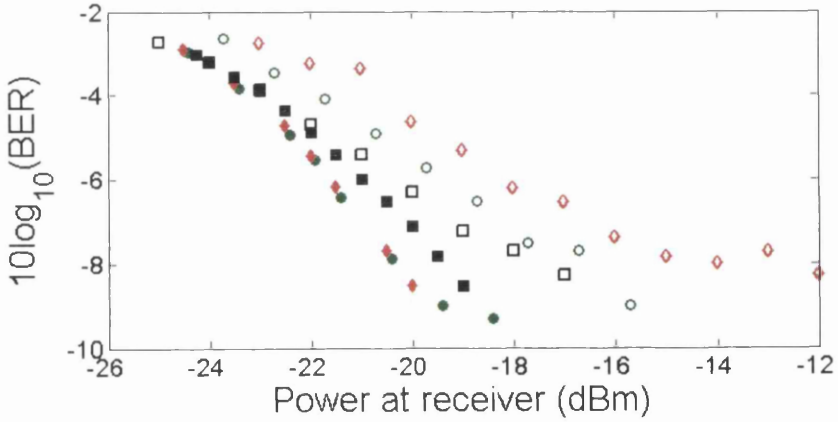

Figure 5.11. Bit Error Rate for channels 1 (blue squares), 2 (red diamonds) and 3 (green circles). Back to back measurements, represented in filled shapes, are made at signal wavelengths, while the demultiplexed channels (non filled shapes) are at the corresponding idler wavelengths.

5.2.6. Simultaneous wavelength- and time-demultiplexing[7]

Using a pulsed pump, one can also in principle demultiplex signals in time and wavelength simultaneously. Indeed, due to the quasi-instantaneous response of OPAs, time demultiplexing at ultrahigh speed has been demonstrated with standard OPAs [**36**]. This feature, used in conjunction with the gain spectrum in vectorial phase-matched Bi-HNLF OPAs, can lead to simultaneous separation of time-multiplexed WDM channels as shown in

Figure 5.13. By tuning the pump pulses at the right time and wavelength, gain is generated on the desired time slot and wavelength and the desired channel can be selected. The generated idler can also be used to enhance the extinction ratio.

We used this concept to demonstrate demultiplexing from 37 wavelength channels to 1 channel and 40 Gb/s to 10 Gb/s simultaneously. The experimental setup is sketched in Figure **5.12**. A mode locked fibre ring laser was used to generate short pulses of about 6 ps duration at a repetition rate of 10 Gb/s. The output pulses could then be further modulated using a Mach-Zehnder intensity modulator to reduce the repetition rate down to as low as 625MHz. The pump was then amplified and filtered by two EDFAs to reach the required multi-watt peak power. 37 wavelength channels were launched from a 40 Gb/s WDM test bed; they were modulated with a 2^{31}-1 PRBS and a half-rate clock to produce a 40Gb/s 67% RZ OOK signal. Using a 64-bit binary word (1 0 0...), we generated an adequate pump to demultiplex a single wavelength from 40 Gb/s down to 625 Mb/s. This effectively demultiplexed a 625Mb/s sub-channel from an initial data rate of 1.48Tb/s. We observed the demultiplexed channel on the idler side for a mean injected pump power of 2 W. Since we use short pulses this average power corresponds to a very high peak power. At this high power level, the splice between the high numerical-aperture fibre and the input of the Bi-HNLF burnt, which prevented us from recording any data.

In order to succeed better with this experiment, it will be necessary to employ a cooling scheme to remove the heat generated at the Bi-HNLF splices.

[7] This experiment was performed by the joint work of me and Dr. Armand Vedadi. Dr. Donald Govan provided valuable ideas and helps.

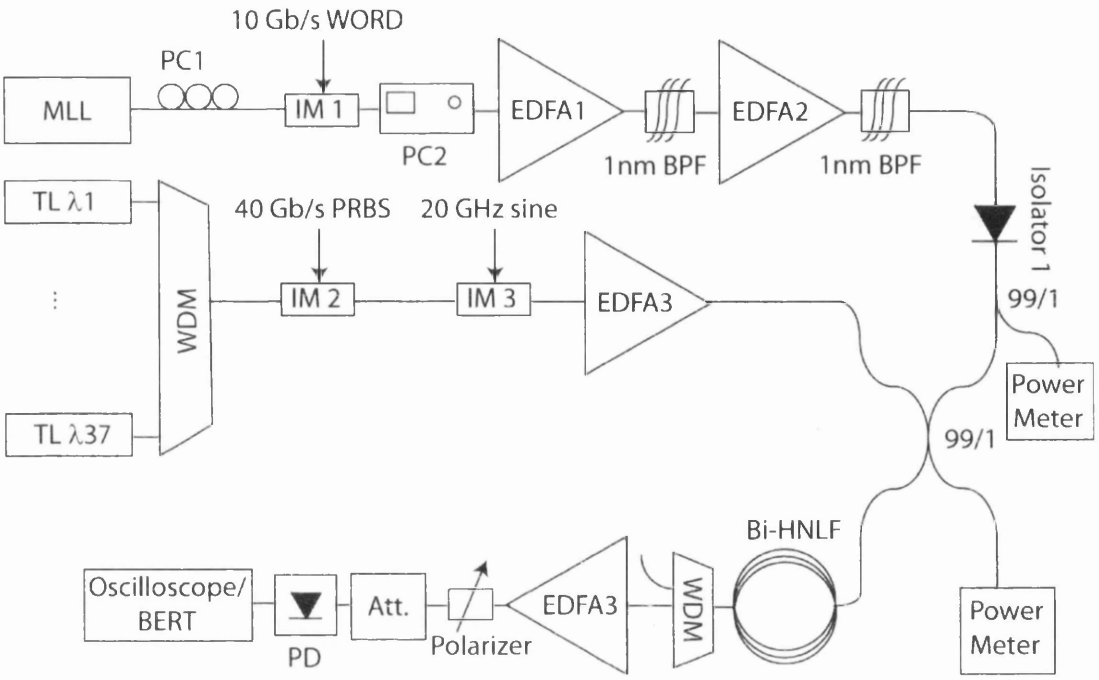

Figure 5.12. Experimental setup for simultaneous time- and wavelength-demultiplexing.

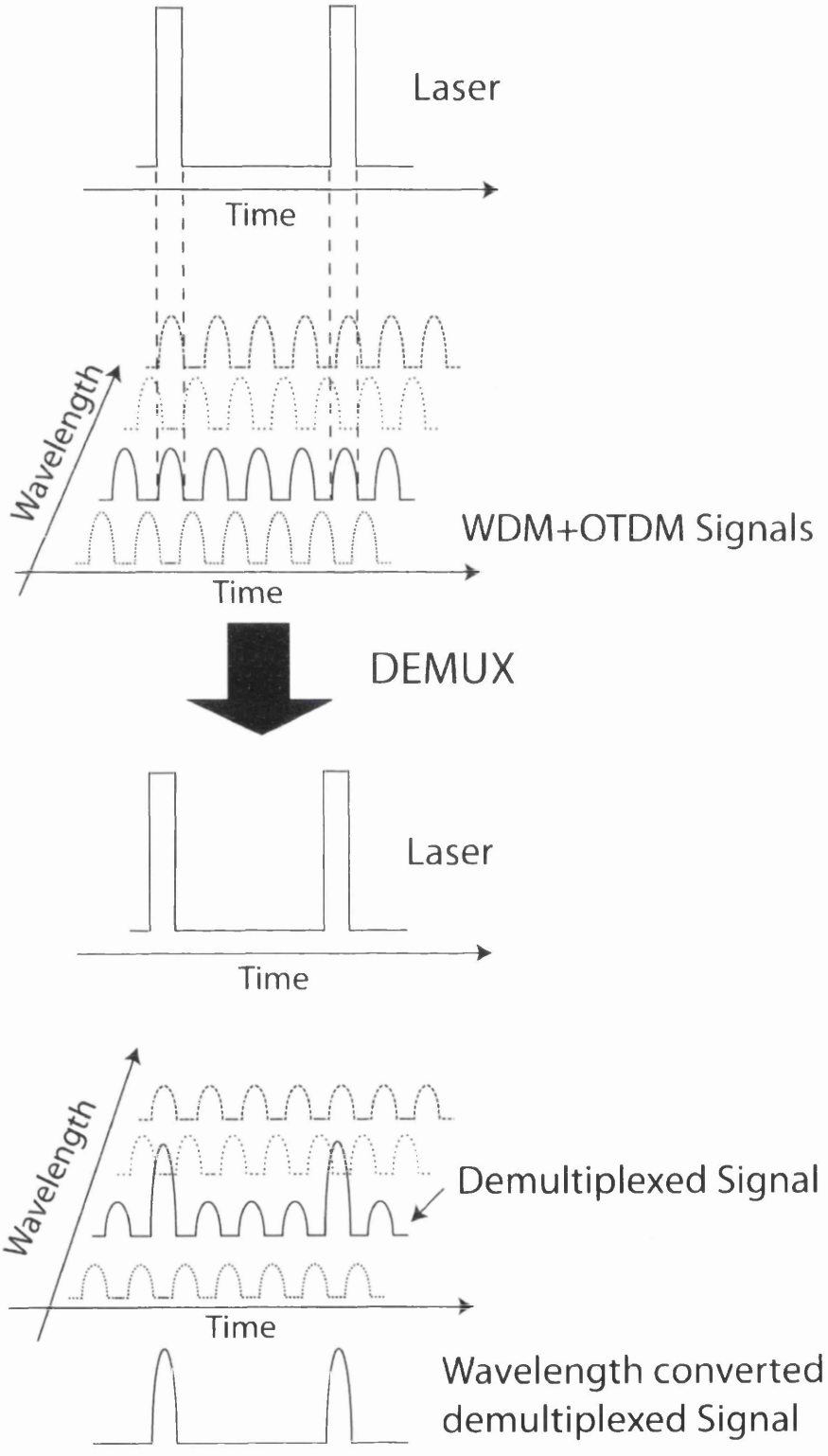

Figure 5.13. Principle of Simultaneous Time and Wavelength demultiplexing; By injecting pump at right wavelength and time slot simultaneous Wavelength- and Time-Demultiplexing is achieved

Summary

This final chapter discusses the newly developed technology for constructing highly-nonlinear fibres with extraordinary nonlinearity coefficient in excess of 1000 $W^{-1}km^{-1}$. The fibre nonlinearity coefficient, γ, is dependent on two parameters, namely the effective area, A_{eff}, and the nonlinear refractive index, n_2. Therefore any approach to increase the γ must either reduce the A_{eff}, or increase n_2 or both.

In order to reduce the A_{eff}, new technologies with promising results have been developed. The important technology of this type is microstructured optical fibres. Holey fibres are another name often used for this type of fibre.

In the direction of increasing n_2 using new materials, known as compound glasses, such as bismuth-oxide, lead-silicate etc are being considered to form the core of the fibre. In fact, using new materials, fibres with extremely high fibre nonlinearities have been reported.

One of the suitable materials for construction of highly-nonlinear fibres, which has attracted a lot of attention, is bismuth-oxide. These fibres, in addition to high nonlinearity coefficient, exhibit constant linear birefringence.

In this chapter, we presented our results of investigation on a sample of bismuth-oxide highly-nonlinear fibres, which are called Bi-HNLF. We first tried to investigate their suitability for actual parametric amplification, which showed that despite the high γ, due to inappropriate dispersion properties they are not suitable for practical OPAs yet. We then proceed to exploit their linear birefringence to generate narrowband gain regions using the method discussed in Chapter **3**. We used that to propose a novel scheme for filtering. At the end the possibility of a simultaneous time- and wavelength-demultiplexing is discussed.

References

[1] M. P. Fok, and C. Shu "Recent Advances in Optical Processing Techniques Using Highly Nonlinear Bismuth Oxide Fibre," *IEEE J. Sel. Topics in Quantum Electronics*, vol. 14, pp. 587-598, 2008.

[2] Y. H. Kuo, H. S. Rong, V. Sih, S. B. Xu, M. Paniccia, and O. Cohen, "All optical wavelength conversion at 40 Gb/s data rate in silicon waveguides," *Opt. Exp.*, vol. 14, pp.11721-6, 2006.

[3] A. K. Popov, S. A. Myslivets, T. F.George, andV. M. Shalaev, "Four-wave mixing, quantum control, and compensating losses in doped negative index photonic metamaterials," *Opt. Lett.*, vol. 32, pp. 3044–3046, 2007.

[4] T. Tanabe, K. Nishiguchi, A. Shinya, E. Kuramochi, H. Inokawa, and M. Notomi, "Fast all-optical switching using ion-implanted silicon photonic crystal nanocavities," *Appl. Phys. Lett.*, vol. 90, pp. 31115-1–31115-3, 2007.

[5] A. Boskovic, S. Chernikov, J. Taylor, L. Gruner-Nielsen, and O. Levring, "Direct continuous-wave measurement of n2 in various types of telecommunication fiber at 1.55 μm," *Opt. Lett.*, vol. 21, pp. 1966-1968, 1996.

[6] L. Prigent and J. P. Hamaide, "Measurement of fiber nonlinear Kerr coefficient by four-wave mixing," *IEEE Photon. Technol. Lett.*, vol. 5, pp. 1092–1095, 1993.

[7] P. Dumais, F. Gonthier, S. Lacroix, J. Bures, A. Villeneuve, P. Wigley, and G. Stegeman, "Enhanced self-phase modulation in tapered fibers," *Opt. Lett.*, vol. 18, pp. 1996-1998 , 1993.

[8] G. P. Agrawal, *Nonlinear Fiber Optics*. 4th Ed. United States Of America: Academic press, 2007.

[9] M. E. Marhic, *Fiber Optical Parametric Amplifiers, Oscillators and Related Devices*. United Kingdom: Cambridge University Press, 2008.

[10] P. St. J. Russell, "Photonic Crystal Fibers," *Science*, vol. 299, pp. 358-362 ,2003.

[11] J. Broeng, D. Mogilevstev, S. E. Barkou, and A. Bjarklev, "Photonic Crystal Fiber: A New Class of Optical Waveguides," *Opt. Fiber Technol.*, vol. 5, pp. 305-330, 1999.

[12] N. Broderick, T. Monro, P. Bennett, and D. Richardson, "Nonlinearity in holey optical fibers: measurement and future opportunities," *Opt. Lett.*, vol. 24, pp. 1395-1397, 1999.

[13] T. White, R. McPhedran, C. de Sterke, L. Botten, and M. Steel, "Confinement losses in microstructured optical fibers," *Opt. Lett.*, vol. 26, pp. 1660-1662, 2001.

[14] C. C. Wang, "Empirical relation between the linear and the third-order nonlinear optical susceptibilities," *Phys. Rev. B.*, vol. 2, pp. 2045–2048, 1970.

[15] X. Feng, A. Mairaj, D. Hewak, and T. Monro, "Nonsilica Glasses for Holey Fibers," *J. Lightwave Technol.*, vol. 23, pp. 2046- 2054, 2005.

[16] H. Ebendorff-Heidepriem, P. Petropoulos, S. Asimakis, V. Finazzi, R. Moore, K. Frampton, F. Koizumi, D. Richardson, and T. Monro, "Bismuth glass holey fibers with high nonlinearity," *Opt. Express.*, vol. 12, pp. 5082-5087, 2004.

[17] A. Camerlingo, X. Feng, F. Poletti, G. Ponzo, F. Parmigiani, P. Horak, M. Petrovich, P. Petropoulos, W. Loh, and D. Richardson, "Near-zero dispersion, highly nonlinear lead-silicate W-type fiber for applications at 1.55μm," *Opt. Express.*, vol.18, pp. 15747-15756, 2010.

[18] K. Kikuchi, K. Taira, and N. Sugimoto, "Highly nonlinear bismuth oxide-based glass fibres for all-optical signal processing," *Electron. Lett.* vol. 38, pp. 156-157, 2002.

[19] N. Sugimoto, T. Nagashima, T. Hasegawa, S. Ohara, K. Taira, and K. Kikuchi, "Bismuth-based optical fiber with nonlinear coefficient of 1360 $W^{-1}km^{-1,}$ " in

Optical Fiber Communication Conference (OFC), Los Angeles, California, 22 Feb.2004, paper PD26.

[20] J. Lee, T. Nagashima, T. Hasegawa, S. Ohara, N. Sugimoto, and K. Kikuchi, "Bismuth-Oxide-Based Nonlinear Fiber With a High SBS Threshold and Its Application to Four-Wave-Mixing Wavelength Conversion Using a Pure Continuous-Wave Pump," *J. Lightwave Technol.* vol. 24, pp. 22-28, 2006.

[21] S. Afshar Vahid, W. Zhang, H. Ebendorff-Heidepriem, and T. Monro, "Small core optical waveguides are more nonlinear than expected: experimental confirmation," *Opt. Lett.*, vol. 34, pp. 3577-3579, 2009.

[22] J. Gopinath, H. Shen, H. Sotobayashi, E. Ippen, T. Hasegawa, T. Nagashima, and N. Sugimoto, "Highly nonlinear bismuth-oxide fiber for smooth supercontinuum generation at 1.5 μm," *Opt. Express.*, vol. 12, pp. 5697-5702, 2004.

[23] K. Chow, K. Kikuchi, T. Nagashima, T. Hasegawa, S. Ohara, and N. Sugimoto, "Four-wave mixing based widely tunable wavelength conversion using 1-m dispersion-shifted bismuth-oxide photonic crystal fiber," *Opt. Express* ., vol.15, pp. 15418-15423, 2007.

[24] T. Nagashima, T. Hasegawa, S. Ohara, and N. Sugimoto, "Multi-step-index Bismuth-based highly nonlinear fiber with low propagation loss and splice loss," in *Optical Fiber Communication Conference (OFC)*, Anaheim, California , 6-11 March 2005, Paper OThA2.

[25] Y. Kuriowa, N. Sugimoto, K. Ochiai, S. Ohara, Y. Fukasawa, and S. Ito, "Fusion Spliceable and High Efficient Bi2O3-based EDF for Short-length and Broadband Application Pumped at 1480 nm," in *Optical Fiber Communication Conference (OFC)*, Anaheim, California, 17 March 2000 , Paper TuI5-1.

[26] P. Petropoulos, H. Ebendorff-Heidepriem, T. Kogure, K. Furusawa, V. Finazzi, T. M. Monro, and D. J. Richardson, "A spliced and connectorized highly nonlinear and anomalously dispersive bismuth-oxide glass holey fiber," in *Conference on Lasers and Electro-Optics (CLEO)*, San Francisco, California,16 March 2004, Paper CTuD3.

[27] J. H. Lee, T. Nagashima, T. Hasegawa, S. Ohara, N. Sugimoto, and K. Kikuchi, "Bismuth-Oxide-Based Nonlinear Fiber With a High SBS Threshold and Its Application to Four-Wave-Mixing Wavelength Conversion Using a Pure Continuous-Wave Pump," *J. Lightwave Technol.*, vol. 24, pp. 22-28, 2006.

[28] K. Croussore, and G. Li, "Phase Regeneration of NRZ-DPSK Signals Based on Symmetric-Pump Phase-Sensitive Amplification," *IEEE Photon. Technol. Lett.* Vol. 19, pp. 864-866, 2007.

[29] J. H. Lee, T. Tanemura, K. Kikuchi, T. Nagashima, T. Hasegawa, S. Ohara, and N. Sugimoto, "Experimental comparison for a Kerr nonlinearity figure of merit including the Stimulated Brillouin Scattering threshold for state-of-the-art nonlinear optical fibers," *Opt. Lett.*, vol. 30, pp. 1698-1700, 2005.

[30] A. Vedadi, M. Jamshidifar, and M. E. Marhic, "Continuous-Wave Bismuth-Oxide One-Pump Fiber Optical Parametric Amplifier," in *European Conference on Optical Communication (ECOC)*, Brussels, Belgium, 2008, Poster P.1.20.

[31] M. O. Van Devender, A. J. Boot, "Polarization properties of SBS in single mode fibers," *J. Lightwave Technol.*, vol. 12, 585-590, 1994.

[32] F. Yaman, E. Mateo, G. Li, "Vectorial Modulational Instability in a Bismuth Fiber," in *Proceedings: Lasers and Electro-Optics Society (LEOS), The 20th Annual Meeting of the IEEE*, 2007, paper WQ2.

[33] K. Seki, S. Yamashita, "Narrowband and Tunable Parametric Amplification in Bismuth-Oxide-Based Highly Nonlinear Fiber," in *Conference on Lasers and Electro-Optics (CLEO)*, 2008, Paper CFL1.

[34] R. H. Stolen, M. A. Bosch, C. Lin, "Phase matching in birefringent fibers," *Opt. Lett.*, vol. 6, pp.213-215, 1981.

[35] A. Vedadi, M. Jamshidifar, M. E. Marhic, "Wavelength Demultiplexing Based on a Continuous-Wave Bismuth-Oxide Fiber Optical Parametric Amplifier," in *European Conference on Optical Communication (ECOC)*, Brussels, Belgium, 21-25 Sept. 2008 , PDP Th.3.C.2.

[36] J. Hansryd, P. A. Andrekson, "O-TDM Demultiplexer with 40-dB Gain Based on a Fiber Optical Parametric Amplifier," *IEEE Photon. Technol. Lett.*, vol. 13, pp. 732-734, 2001.

[37] T. Hasegawa, T. Nagashima, S. Ohara, and N. Sugimoto, "High Nonlinear Bismuth Fibers and Their Applications," in *Optical Fiber Communication Conference (OFC)*, Anaheim, California, March 2006, Paper OTuH.

[38] T. Nagashima, T. Hasegawa, S. Ohara, and N. Sugimoto, "Dispersion shifted Bi_2O_3-based photonic crystal fiber," in *European Conference on Optical Communication (ECOC)*, Cannes, France, 2006, Paper We1.3.2.

Chapter 6. Conclusion

6.1. Conclusion

The objective of this thesis was to investigate the possible role of fibre optical parametric amplifiers in practical telecommunication systems. Although, OPAs and their main feature, which is the capability of providing very broad gain bandwidth, have been investigated for many applications for years, what makes them potentially attractive at this time is firstly the ever-increasing demand for high bit-rate transmission capacity. The capacity of current telecommunication systems is limited to the quite small bandwidth of EDFAs and is about to be fully occupied. Therefore, novel amplifier technologies with greater bandwidth can be the solution to the current situation.

The other motivation for reinvestigation of OPAs within the past few years is that, high power pumps and highly-nonlinear fibres that have emerged recently have made it possible to construct more compact OPAs with improved performance.

While the nonlinearity coefficient of DSFs as the most widely-used medium for OPAs is only about 2 $W^{-1}km^{-1}$, new highly-nonlinear fibres have γ of about 20 $W^{-1}km^{-1}$, which in turn reduces the length of the fibre required.

The technology of highly-nonlinear fibres is growing beyond silica-based fibres and step-index designs. Novel materials are being considered to be used to make new fibres with extraordinary nonlinearity [**1**]. Moreover, new fibre structures have been developed recently, which makes it possible to reduce the effective area and hence improve the nonlinearity even more. Bismuth-oxide fibres are one of the promising classes of fibres of this type.

As part of my thesis, I investigated a sample of Bi-HNLF for OPA work. The sample has a γ of 1360 $W^{-1}km^{-1}$. It was found that despite such high γ, due to the high loss and large dispersion (-240 ps/nm/km) in the C-band, no meaningful parametric gain is obtainable with this kind of fibre currently. However, as soon as the ZDW of these novel HNLFs is brought to the C-band, OPAs will experience an astonishing improvement.

Nonetheless, still innovative ideas in the context of all optical signal processing can benefit from these fibres. In an experiment, making use of linear birefringence a new filtering scheme is proposed and demonstrated in the thesis with the capability of providing gain. The scheme is extendable to simultaneous time- and wavelength-demultiplexing, which can be a very useful functionality.

In the laboratory experiments with OPAs, the pump in almost all cases is provided by an EDFA. Novel very high-power EDFAs that have become commercially available can deliver up to 10 W of CW power, which enables researchers to build very broadband CW OPAs. However, it may not seem very practical to use an EDFA for each OPA. Thus, laser sources with suitable characteristics, namely high power, narrow linewidth, and low relative intensity noise (RIN) should be sought.

At any rate, when talking about OPAs, the main interest is to exploit the broadband features of them. As mentioned before, OPAs are capable of providing unbeatable gain bandwidths [**2**]. In fact, OPAs with 730 nm of bandwidth in one-pump arrangement and pulsed-mode [**3**] and 155 nm of bandwidth in a two-pump arrangement [**4**] have been demonstrated. The interesting point about the gain spectra of OPAs is that they are 'man-made'. It means that the designer can determine the shape and the centre frequency of the gain spectrum of OPAs almost at will providing that he possesses the right pump and fibre.

Besides, OPAs are capable of providing very large gain. This is mainly due to the fact the parametric gain is only available in the direction of the pump i.e. the gain is uni-directional. This reduces the growth of the parasitic reflections, which is a limiting factor for very high gain amplifiers [**5**].

Fibre optical parametric amplifiers suffer from a number of problems, which have prevented OPAs from being used in practice. The major problems are the impact of Raman gain, the impact of SBS, the polarisation dependence and the nonlinear crosstalk.

In very broadband OPAs, for which the gain bandwidth is above 100 nm the mutual effect between parametric process and the Raman gain becomes important. The full description of the problem requires including the Raman gain in the coupled equations of OPAs and computational simulations are necessary. However, the immediate effect is

distortion in the gain spectrum of the OPA. The situation is more problematic in the novel HNLFs made up of compound glasses. Since the Raman shift is much smaller in this case. For example in Figure **5.6** it is seen that for Bi-HNLF the Raman shift is about 30 nm. Therefore, the impact of the Raman gain is to be carefully considered when designing broadband OPAs.

Stimulated Brillouin scattering is another problem facing OPAs. SBS prevents injection of high pump-power into the HNLF. This is essential to achieve broadband OPAs. Moreover, SBS is a chaotic process which deteriorates the performance. Therefore, sufficient suppression of SBS is necessary for the operation of OPAs. Currently, the most widely-used technique for SBS suppression is pump broadening by means of phase-dithering [**6**].

The FWM process as the underlying process through which the amplification takes place in OPAs is fundamentally polarisation dependent [**7**]. As a result, the gain in OPAs is also dependent on the SOP of the incoming signal. The gain is maximum when both the pump and the signal are linearly polarised with the same orientation and it minimum for orthogonal linear SOP of the pump and the signal. The dependency of the gain on the SOP of the signal is problematic as in real systems the SOP of the signal is completely random. As the problem is of a fundamental nature, there is not any measures one could take to solve it other than using some techniques. Today, making use of polarisation diversity method seems to be the solution to this problem [**8**].

Nonlinear crosstalk has been one of the main criticisms on the OPAs for years [**9**]. In the OPAs, one needs to place the pump and signals near ZDW of the fibre in order to have phase-matching condition met. This leads to good phase-matching among the channels as well. Spurious FWM terms generated among the channels deteriorate the quality of the channels. This problem has been looked into more closely in this thesis. In fact, it has been shown that this problem can be solved by shortening the fibre [**10**] and the crosstalk can be kept with in a tolerable limit.

6.2. Summary of contribution to the knowledge

The contributions to the knowledge of fibre optical parametric amplifiers that have been achieved during my PhD period and reported in this thesis is summarised as follows:

- Investigation of very high-gain OPAs in two-pump arrangement and report of a two-pump OPA with 60 dB of gain.
- Investigation of very broadband OPAs in CW operating in CW regime and report of the operation of a one-pump CW OPA with a 270 nm of bandwidth.
- Investigation of the problem of the Raman gain on the bandwidth of the one-pump OPAs. It was shown that deliberately misaligning the SOP of the pump and the signal may be a good idea to improve the smoothness of the gain spectrum in the expense of loosing some gain.
- Investigation of the problem of the nonlinear crosstalk in OPAs. It was shown that shortening the length of the fibre, the amount of crosstalk can be reduced to tolerable limits. In a experiment, I showed that reducing the length of the fibre from 340 m to 50 m the amount of crosstalk is reduced by 16 dB. In another experiment I initiated, we transmitted 26 channels in an OPA and obtained performance results close to that of EDFA.
- Investigation of a sample of newly emerged bismuth-oxide HNLF for OPA work. It was shown that despite the very high γ and quite improved SBS threshold, these fibres are not very useful for OPA work until their dispersion properties are modified.
- Proposing and demonstration of a scheme for filtering while providing gain. Making use of the Bi-HNLF sample, I managed to demonstrate the possibility of channels filtering while providing gain. The scheme is shown to be extendible to simultaneous time- and wavelength-demultiplexing.

References

[1] X. Feng, A. Mairaj, D. Hewak, and T. Monro, "Nonsilica Glasses for Holey Fibers," *J. Lightwave Technol.*, vol. 23, pp. 2046- 2054, 2005.

[2] J. Hansryd, and P. A. Andrekson, "Broad-band continuous-wave-pumped fiber optical parametric amplifier with 49-dB gain and wavelength-conversion efficiency," *IEEE Photon. Technol. Lett.*, vol. 13, pp. 194–196, 2001.

[3] J. Chavez Boggio, J. Windmiller, M. Knutzen, R. Jiang, C. Bres, N. Alic, B. Stossel, K. Rottwitt, and S. Radic, "730-nm optical parametric conversion from near- to short-wave infrared band," *Opt. Express.*, vol. 16, pp. 5435-5443, 2008.

[4] J. M. C. Boggio, S. Moro, E. Myslivets, J. R. Windmiller, N. Alic, and S. Radic," 155-nm Continuous-Wave Two-Pump Parametric Amplification," *IEEE Photon. Technol. Lett.*, vol. 21, pp. 612-614, 2009.

[5] T. Torounidis, P. A. Andrekson, B. E. Olsson, "Fiber-optical parametric amplifier with 70-dB gain," *IEEE Photon. Technol. Lett.*, vol. 18, pp. 1194-1196, 2006.

[6] K. K. Y. Wong, M. E. Marhic, and L. G. Kazovsky, "Phase-conjugate pump dithering for high-quality idler generation in a fiber optical parametric amplifier," *IEEE Photon. Technol. Lett.*, vol. 15, pp. 33–550, 2003.

[7] G. P. Agrawal, *Nonlinear Fiber Optics*.4th Ed. United States of America: Academic press, 2007.

[8] G. Kalogerakis, M. E. Marhic, and L. G. Kazovsky, "Polarization-Independent Two-Pump Fiber Optical Parametric Amplifier with Polarization Diversity Technique", in *Optical Fiber Conference (OFC)*, 2006, Anaheim, Paper OWT4.

[9] J. L. Blows, and P. Hu, "Cross-talk-induced limitations of two-pump optical fibre parametric amplifiers," *J. Opt. Soc. Amer. -B.*, vol. 21, pp. 989-995, 2004.

[10] M. Jamshidifar, A. Vedadi, and M. E. Marhic, "Reduction of Four-Wave-Mixing Crosstalk in a Short Fibre-Optical Parametric Amplifier," *IEEE Photon. Technol. Lett.*, vol. 21, pp. 1244-1246, 2009.

Index of symbols

$\vec{E}$	Electrical Field
$\vec{P}$	Polarisation vector
$\vec{P}_L$	Linear polarisation vector
$\vec{P}_{NL}$	Nonlinear polarisation vector
$\chi^{(i)}$	i^{th}-order susceptibility
n	Refractive index
n_2	Nonlinear refractive index
n_0	Weak-field refractive index
c	Attenuation factor
γ	Fibre nonlinearity coefficient
A_{eff}	Effective area
L_{eff}	Effective length
α	Attenuation factor
β	Propagation constant
$\beta^{(i)}$	i^{th} derivative of propagation constant with respect to ω
$A(z,t)$	Slowly-varying envelop
P	Optical power
g	Gain coefficient
I	Irradiance
λ	Wavelength

List of Publications

1. "Parametric Amplifiers for Terabit Transmission Systems", Donald. S. Govan, *Mehdi Jamshidifar*, Nayla El-dahdah, Nick Doran, Michel E. Marhic, (Invited Paper), under preparation for IEEE Journal of Selected Topics in Quantum Electronics.

2. "Continuous Wave Parametric Amplification in Bismuth Oxide Fibers", *Mehdi Jamshidifar*, Armand Vedadi, Donald S. Govan, Michel E. Marhic, (Invited Paper) Opt. Fiber. Technol. Special Issue. In Press (End of 2010)

3. "1-Tb/s DWDM Long-Haul Transmission employing a Fiber Optical Parametric Amplifier", Nayla El-dahdah, Donald S. Govan, *Mehdi Jamshidifar*, Nick Doran, Michel E. Marhic, IEEE Photon. Technol. Lett. Vol. 22 (2010) 1171-1173.

4. "Reduction of Four-Wave Mixing Crosstalk in a Short Fiber Optical Parametric Amplifier", *Mehdi Jamshidifar*, Armand Vedadi, Michel E. Marhic, IEEE Photon. Technol. Lett. Vol. 21, (2009) 1041-1135.

5. "Continuous-wave parametric amplification and signal possessing in bismuth-oxide microstructured fibres", Armand Vedadi, *Mehdi Jamshidifar*, Michel E. Marhic, (Invited Talk), to be given in IEEE/Photonics Society Winter Topical Meeting, 2011, Colorado.

6. "Fiber Optical Parametric Amplifier in High-Speed WDM Networks", Nayla El Dahdah, Donald S. Govan, *Mehdi Jamshidifar*, Nick J. Doran, IEEE Photonics Soc. Topical Meetings, 2010, New Mexico.

7. "1-Tb/s DWDM Amplification in a Fiber Optical Parametric Amplifier", Optical Fiber Communication Conference (OFC), *Mehdi Jamshidifar*, Nayla El Dahdah, Donald S. Govan, Nick J. Doran, Michel E. Marhic, 2010, San Diego

8. "Continuous-Wave One-Pump Fiber Optical Parametric Amplifier with 270 nm Gain Bandwidth", *Mehdi Jamshidifar*, Armand Vedadi, Michel E. Marhic, European Conference on Optical Communication (ECOC), 2009, Vienna.

9. "Reduced Four-Wave Mixing Crosstalk in a Short Fiber Optical Parametric Amplifier", *Mehdi Jamshidifar*, Armand Vedadi, Michel E. Marhic, European Conference on Optical Communication (ECOC), 2009, Vienna.

10. "Continuous-Wave Two-pump Fiber Optical Parametric Amplifier with 60 dB Gain", *Mehdi Jamshidifar*, Armand Vedadi, Michel E. Marhic , Optical Fiber Communication Conference (OFC), 2009, San Diego.

11. "Continuous-Wave One-Pump Fiber Optical Parametric Amplifier with 230 nm Gain Bandwidth", *Mehdi Jamshidifar*, Armand Vedadi, Michel E. Marhic, IEEE Photonics Soc. Topical Meetings, 2009, Innsbruck.

12. "Wavelength Demultiplexer Based on a Continuous-Wave Bismuth-Oxide Fiber Optical Parametric Amplifier", *Mehdi Jamshidifar*, Armand Vedadi, Michel E. Marhic, (Post-Deadline paper) European Conference on Optical Communication (ECOC), 2008, Brussels.

13. "Continuous-Wave Bismuth-Oxide One-Pump Fiber Optical Parametric Amplifier", *Mehdi Jamshidifar*, Armand Vedadi, Michel E. Marhic, European Conference on Optical Communication (ECOC), 2008, Brussels.